Supplementary Information for: A Phanerozoic-style icehouse climate in the middle Ediacaran

Thomas W. Wong Hearing[1], Alexandre Pohl[2], Thomas M. Vandyk[1], Benjamin H. Tindal[3], Frédéric Fluteau[4], Alexander G. Liu[5], Thomas H. P. Harvey[1], Mark Williams[1]

[1]Centre for Palaeobiology and Biosphere Evolution, School of Geography, Geology and the Environment, University of Leicester, Leicester, LE1 7RH, UK.
[2]Université Bourgogne Europe, CNRS, Biogéosciences UMR 6282, 21000 Dijon, France.
[3]Chief Scientist's Directorate, Natural England, 8 City Walk, Leeds, LS11 9AT, UK.
[4]Université Paris Cité, Institut de physique du globe de Paris, CNRS, 1 Rue Jussieu, F-75005, Paris, France
[5]Department of Earth Sciences, Downing Street, University of Cambridge, Cambridge, CB2 3EQ, UK.
Correspondence to: Thomas W. Wong Hearing(twonghearing@gmail.com); Alexandre Pohl (alexandre.pohl@cnrs.fr); Thomas H. P. Harvey (thph2@le.ac.uk); Mark Williams (mri@le.ac.uk)

CONTENTS

1 Supplementary Data

The following supplementary data files are available on Zenodo at https://doi.org/10.5281/zenodo.17158910.

Data S1. Excel file containing the dataset of candidate mid- and late Ediacaran glaciogenic deposits.

Data S2. Excel file detailing the latitudinal extent of glaciation by 1 Myr steps from the Cryogenian (720 Ma) to Quaternary (0 Ma).

Data S3. Mid-Ediacaran icehouse Fast Ocean Atmosphere Model (FOAM) global circulation model climate simulation netCDF files.

Data S4. Mid-Ediacaran icehouse LMDZ atmospheric circulation model simulation netCDF files used to force the GRISLI ice sheet model.

Data S5. Mid-Ediacaran icehouse glacial onset GRISLI ice sheet model simulation netCDF files.

Data S6. CSV file of palaeo-rotated candidate MEIH deposits produced from these analyses.

Supplementary code files are available on GitHub at: https://github.com/twwh01/MEIH.

2 Phanerozoic- and Cryogenian-style icehouse climate states

Table S1. Comparison of Phanerozoic and Cryogenian icehouse climate states.

Criteria	Phanerozoic	Cryogenian
Sedimentology	Similar to modern glacial deposits.	Similar to modern glacial deposits with addition of post-glacial 'cap carbonates' (Hoffman et al., 2017).
Geographical extent of ice sheets	Low altitude ice sheets restricted to mid- to high latitudes (i.e. glaciogenic deposits found polewards of ~30 ° latitudes) (Evans, 2003; Macdonald et al., 2019; Merdith et al., 2025).	Depending on the model followed, low altitude ice sheets are either: (i) globally distributed, in a full 'snowball' state (Evans, 2003; Hoffman et al., 1998, 2017; Kirschvink, 1992) or a less intense 'slushball' state (e.g. Allen and Etienne, 2008; Micheels and Montenari, 2008), or (ii) concentrated at low latitudes resulting from strongly seasonal continental glaciation of paleomagnetically-equatorial continents with Earth in a high obliquity orbit (e.g. Evans, 2003; Williams et al., 2016).
Duration	Several to tens of millions of years (see Table 1 and Fig. 5) (Etienne et al., 2007; Evans, 2003; Macdonald et al., 2019; van der Meer et al., 2022; Merdith et al., 2025; Montañez and Poulsen, 2013; Raymond and Metz, 2004; Wicander et al., 2011).	Several millions to tens of millions of years (see Table 1 and Fig. 5) (Hoffman et al., 1998, 2017; Prave et al., 2016; Rooney et al., 2015; Tasistro-Hart et al., 2025).
Internal dynamics	Ice sheets fluctuate on orbitally-driven time scales producing significant sea level change of up to ~130 m within 15 kyr (Clark et al., 2009), ~200 m within 100 kyr, and up to ~300 m over 1 Myr (van der Meer et al., 2022), with associated sedimentary facies change (Ghienne et al., 2014).	Geological data are inconclusive. Some studies support Phanerozoic-like orbital forcing of Cryogenian ice advance and retreat (Etienne et al., 2007; Leather et al., 2002; Spencer, 1985), including marked climatic variation (Ye et al., 2024) and intervals with open marine conditions (Prave et al., 2016). Other studies have shown very limited Marinoan ice sheet grounding line oscillation over the whole four million year interval (e.g. Tasistro-Hart et al., 2025), with stable ice sheets eventually melting rapidly due to very high CO_2 build-up (Evans, 2003; Hoffman et al., 1998, 2017). This uncertainty may be partly due to different study locations with respect to the ice sheet (i.e. near the centre or on the fringes).
Inferred climate conditions	By comparison to greenhouse intervals, lower global mean surface temperatures, and stronger vertical and latitudinal temperature gradients (Fenton et al., 2023; Judd et al., 2024; Scotese et al., 2021; Woodhouse et al., 2023).	Characterised by extreme ('freeze-fry') climate oscillations governed by hysteresis (tipping-point) effects; nearly uniform very cold (freezing) global temperatures with a geologically rapid onset and termination globally when atmospheric CO_2 levels build to a catastrophic tipping-point (Evans, 2003; Hoffman et al., 1998, 2017).
Our preferred definition	Low altitude ice sheets in polar and mid-latitudes (i.e. non-tropical), exhibiting cyclic (orbitally-driven) fluctuations; ice sheets persisting for several millions to tens of millions of years.	Rapid onset of freezing at all latitudes, with or without cyclic ice sheet fluctuation, ice sheets persisting for several millions to tens of millions of years.

3 Assessing glaciogenic deposits

Sedimentary deposits can indicate either that freezing conditions were present in the proximal vicinity (e.g. a tillite), or that (low altitude) freezing conditions were present somewhere on Earth (e.g. a dropstone). Ice-related sediments can be grouped into two depositional categories: glacial ice, and non-glacial ice. Although such sedimentary deposits represent different formation conditions, they both indicate freezing temperatures. Furthermore, putatively glaciogenic sediments take many forms and are often open to multiple non-glaciogenic interpretations.

In this section, we briefly describe and evaluate different types of ice-related deposits, and outline how we can semi-quantitatively integrate them into data-model comparison studies. We begin by outlining how we can assess the likelihood of an icy origin for sedimentary deposits, i.e. how likely it is that the available evidence indicates an ice-related depositional mechanism rather than any other depositional mechanism.

3.1 Distal indicators of ice: how far can icebergs get?

Properly identified ice-rafted debris (IRD) or iceberg scours can be regarded as distal evidence for low altitude glaciation, in the absence of any indicators of proximal glaciation (e.g. low frequency occurrences of dropstones or till pellets not otherwise associated with striated pavements or tillites). Hill and Condron (2014) used scour marks off the coast of Florida, USA, to show that large "icebergs up to 300 m thick drifted to southern Florida (24.5° N)" after calving in the Arctic during the Last Glacial Maximum (LGM). Headland et al. (2023) found that Antarctic-origin icebergs have been recorded as far north as 26.83° S, in the middle of the South Atlantic Ocean (approximately 26° W) by the barque *Dochra* on 30 April 1894 (Munn, 1911). During the LGM and in the recent past, icebergs have been able to drift from northern and southern polar latitudes to near-tropical latitudes in both continental shelf and ocean settings.

A 1980 Institute of Oceanographic Sciences (IOS) project evaluating sediment dredge hauls of the northeast Atlantic Ocean found that glacially-derived material dominates hauls from ridges and seamounts from polar latitudes to approximately 40 °N, and that glacial erratics have been found as far south as 30°N (Davies and Laughton, 1972; Kidd and Huggett, 1981) – similar to the independently documented near-tropical latitudes of iceberg occurrences. Kidd and Huggett (1981) also note that neither seabed photographs nor dredge hauls showed evidence of clasts larger than 14 cm in diameter, and that 6 cm was a more typical maximum diameter, even though the dredge can recover clasts with a volume of 1 m^3. Those authors consequently inferred that glacially-derived boulders are rare in settings distal of present day ice sheets (Kidd and Huggett, 1981). Sedimentological evidence for low-altitude glacial ice throughout Phanerozoic icehouse intervals spans polar to mid-latitudes (approximately ±90 to 40 °; Evans, 2003; Macdonald et al., 2019), possibly reaching near-tropical latitudes during the peak of the Late Palaeozoic Ice Age (see Fig. 5; Merdith et al., 2025). This pattern is consistent with the ocean floor studies of the late Cenozoic north Atlantic Ocean (Davies and Laughton, 1972; Kidd and Huggett, 1981) and suggests that evidence of large, outsized clasts in marine settings interpreted as glaciogenic in origin may therefore be good evidence for the maximum palaeolatitudinal extent of ice sheets and low-altitude glaciers in deep time.

Icebergs have not been documented as crossing the Equator. Ice-rafted debris may therefore be a useful indicator that there was grounded ice at sea level somewhere in the same hemisphere, except during very cold ('snowball Earth') conditions. However, the location at which the IRD is found need not itself be particularly cold. Abundant and locally widespread IRD may be used to indicate proximity to an iceberg source, but the presence of lone or sparse IRD only indicates that low altitude ice was present on Earth, likely in the same hemisphere, at the time of deposition.

3.2 Weighting confidence of glaciogenicity

Here, we build on the method of assessing likely glaciogenicity of geological deposits developed by Tindal (2023) and updated by Wong Hearing et al. (2026). The five-star rating system can be used to assess the likelihood that any particular sedimentary deposit had a glacial origin (see Table 1 and Data S1). Importantly, this scheme takes account of the diversity of possible sedimentological and depositional setting evidence for glaciogenicity, much of which evidence can also result from non-glacial origins.

Five qualitatively-defined categories of confidence are used, with individual lines of evidence being given a rating of zero to five stars (Tindal, 2023). Each deposit may have multiple different lines of evidence, all of which contribute to an overall rating for the whole deposit. In this way, a deposit may be confidently considered glaciogenic if it has either one "unequivocal" line of evidence or several weaker ("strong", "circumstantial", "weak", "equivocal") lines of evidence (Tindal, 2023). We have added a "zero star" or "insufficient" category (see Table 1; Wong Hearing et al., 2026), which Tindal (2023) implicitly included but did not define.

Tindal's (2023) approach to semi-quantitatively combining lines of evidence was to use a geometric progression with an interval ratio of ½, making two lines of evidence from one level equivalent to one line of evidence from the next level. For example, two three-star ("circumstantial") lines of evidence in one deposit would be equivalent to one four-star ("strong") line of evidence. It is therefore theoretically possible to have a 'greater than five-star' deposit, though in practice this is not a concern for potential Ediacaran glaciogenic deposits.

3.3 Diamictites and dropstones

Diamictites are "any non-sorted or poorly sorted terrigenous sediment that consists of sand and/or larger particles in a muddy matrix" that has been lithified (Flint et al., 1960a, b). Since this definition was developed, the term "diamictite" has been considered non-genetic (Eyles et al., 1983; Flint et al., 1960a, b) as it is recognized that poorly sorted sediment in a muddy matrix can have many different depositional origins. Consequently, though this is often overlooked, not all diamictites are tillites or even glaciogenic deposits. As noted by Tindal (2023), "a mudrock with a single boulder; a sandy mudstone; and a clast supported conglomerate with a muddy matrix can all be considered to be diamictites."

For ancient diamictites to be confidently considered to represent tillites, they should be supported by several lines of evidence, not all of which will be available in the published literature, or even possible to determine from the geological record.

3.3.1 Clast-rich diamictites (candidate tillites)

A rock comprising a muddy matrix with floating outsized clasts of at least sand size could be classed as a diamictite (Flint et al., 1960a, b; Tindal, 2023). A variety of processes can result in the deposition of sediment with a diamict fabric, including sediment rafting, floatation and gravitational processes, and proximal glacial action. The depositional mechanisms of infrequent lonestones are addressed in the section below. The formation of clast-rich diamictites that could arguably be proximal tillites are dealt with here.

Gravitational processes that incorporate outsized clasts into a deposit include turbidity currents and debris flows, which can transport cobble- and boulder-sized clasts, and that result in a wide range of sedimentary structures. These include chaotic, unstructured deposits as well as laminae in finer material that larger clasts may disrupt, "giving the appearance of a dropstone bearing deposit" (Bennett et al., 1996). Outsized clasts can also be deposited after rolling or bouncing either down a slope, or by escaping as outrunners from the sides or end of a mass flow – "outrunner blocks" up to 18 m high and 70 m long can travel at least 25 km on a slope of <1° after separating from a submarine landslide, and may produce large scour marks (Nielsen and Kuijpers, 2004). Gravitational processes can therefore cause deposition of very large, outsized clasts in fine grained sediment. The depositional context is as important as the sedimentological characteristics of a deposit for assessing likely glaciogenicity (Tindal, 2023). Sedimentological characteristics are assessed separately below as these apply equally to lonestone and clast-rich diamictite deposits. Here, we consider that outsized clasts deposited as massive or stratified diamictites are good indicators of proximal glacial activity if the depositional setting shows no indicators of downslope transport in the target deposit or stratigraphically adjacent deposits; i.e. the sediments were deposited in a flat or distal setting (Table S2). Outsized clasts deposited as massive or stratified diamictites in settings with evidence for downslope transport or associated with other, non-diamictite, reworked deposits provide weak evidence for a glacial origin, i.e. whilst plausibly glaciogenic this is not the most parsimonious mechanism for deposition.

Table S2. Clast-rich diamictites as an indicator of glaciogenicity. Clast-rich diamictites are distinct from isolated or infrequent lonestones in a muddy matrix (for which see Table S3). Note that the substantial increase in land plants and nektonic vertebrates in the late Silurian and Devonian increases the number of non-ice raft sources from the Devonian Period onwards. After Tindal (2023, table 2.2).

Rating	Clast-rich diamictite
★★★	Outsized clasts deposited as a massive or stratified diamictite in a flat or distal setting not on or near the base of a slope.
★★	N/A
★	Outsized clasts deposited as a massive or stratified diamictite in a setting with other reworked deposits.

3.3.2 Clast-poor diamictites (candidate dropstones and ice-rafted debris)

Ice-rafted debris, typically in marine sediments, is routinely used for understanding Cenozoic cryosphere dynamics and should be considered as a separate line of evidence to tillites: both lithologies may be considered diamictites (following Tindal, 2023).

A rock comprising a muddy matrix with floating outsized clasts of at least sand size would be classed as a diamictite (Flint et al., 1960a, b; Tindal, 2023). Bennett et al. (1996) define "a dropstone as a clast of anomalous size, and/or lithology, indicative of vertical or oblique introduction into the host sediment"; 'dropstone' is therefore a genetic term, linking the presence of an outsized clast with its method of emplacement (Tindal, 2023). Separating the emplacement mechanism from structures observed in a rock, one may consider interpreting a lonestone disrupting (bending, penetrating, rucking, or rupturing) laminae above and below it as a dropstone (Evans and Benn, 2004; Tindal, 2023). There are many ways of emplacing outsized clasts in water-lain sediments, including rafting (biological, ice, pumice), floatation processes, gravitational processes, and projectile processes (Bennett et al., 1996, fig. 2).

In an Ediacaran and Cambrian context, the only plausible biological agent of dropstone emplacement is via uprooted algal (or arguably soft-bodied metazoan) holdfasts which in the present can reach the open ocean and transport clasts up to boulder size (400 mm; Bennett et al., 1996; Huggett and Kidd, 1983); there would have been no plants, no corals, and no pelagic animals with gastroliths (Bennett et al., 1996). Ice-rafting can carry sediment ranging from very fine to large boulder size over long distances and may deposit either isolated lonestones or clusters of finer grained material as dump structures. Ice-rafting may be caused by the flow of a grounded ice sheet into the sea (or a lake) and subsequent transport as an iceberg. Ice-rafting may also derive from seasonally frozen settings (seas, rivers, lakes) which may result in considerable volumes of ice-transported material (Bennett et al., 1996). Pumice rafting would usually result in only lithic fragments of pumice (or similar felsic volcanic rock) being deposited. Other floatation processes typically only apply to finer sediments (long axis ≤ 15 mm) that can be supported by surface tension (Bennett et al., 1996; Moeller and Ingolefsson, 1994).

Gravitational processes can introduce outsized clasts into a deposit include turbidity currents and debris flows (see above). Outsized clasts can also be deposited after rolling or bouncing down a slope or by escaping from the sides or end of mass flows as outrunners. Gravitational processes can, therefore, cause deposition of very large, outsized clasts in fine grained sediment.

Projectile processes – volcanic eruptions and bolide impacts – may result in dropstone deposition, typically close to the source for large clasts (Bennett et al., 1996). Volcanic sources will usually be readily identifiable from the clast composition, shape, and surface characteristics, as well as the geological setting (Bennett et al., 1996). Bolide sources are a vanishingly rare prospect at most intervals in the geological record, and clast lithology can be an indicator (Bennett et al., 1996).

Glaciogenic dropstones do not necessarily indicate proximal grounded ice; rather they indicate that once-grounded ice has floated above the location at which the dropstone was deposited. Ice-rafted debris is likewise a useful indicator that there was grounded ice at sea level. However, the location of the IRD deposit need not necessarily be particularly cold. Abundant and locally widespread IRD may be used to indicate proximity to an iceberg source, but the presence of lone or sparse IRD only indicates that low altitude ice was present on Earth (likely in the same hemisphere) at the time of deposition.

Clast shape and surface characteristics may aid in diagnosing the depositional mechanism of lonestones (Bennett et al., 1996). Faceting – 'iron-wedging' – and striation would support a glaciogenic origin for a lonestone, but one must also consider the possibility of reworking of older material (Bennett et al., 1996), so depositional setting is also important particularly if the stone is deposited on or near the base of a slope (Tindal, 2023).

Table S3. Clast-poor diamictites as an indicator of glaciogenicity. Clast-poor diamictites: fine-grained rocks with outsized clasts or lonestones which may or may not disrupt laminae in the surrounding sediment, as distinct from clast-rich diamictites (for which see Table S2). Note that the substantial increase in land plants and nektonic vertebrates in the late Silurian and Devonian increases the number of non-ice raft sources from the Devonian Period onwards. After Tindal (2023, table 2.2)

Rating	Clast-poor diamictite
★★★	Outsized clasts that: (i) disrupt laminae above/below in a flat or distal setting not on or near the base of a slope; or (ii) are deposited as a massive or stratified diamictite in a flat or distal setting not on or near the base of a slope.
★★	Outsized clasts that disrupt laminae above/below, from a setting where downslope transport is not reported, or confirmed absent.
★	Outsized clasts that may disrupt laminae above/below in or associated with reworked deposits.

3.3.3 Clast shape and clast surface

Clast shape is frequently reported in sedimentological studies and may be useful in diagnosing transportation mechanism and distance. Following the Powers (1953) roundness scale of (1) very angular, (2) angular, (3) subangular, (4) subrounded, (5) rounded, and (6) well-rounded, Hambrey and Harland (1981) suggest that glacial deposits typically comprise angular to well-rounded clasts and must have both subangular and subrounded clasts. Following Tindal (2023), a conservative requirement for possible glaciogenicity from clast roundness is to require at least four classes from Powers' (1953) scale, including subangular and subrounded. More crudely, ice can transport elongate clasts further than a higher energy or turbulent flow (Evans and Benn, 2004). A deposit with several elongate clasts may be more readily interpreted as having an ice-related depositional process, or may have only had a short transport distance (Tindal, 2023).

Table S4. Clast shape as an indicator of glaciogenicity. After Tindal (2023, table 2.3).

Rating	Clast shape
★★	Several elongate clasts.
★	Clasts with at least four different grades of roundness, including subangular and subrounded, or a few elongate clasts.

Clast surface – faceting and striation – can also be used to help diagnose the depositional mechanism of a rock with outsized clasts. Clasts entrained either at the bottom or the margins of a glacier or ice sheet can be abraded by scraping against the underlying bedrock or other clasts also entrained in the ice, typically producing one or multiple smoothed faces (facets), but such smooth surfaces can be produced by non-glacial means as well (Knight, 2008; Várkonyi and Laity, 2012). Faceted clasts can present as ‘flat-iron’/dreikanter stones, or ‘bullet-shaped’ clasts. Striations on clast surfaces can only form from a directional contact with a harder object, which can occur during downslope reworking (Van Hoesen and Orndorff, 2003), fault plane movement (Eyles and Boyce, 1998), and glacial action, all of which can produce diamictites with striated clasts. Glacial action and turbulent currents may cause scratching that develops grooves without a preferred orientation (Van Hoesen and

Orndorff, 2004), and aligned striae can be caused by both glacial ice and fault-actions. In practice, it may be difficult to differentiate poly-directional scratches and aligned striae in published literature unless the specimens are well figured (Tindal, 2023). Producing and preserving clasts with both striated and faceted surfaces is challenging without a glacial mechanism, particularly if there are multiple striated or faceted surfaces.

Table S5. Clast surface texture as an indicator of glaciogenicity. After Tindal (2023, table 2.4).

Rating	Clast surface
★★★	Clasts with striated and facetted surfaces.
★★	N/A
★	Clasts with either facetted surfaces or striae.

Clast lithologies. The lithologies of outsized clasts in a diamictite can be informative about the processes that collected those clasts together. Extra-basinal lithologies not found in local lithologies or basement rocks can be indicative of a glacial origin. In practice, this is hard to test in deep time contexts since a complete sedimentary basin is rarely preserved, or at least rarely exposed. Following Tindal (2023), a pragmatic approach can be taken for using clast lithology as an indicator of potential glaciogenicity of a diamictite: the presence of siliciclastic, carbonate, metamorphic, and igneous clasts. This categorization of clast lithologies can be combined with stricter criteria, such as a known extra-basinal or very long-distance source to produce a framework for interpreting clast lithologies as a possible indicator of glaciogenicity (Table S6) (Tindal, 2023).

Table S6. Clast lithology as an indicator of glaciogenicity. After Tindal (2023, table 2.5).

Rating	Clast lithology
★★★	Clasts include all of siliciclastic, carbonate, metamorphic, and igneous lithologies; or clasts of a lithology not otherwise known from the basin; or non-abraded clasts (i.e. with little physical weathering) that must have travelled at least 100 km.
★★	Clasts include three of siliciclastic, carbonate, metamorphic, and igneous lithologies.
★	Clasts include two of siliciclastic, carbonate, metamorphic, and igneous lithologies; or diamictite described as "heterogeneous" or "polymict" without further description.

3.3.4 Grain clusters (frozen aggregates; till pellets)

Frozen aggregates are clusters of sediment grains temporarily 'cemented' by interstitial ice which can break off from larger icebergs in blocks with more that 7.5% lithic fragments and sink to the seafloor before the ice completely melts (Gilbert, 1990; Huggett and Kidd, 1983; Ovenshine, 1970). Goldschmidt et al. (1992) found that frozen aggregates could maintain their form over a 4 km fall through seawater and initial burial in the cold waters of the Arctic Ocean and peripheral seas. Icebergs from which frozen aggregates calve may derive from glaciers that embedded sediment grains during their transit over land, from lacustrine or fluvial ice that drifts out to sea, or from sea ice that formed in contact with a beach or shallow coastal seafloor.

Frozen aggregates behave like dropstones – i.e. are 'dropped' from the iceberg and fall to the seafloor intact – until the interstitial ice melts and they enter the geological record as a cluster of interlocking outsized sediment grains in a finer matrix. Clusters of sediment grains may also form as lag deposits from currents, so a current-origin for clusters of sediment grains must be excluded for confident interpretation of grain clusters as frozen aggregates.

Table S7. Grain clusters as an indicator of glaciogenicity.

Rating	Grain clusters
★★★★	Uncemented clusters of close-packed interlocking outsized grains, isolated in a fine-grained sediment without evidence of current flow, disrupting laminae (if present), and occurring at multiple closely spaced stratigraphic horizons.
★★★	Uncemented clusters of close-packed interlocking outsized grains, isolated in a fine-grained sediment without evidence of current flow and disrupting laminae (if present).
★★	Uncemented clusters of outsized granules in a fine-grained matrix that may host other sediment grains without specific evidence of current flow for their deposition though surrounding sediment may show signs of current flow for deposition.
★	Uncemented clusters of outsized clasts without evidence of erosive lower contacts.
☆	Lag deposits of outsized clasts in a fine-grained sediment where there is direct evidence of an erosive base, current deposition, or several laterally extensive deposits confined to one or several specific horizons.

3.4 Geomorphology and erosion surfaces

Geomorphology is a crucial lens through which to understand relatively recent glacial activity, and can be used to understand ancient glaciers as well (Hambrey and Harland, 1981; Tindal, 2023). Glacially striated rock surfaces are unequivocal evidence for grounded ice at a given location, but as with diamictites there are non-glacial processes that can produce striated surfaces. Such non-glacial processes include human activity, movement on fault planes (slickensides), and landslides (Gee et al., 2005; Means, 1987; Tindal, 2023). Moreover, it can be difficult to date the age of striation of a striated surface. A recent review of a "classic" Cryogenian striated pavement in North America found it more likely to be a "recent erosional phenomenon" (Vandyk et al., 2021). Whilst it is possible to differentiate ancient glaciogenic from other striated surfaces, even "classic" examples should be considered carefully on a case-by-case basis. Structural features that indicate a probable glacial origin of a striated surface include crescentic gouges, chatter marks, and s-forms (Hambrey and Harland, 1981; Shaw et al., 2020; Tindal, 2023), in the absence of evidence for non-glacial fluvial processes which can also produce similar erosive features (Shaw et al., 2020). Valleys with a U-shaped cross section are typical of large-scale glacial erosion and can be recognised by mappable unconformities and lateral variation in unit thickness, even in ancient deposits (Dietrich et al., 2021; Tedesco et al., 2016). Recessive erosion of glacial valley fill deposits can also reveal ancient ice-stream morphologies in modern landscapes (Dietrich et al., 2021; Le Heron, 2017). To be sure of a glacial origin for ancient geomorphological features there should be other direct evidence of ice, such as extensive striation of surfaces within the feature (following Tindal, 2023).

Roches moutoneés are glacial erosion features comprising asymmetrical hills with striated upstream faces and ice-fractured downstream faces. In practice, it is difficult to identify such features in very ancient deposits. Moraine ridges are glacial depositional features that form in sub- and pro-glacial settings (Evans and Benn, 2004). Although difficult, it is possible to identify ancient moraine ridges from diamictite dimensions though, as Tindal (2023) notes, there are other processes that could cause variations in diamictite thickness, including erosion or reworking.

Table S8. Star rating scheme for geomorphological or erosional feature evidence for ice. After Tindal (2023, table 2.6).

Rating	Geomorphology and erosion surfaces
★★★★★	Extensive striated surfaces with crescentic gouges, chatter marks and s-forms.
★★★★	Extensive surfaces with striae and some, but not all, of crescentic gouges, chatter marks and s-forms.
★★★	Extensive surfaces with striae and/or small surfaces with crescentic gouges, chatter marks, and s-forms. U-shaped valleys or branching valley networks.
★★	Large smooth surfaces and/or small surfaces with striae. Palaeotopography resembling: (i) roche moutoneé structures, or (ii) (ii) moraine-like ridges.
★	Small smooth surfaces.
☆	Uneven bedrock topography.

3.5 Glendonites (ikaite)

Ikaite is a metastable hydrous calcium carbonate ($CaCO_3 \cdot 6H_2O$) mineral that precipitates a characteristically stellate morph in cold marine settings in the water column or at the sediment-water interface (Buchardt et al., 1997; Pauly, 1963), just below the sediment-water interface (Stein and Smith, 1986; Suess et al., 1982; Zhou et al., 2015), and in sea ice (Dieckmann et al., 2008), as well as in non-marine lacustrine (Council and Bennett, 1993) and terrestrial settings (Field et al., 2017).

Experimental work has shown that low temperatures are not sufficient to favour ikaite precipitation over other more stable carbonate forms like aragonite, calcite, and vaterite, though the difference in saturation between ikaite and other carbonates decreases substantially as temperatures cool towards 0 °C (Bischoff et al., 1993). In modern oceans, ikaite typically precipitates where bottom-water temperatures are below 4 °C, though it may rarely precipitate at up to 10 °C (Zhou et al., 2015), which is close to the reported maximum precipitation temperature of 8 °C to 9 °C in a terrestrial setting (Field et al., 2017). However, ikaite has been experimentally precipitated at temperatures up to 35 °C in high pH conditions (pH > 9.2; Tollefsen et al., 2020), and in the field ikaite is commonly not found in seafloor sediments with suitable water temperatures for its precipitation (i.e. <10 °C; Zhou et al., 2015). Ikaite is therefore not a simple palaeo-thermometer.

Factors that favour ikaite precipitation are low temperature (<10 °C, typically <4 °), low pCO_2, high pressure (e.g. deeper water), high phosphate, and high alkalinity (particularly Mg) conditions (Bischoff et al., 1993; Zhou et al., 2015). Organic-rich sediments are also associated with favouring ikaite precipitation (Stein and Smith, 1986; Suess et al., 1982), which may

be due to their high phosphate concentrations (Bischoff et al., 1993; Zhou et al., 2015). There is also geochemical evidence that microbial action (bacterial sulfate reduction) may be important in promoting ikaite formation (Qu et al., 2017). In the absence of evidence for exceptionally high alkalinity, ikaite precipitation may be taken as indicative of cool (<10 °C and likely <4 °C) phosphate-rich seafloor conditions.

Ikaites are typically preserved in the geological record as glendonites: pseudomorphs of ikaite by more stable minerals including various carbonates or silica. Although most geological occurrences of glendonites are small, the original report of ikaite described columns of typically 1 m but up to 10 m in diameter and 0.5 m to 20 m high from the seafloor of Ika Fjord, Greenland, and reaching up to just 0.5 m below the low tide sea level (Pauly, 1963). At Ika Fjord, sea temperatures were 3 °C at the seafloor and 7 °C 1 m above the seafloor (Pauly, 1963).

Whilst glendonites do not necessarily indicate anything about sea surface conditions, or whether ice was present at sea level at the time of formation, their presence can provide useful contextual evidence for a cold climate locally, especially when combined with other lines of evidence.

4 Candidate mid-Ediacaran glaciogenic deposits

Here we review the evidence for potential glaciogenicity and depositional age of all candidate glaciogenic deposits identified as plausibly of MEIH-interval age (i.e. deposited between ~600 to 579 Ma; see Figure 1).

4.1 Amazon Craton

4.1.1 Serra Azul Formation (Parecis Basin, Brazil)

The Serra Azul Formation (Alvarenga et al., 2007) was deposited in the Juruena sub-basin of the Parecis Basin, northwest Brazil, and lies between carbonates of the Araras Group and siliciclastics of the Alto Paraguay Group, which are interpreted as recording the opening of the Clymene Ocean basin and its closure in the Brasiliano orogeny, respectively (Figueiredo et al., 2011; Lamoso et al., 2023; McGee et al., 2015a).

Sedimentology. The Nobres Formation (uppermost Araras Group) is overlain by the Serra Azul Formation, and the contact, though unobserved, is thought to be unconformable as carbonate clasts similar to the Araras Group are found in the lower Serra Azul Formation (Alvarenga et al., 2007; McGee et al., 2013, 2015a). The Nobres Formation comprises shallow marine dolomitic carbonates including dolostones, silicified carbonates, and a cross-bedded dolostone with peloids, and oolites, and towards the top of the formation includes stromatolitic dolostones and evaporative sedimentary features, indicating further shallowing (containing mud cracks and evaporites) (Figueiredo et al., 2011).

The Serra Azul Formation is typically up to 300 m thick, with the diamictite (sometimes known as 'Unit A') typically about 70 m thick (Alvarenga et al., 2007; Figueiredo et al., 2011), though it has been reported locally as ~180 m thick and up to 1 km thick (McGee et al., 2013). Above the diamictite, 'Unit B' comprises laminated mudstones and siltstones with granules of quartz and chert, as well as claystones, with very fine and fine sandstones becoming more common up-section forming a coarsening-upwards sequence (Alvarenga et al., 2007).

Unit A, the diamictite unit, comprises massive diamictite with a clay- to silt-grade matrix hosting millimetre- to centimetre-scale clasts and rare larger clasts up to 30 cm diameter (Alvarenga et al., 2007). The clasts include carbonates, cherts, sandstones, mudstones, quartzites and quartz grains, as well as mafic and (weathered) granitic igneous rocks, and gneiss (Alvarenga et al., 2007; McGee et al., 2013, 2015b). Clasts of typically 0.5 cm to 10 cm range from rounded or well-rounded to very angular (Alvarenga et al., 2007; McGee et al., 2013, 2015b). Clasts may also be polished, striated, and faceted, including possible bullet-shaped clasts (Alvarenga et al., 2007; McGee et al., 2013, 2015b).

McGee et al. (2013, 2015b) interpret the Serra Azul diamictite as recording a transitional environment from a grounded icesheet to a glaciomarine setting, with the depositional setting becoming deeper up-section due to glacioeustatic sea level rise in the immediate aftermath of glaciation. McGee et al. (2013) also infer glacial erosion and incision from the highly variable thickness of the Serra Azul Unit A and underlying Araras Group, which is locally absent, although carbonate clasts similar to rocks of

the Araras Group appear in the Serra Azul diamictite even in sections missing the whole Araras Group. McGee et al. (2013) rely on changing stratigraphic thicknesses and local mapping to evidence the palaeotopography onto which the Serra Azul Formation was deposited; no erosive contact surface is described.

Age constraints. The depositional age of the Serra Azul Formation is poorly constrained. The Mirassol d'Oeste Formation (lowermost Araras Group) carbonates have produced a Pb-Pb whole-rock isochron age of 627 ± 32 Ma (Babinski et al., 2006; cited as 633 ± 25 Ma in Figueiredo et al., 2011), supporting an Ediacaran maximum age for the Serra Azul Formation. Detrital zircon U-Pb dates from the Serra Azul diamictite indicate a depositional age after 650 Ma and probably after 646 Ma (McGee et al., 2015a). Detrital muscovite Ar-Ar dates from the Serra Azul Formation have provided a maximum depositional age of 640 ± 15 Ma (McGee et al., 2015b). Detrital zircon U-Pb dates from the Spotuba Formation (middle to upper Alto Paraguay Group) provide a maximum depositional age for this formation of 615 Ma, and detrital zircons from the Diamantino Formation (uppermost Alto Paraguay Group) provide a maximum depositional age for this formation of 528 ± 9 Ma from the youngest grain, or 560 ± 13 Ma from a weighted average of the second and third youngest grains (McGee et al., 2015a). Detrital muscovite Ar-Ar dates clustering around 544 ± 7 Ma support the younger, Cambrian, maximum depositional age for the Diamantino Formation (McGee et al., 2015b).

Chemostratigraphic evidence supports a mid-Ediacaran age for the Serra Azul diamictite. Stable carbon isotope ($\delta^{13}C$) values through the Araras Group (Mirassol d'Oeste, Guia, and Nobres formations) rise steeply from approximately –10 ‰ directly above the Puga Formation to approximately –1 ‰ to 0 ‰ through the Guia Formation and most of the Nobres Formation (Alvarenga et al., 2011). Carbon isotope values peak close to the top of the Nobres Formation with values up to approximately +10 ‰ (Alvarenga et al., 2011). This is similar to the global early Ediacaran $\delta^{13}C$ curve, which recovers quickly from a basal Ediacaran negative excursion to a low positive plateau throughout the early Ediacaran, with a small negative excursion (to ~0 ‰) between 590 to 585 Ma and a return to more positive values between 586 to 580 Ma before a negative excursion at ~580 to 578 Ma (Yang et al., 2021). An alternative reading of the Araras Group $\delta^{13}C$ data is that it represents only early Ediacaran values, i.e. the post-Cryogenian negative excursion recovery and rise into the positive plateau at ~620 Ma (Yang et al., 2021).

Summary. The upper Alto Paraguay Group is either latest Ediacaran or early Cambrian in age (<540 Ma, possibly <528 Ma; McGee et al., 2015a, b). The Araras Group is likely early to mid-Ediacaran in age, though this relies on sparse and difficult to interpret chemostratigraphy, as the available radiometric age constraints have large uncertainties. The Serra Azul Formation is not likely to be much older than 600 Ma, based on this chemostratigraphy and the loose radiometric age constraints. The Serra Azul Formation is also likely to be older than Cambrian age, based on the absence of paleontological data (particularly trace fossils) in the Alto Paraguay Group and the few available radiometric age constraints. It is probable that the Serra Azul Formation is older than or coeval with the Shuram excursion, which is not captured in the Araras Group $\delta^{13}C$ data; one of the early (~620 Ma) or mid-Ediacaran (~585 to 580 Ma) positive $\delta^{13}C$ peaks may be captured. It is probable that the Serra Azul diamictite is of approximately mid-Ediacaran age, though younger and older Ediacaran ages cannot be ruled out.

Table S9. Rating of possible glacial influence on the Serra Azul diamictite.

Category	Description	Rating
Outsized clasts	Outsized clasts deposited as a massive (but not stratified) diamictite in a flat or distal setting not on or near the base of a slope.	★★★
Clast shape	Clasts are well rounded to very angular.	★
Clast surface	Clasts with striated and faceted surfaces.	★★★
Clast lithology	Clasts of four lithology classes (siliciclastic, carbonate, metamorphic, igneous).	★★★
Geomorphology	Uneven bedrock topography. (No erosional surfaces have been observed but erosion clearly occurred.)	
Summary	Strong: no realistic ice-free depositional environment is likely to produce this evidence.	★★★★

4.2 Arabian Shield

4.2.1 Antaq Polymictic Conglomerate (and other Jibalah Group conglomerates: Jifn, Mataar)

Here, we follow Tindal (2023) in considering the Antaq Polymictic Conglomerate as representative of other polymictic conglomerates in the geographically restricted Jibalah Group, excluding the Dhaiqa Formation (see below). This approach follows the correlations of Al-Husseini (2014).

Sedimentology. Kusky and Matsah (2003) described several conglomeratic facies of the Jifn Formation in the Jifn Basin, including a "polymict basal conglomerate" (p. 336) that is distinct from other conglomerates higher in the succession which comprise entirely and evidently local clasts. The polymict conglomerate apparently both unconformably overlies and, in some places, is intercalated with Jibalah Group volcanic deposits (Kusky and Matsah, 2003), implying a short time gap and local erosion at the base of the conglomerate. The Jifn Formation basal conglomerate is characterized as a massive conglomerate with rounded to subrounded sand to boulder grade (up to 35 cm diameter) clasts of granite, rhyolite, andesite, and sedimentary lithologies from the underlying Murdamah Sandstone Conglomerate (Kusky and Matsah, 2003); carbonate clasts are also mentioned in logs (e.g. Vickers-Rich et al., 2012), but not in primary reports. The Jifn Formation polymict conglomerate occurs around the flanks and base of the basin: the polymict conglomerate is thickest around the northeastern side of the basin, and is thinner in the south, southwest, and west where it can be intercalated with mafic volcanic rocks (Kusky and Matsah, 2003). The northeastern side of the Jifn Basin is defined by the main branch of the Halaban-Zaeghat fault which was active during deposition of the Jibalah Group, controlling the shape and evolution of the Jifn Basin as a pull-apart basin (Kusky and Matsah, 2003). That the thickest deposits of the polymict conglomerate are found on the faulted sides of the Jifn Basin led Kusky and Matsah (2003) to conclude that it is a high energy downslope deposit with pulses of deposition controlled by fault movement. Since Kusky and Matsah (2003), Al-Husseini (2014) reported the description of the Antaq Polymictic Conglomerate (Rubtayn Formation, Antaq Basin) from an unpublished honours thesis (Nettle, 2009; University of Adelaide) as being a blocky, massive, deposit of predominantly sub-rounded quartz clasts in a quartzofeldspathic matrix, with occasional sedimentary structures (cross bedding). In turn, Nettle et al. (2014) gave only brief mention of the Antaq Polymictic Conglomerate, whilst

describing the overlying deposits in more detail as fine and medium sandstones and siltstones, with carbonate concretions and metre-scale soft sediment deformation structures, including fluid escape structures, convolute bedding, and slump folds. The middle Rubtayn Formation apparently comprises similar sandy and silty facies to the lower part of the formation, without the conglomerates which do return in the upper part of the formation as a more than 200 m thick predominantly massive polymictic conglomerate, which is interpreted as an alluvial deposit (Nettle et al., 2014). Soft sediment deformation structures are also reported, though are less common, in the upper Rubtayn Formation (Nettle et al., 2014). The Antaq Basin is interpreted similarly to the Jifn Basin as a dextral pull-apart basin which was actively faulting during deposition of the Rubtayn Formation sediments (Al-Husseini, 2014).

Age constraints. In the Jifn Basin, the Jibalah Group is constrained by zircon U-Pb TIMS dates from the underlying rhyolite of 624.9 ± 4.2 Ma and from an intruding felsic dyke in the upper Jibalah Group of 576 ± 5.3 Ma (Kusky and Matsah, 2003). In the Dhaiqa Basin, the upper Jibalah Group (Dhaiqa Formation) is constrained by a tuff zircon U-Pb LA-ICP-MS date of 569 ± 3 Ma (Vickers-Rich et al., 2012).

In the Antaq Basin, the Jibalah Group is constrained by a series of dates from Nettle et al. (2014): the underlying basement microgranite yielded a zircon U-Pb CA-TIMS date of 618.17 ± 0.2 Ma, a tuff in the upper Rubtayn Formation (sample WP065) yielded a zircon U-Pb LA-ICP-MS date of 596 ± 17 Ma, and two tuffs in the middle Muraykah Formation yielded stratigraphically incongruent LA-ICP-MS dates of 579 ± 17 Ma (sample S02-04) and 604 ± 18 Ma (sample S02-23) from their youngest concordant ages.

In the Dhaiqa Formation, putative Ediacaran fossils, possibly resembling a frondose taxon and *Aspidella* discs, have been reported from the middle Muraykhah Formation, offering support for a late Ediacaran (<579 Ma) age for the upper Jibalah Group (Vickers-Rich et al., 2012).

Summary. The Antaq and other Jibalah Group polymictic conglomerates were likely deposited in the mid-Ediacaran, after 625 Ma and before ~579 Ma, based on radiometric and palaeontological constraints (Kusky and Matsah, 2003; Nettle et al., 2014; Vickers-Rich et al., 2012).

The Jibalah Group polymictic conglomerates are generally interpreted as fault-controlled gravity-driven deposits around the margins of small pull-apart basins, with the respective overlying finer siliciclastic units reflecting a facies change as deposition becomes more distal with respect to the basin margins (Al-Husseini, 2014; Kusky and Matsah, 2003; Nettle et al., 2014). Much of the Jibalah Group is interpreted as being deposited in a non-marine setting: many of the coarser siliciclastics, including tabular and trough cross-stratified sandstones, and some of the conglomerates, are interpreted as fluvial to delta plain facies which transition upwards into finer grained siliciclastic units, some of which (at least in the Antaq Basin) were likely deposited in a shallow marine, tidal, setting (Nettle et al., 2014).

Table S10. Rating of possible glacial influence on the Antaq Polymictic Conglomerate and other Jibalah Group polymict conglomerates.

Category	Description	Rating
Outsized clasts	Outsized clasts deposited as a massive diamictite in a setting with evidence for downslope reworking of deposits.	★
Clast shape	Clasts are rounded to subrounded.	
Clast lithology	Clasts of two lithology classes (siliciclastic, igneous). Note that carbonates are described from the area but are not mentioned as being represented in the conglomerate clasts.	★
Summary	Weak: some ice-free depositional environments could produce this evidence.	★★

4.3 Avalonia

4.3.1 Gaskiers Formation (Conception Group)

The Gaskiers Formation crops out on the eastern side of St. Mary's Bay, southern Avalon Peninsula. It conformably overlies the Mall Bay Formation and is conformably overlain by the Drook Formation (Carto and Eyles, 2011; Eyles and Eyles, 1989). The Mall Bay and Drook formations comprise fine-to-medium and fine-to-coarse sandy turbidites, respectively, with common soft-sediment deformation and slumping (Carto and Eyles, 2011; Eyles and Eyles, 1989).

Sedimentology. The Gaskiers Formation is up to 300 m thick and comprises four main facies: massive diamictite, slumped diamictite, stratified diamictite, and turbidites (Carto and Eyles, 2011; Eyles and Eyles, 1989; Tindal, 2023). The formation "consists predominantly of massive and crudely-stratified diamictites" (Eyles and Eyles, 1989). Both massive and stratified diamictite facies typically have sharp, locally erosive basal contacts (Eyles and Eyles, 1989). The stratified diamictite facies comprises crudely stratified (10 cm to 40 cm layers) units that grade into the massive diamictite facies (Eyles and Eyles, 1989; Tindal, 2023). The slumped polymict diamictite facies includes sediment rafts of sandstones, siltstones, mudstones, carbonates, and diamictites that can be up to tens of metres in length (Eyles and Eyles, 1989). The sediment rafts may include striated clasts (Eyles and Eyles, 1989). The Gaskiers Formation turbidites grade up from polymict granules, consistent with reworking of a glacial source (Tindal, 2023).

The massive and stratified diamictite facies clasts include a wide range of different lithologies, are rounded to very angular, typically 3 cm to 10 cm in diameter, but reach up to 80 cm (Eyles and Eyles, 1989; Myrow and Kaufman, 1999; Tindal, 2023). Moreover, the diamictites include faceted ('bullet-shaped') and elongate clasts, clasts with multiple striated faces, and chatter-marked garnets which all indicate a glaciated source for the diamictite material (Brückner and Anderson, 1971; Carto and Eyles, 2011; Gravenor, 1980). Laminated siltstones and sandstones are interbedded with the diamictite units and have outsized clasts which appear to have been vertically emplaced (Williams and King, 1979). Clast lithologies comprise siliciclastics (mudstone, siltstone, quartzite, conglomerate), rarer carbonates, and various igneous rocks (basalt, granite, diorite, granophyre), though no metamorphic lithologies have been reported (Carto and Eyles, 2011; Eyles and Eyles, 1989).

The Gaskiers Formation is interpreted as having been deposited by submarine downslope reworking of glacially-derived sediment, consistent with the inferred depositional setting of the conformable overlying and underlying formations and the evidence for intraformational slumping in the Gaskiers Formation itself (Carto and Eyles, 2011; Eyles and Eyles, 1989; Tindal, 2023).

Age constraints. The Gaskiers Formation has been associated with a thin (15 cm to 50 cm thick) 'cap carbonate' unit with $\delta^{13}C_{carb}$ values averaging about –5 ‰ but as low as –7.6 ‰ in the *in situ* carbonates (Myrow and Kaufman, 1999). Lower $\delta^{13}C_{carb}$ values (down to –7.8 ‰) were recovered from limestone intraclasts in the upper beds of the diamictite (Myrow and Kaufman, 1999). Tindal (2023) confirmed that the 'cap carbonate' is only found in the northern part of the Avalon Peninsula, at the Kitchuses and Harbour Main sections, where the Gaskiers Formation is thinnest. The limestone clasts within the diamictite (Myrow and Kaufman, 1999) comprise slumped rafts up to 40 cm thick in which the limestone may be interbedded with siltstone or diamictite facies and only occur in the upper 1.5 m of the Gaskiers diamictite (Tindal, 2023). Tindal (2023) associates the thinning of deposits to the north as an indicator of reduced sediment supply, rather than reduced accommodation space, and uses this as a supporting argument for a sediment-starvation model (Kennedy and Christie-Blick, 2011) for carbonate deposition directly above the Gaskiers diamictites. Reduced clastic supply in northern Newfoundland is also supported by the prevalence of phosphate nodules in the 19 m of siltstones that overly the carbonate units at Kitchuses and at least 6 cm at Harbour Main (Tindal, 2023).

The depositional age of the Gaskiers Formation is tightly constrained by two radiometric dates close below and one radiometric date close above the diamicite in the St. Mary's Bay area (Pu et al., 2016):

- 580.34 ± 0.52 Ma (tuff 7.75 m below diamictite; sample GCI-7.75, Mall Bay Formation, Great Colinet Island);
- 580.90 ± 0.40 Ma (tuff 6.55 m below diamictite; sample GCI-6.55, Mall Bay Formation, Great Colinet Island);
- 579.63 ± 0.44 Ma from tuff 0.90 m above diamictite (sample NoP-0.9, Drook Formation, North Point Bay).

These radiometric constraints give a maximum depositional duration for the ~300 m thick diamictites of 1.67 Myrs, and potentially less than 1 Myr (Pu et al., 2016). Glaciogenic sedimentary deposits have not been reported from the overlying Drook Formation. A recent report has found candidate glaciogenic sedimentary deposits in the underlying Mall Bay Formation on the Colinet Islands (see 4.3.2; Fitzgerald et al., 2024).

Summary. The Gaskiers Formation is interpreted as having been deposited by submarine downslope reworking of glacially-derived sediment, consistent with the inferred depositional setting of the conformable overlying and underlying formations (Carto and Eyles, 2011; Eyles and Eyles, 1989; Tindal, 2023). The geological setting - a slope setting within which gravity flows are the predominant means of deposition for Gaskiers Formation sediments as well as for the overlying and underlying formations -substantially down-weights glaciogenicity scores for outsized clasts (lonestones and diamictites). Nevertheless, the Gaskiers Formation remains one of the most likely candidates for a mid-Ediacaran glaciogenic deposit and is considered glaciogenic here.

Radiometric constraints give a maximum depositional duration for the ~300 m thick diamictites of 1.67 Myrs and a minimum duration of <1 Myrs (Pu et al., 2016). Glaciogenic sedimentary deposits have not been reported from the overlying Drook Formation, but a recent report has found glaciogenic sedimentary deposits in the underlying Mall Bay Formation on the Colinet Islands which extends mid-Ediacaran glacial conditions on the Avalon Peninsula to much more than 1 Myr in duration (see 4.3.2; Fitzgerald et al., 2024).

Table S11. Rating of possible glacial influence on the Gaskiers Formation.

Category	Description	Rating
Outsized clasts	Outsized clasts deposited as massive and stratified diamictites in a setting with other reworked deposits.	★
	Outsized clasts that may disrupt laminae above/below in or associated with reworked deposits.	★
Clast shape	Elongate clasts are present.	★★
	Clasts are well rounded to very angular.	★
Clast surface	Clasts with striated and faceted surfaces.	★★★
Clast lithology	Clasts of three lithology classes (siliciclastic, carbonate, igneous).	★★
Summary	Strong: no realistic ice-free depositional environment is likely to produce this evidence.	★★★★

4.3.2 Mall Bay Formation (Conception Group)

The Mall Bay Formation is the lowest formation of the Conception Group on the southern Avalon Peninsula, SE Newfoundland, Canada. A recent study (Fitzgerald et al., 2024) has reported sedimentary evidence for cold (freezing) climate conditions in the upper 550 m of the Mall Bay Formation (total thickness >1000 m), directly and conformably beneath the glaciomarine Gaskiers Formation (see 4.3.1).

Sedimentology. Fitzgerald et al. (2024) reported glendonites, outsized clasts, frozen sand aggregates, and coarse sandstone lags in the upper half of the Mall Bay Formation. In particular, they suggest that the types and intensity of glacial indicators increase up through the Mall Bay Formation towards the Gaskiers Formation (Fitzgerald et al., 2024). Fitzgerald et al. (2024) identified eight distinct facies in the Mall Bay Formation. These include distal turbidites (F1: Bouma sequence $T_{d,e,f}$), volcaniclastics and tuffs (F2), massive mudstones (F3), syn-sedimentary folded (slumped) mudstone (F4), feldspar-rich turbiditic sandstones (F5–F7), and diamictite (F8). F1 includes rare granule to pebble-grade acidic to intermediate intrusive igneous outsized clasts that deform underlying laminae and are draped by overlying laminae, as well as common glendonites (Fitzgerald et al., 2024). The background sediment of F1 includes outsized clasts that occur both isolated and in clusters at discrete levels; these levels are overlain by thick units of massive mudstone (Fitzgerald et al., 2024). Convolute laminae are also present in F1, suggesting intervals of rapid deposition (Fitzgerald et al., 2024). Isolated large unweathered basaltic clasts occur in F1 and are interpreted as volcanic bombs (which have also been identified in the overlying Gaskiers Formation; see

Eyles and Eyles, 1989). There are also clast aggregates present that are composed of interlocking grains of variable size and roundness lacking obvious cement (Fitzgerald et al., 2024). The chaotic diamictite facies (F8) comprises a muddy to medium sandy matrix supporting granule to cobble-sized well-rounded to angular clasts, primarily of bimodal volcanic and intrusive igneous lithologies reflecting the underlying basement, some of which are faceted (bullet-shaped), break or deform underlying laminae, and are draped by overlying laminae, including some near-vertically emplaced elongate clasts (Fitzgerald et al., 2024).

Age constraints. The Mall Bay Formation is the lowest unit in the Conception Group and rests unconformably on the upper Harbour Main Group, which has been dated at 606.8 ± 3.7 Ma (Krogh et al., 1988). The uppermost Mall Bay Formation has been dated at 580.90 ± 0.82 Ma (sample GCI-neg6.55, 6.55 m below the top of the formation) and 580.48 ± 0.87 (sample GCI-neg7.75, 7.75 m below the top of the formation), giving a minimum age constraint of 580.90 ± 0.82 Ma for deposition of the Mall Bay Formation (Pu et al., 2016). Given that the glaciogenic deposits are all in the upper 500 m of the Mall Bay Formation, it may be assumed that the glacial interval is closer to 580 Ma than it is to 606 Ma. Matthews et al. (2021) obtained radiometric dates throughout the Conception Group, including from the upper Drook Formation and lower Briscal Formation (samples DRK-10 and DRK-1, respectively), which yielded radiometric ages of 574.17 ± 0.66 Ma and 571.38 ± 0.66 Ma. Taking 571.38 Ma as the minimum age of Drook Formation deposition (Matthews et al., 2021), and 579.88 Ma as the maximum age of Drook Formation deposition (Pu et al., 2016), with a total thickness of 770 m (Fitzgerald et al., 2024) the average sedimentation rate of the Drook Formation was 9 cm kyr^{-1}. Assuming little change in depositional setting between the Mall Bay and Drook formations and a similar sedimentation rate, the top 500 m of the Mall Bay Formation may have been deposited over ~5.5 Myr, but we note that sedimentation rate is known to vary substantially locally and regionally (Grace and Lowe, 2025; Matthews et al., 2021) and so this estimate should be treated with caution.

Summary. The upper Mall Bay Formation was deposited immediately prior to the Gaskiers Formation diamictite (~580 Ma) and above the Harbour Main Group (<606 Ma), with evidence for proximal glaciation in the upper half of the formation, assumed to be at least ~5 million years in duration.

Table S12. Rating of possible glacial influence on the Mall Bay Formation.

Category	Description	Rating
Outsized clasts	Outsized clasts that may disrupt laminae above/below in or associated with reworked deposits and volcanically-emplaced outsized clasts.	★
Clast shape	Some elongate clasts are reported.	★★
	Clasts are well rounded to angular.	★
Clast surface	Clasts with faceted surfaces are reported.	★
Clast lithology	Clasts of two lithology classes (siliciclastic, igneous).	★
Grain clusters	Uncemented clusters of outsized granules without specific evidence of current flow for their deposition (surrounding sediment shows signs of current-related deposition).	★★
Glendonites	Glendonites present in the background mudstones.	–
Summary	Strong: no realistic ice-free depositional environment is likely to produce this evidence.	★★★★

4.3.3 Trinity diamictite (Rocky Harbour Group)

The Trinity diamictite, or Trinity facies, of the Rocky Harbour Group, crops out in the Trinity area on the Bonavista Peninsula, northeast Newfoundland, Canada, where it ranges from ~15 m thick in the south to >100 m in the north (Normore, 2011). The spatial distribution of candidate glaciogenic deposits on the Bonavista Peninsula have been poorly understood, even as the evidence for glaciogenicity has been well developed across different outcrops. Recent work has now better illuminated the spatial, stratigraphic, and temporal distributions of candidate glaciogenic deposits in the Bonavista Peninsula, allowing the previous lumping under the heading of 'Trinity diamictite' (e.g. Tindal, 2023; Wong Hearing et al., 2026) to be better elaborated upon here (following Gómez et al., 2025b, a, 2026; Mills et al., 2024).

Sedimentology. The Trinity facies comprises a green or purple poorly sorted internally laminated and sometimes massive siltstone or sandstone matrix-supported diamictite with well-rounded pebbles and cobbles, and rarer angular boulders, some of which are striated, faceted (flat-iron and bullet-shaped), and deflect or penetrate underlying laminae and are draped by overlying laminae (Mills et al., 2024; Normore, 2011; Pu et al., 2016). The outsized clasts exhibit mostly mafic and felsic igneous lithologies, commonly with feldspar phenocrysts, similar to those of the older Bull Arm Formation (Mills et al., 2024; Pu et al., 2016), but other lithologies certainly occur in this unit with Tindal (2023) noting three lithology classes. As well as outsized clasts, there are wispy lenses of coarse sandstone, which have been interpreted as ice-rafted debris (Pu et al., 2016). South of New Bonaventure, the basal Trinity facies includes bi-directional cross-bedded sandstones with lenses of pebble-rich sediment, which have been interpreted as an iceberg dump structure (Normore, 2011). The unit broadly thickens from south (~15 m) to north (>100 m), and the matrix grain size decreases from south to north (Normore, 2011).

The Trinity facies is interpreted as a Gaskiers Formation-correlative glaciomarine or glaciolacustrine deposit formed by rapid progradation northwards, in part informed by the apparent variety of lower and upper contacting units (Normore, 2011). The lower contact of the Trinity facies is at least locally abrupt (Pu et al., 2016). The upper contact of the Trinity facies is typically transitional into parallel laminated siltstones, with a decreasing outsized clast content (Normore, 2011).

The sedimentary deposits surrounding the Trinity facies are known as the Monk Bay, Cape Bonavista, Kings Cove Lighthouse, Herring Cove, and Kings Cove North facies (Normore, 2011; Pu et al., 2016). These units include conglomerates, sandstones, siltstones, mudstones, and tuffs, with the finer sediments sometimes laminated and many of the deposits showing evidence of reworking in both shallow water and deeper water downslope settings (Normore, 2011). The strata immediately underlying the Trinity facies are interpreted as recording multiple glacial advances and retreats over a shallow marine shelf resulting in well-developed parasequences (Gómez et al., 2024, 2025b, a; Mills et al., 2024).

Age constraints. The Trinity diamictite is one of the best constrained candidate Ediacaran glaciogenic deposits (Tindal, 2023). The unit is constrained by stratigraphically congruent zircon U-Pb CA-ID-TIMS dates from samples below (B1552; tuff bed;

579.63 ± 0.15 Ma), within (OBJP-03; detrital zircon, diamictite matrix; 579.35 ± 0.33 Ma), and above (OBJP-01; tuff bed; 579.24 ± 0.17 Ma) the diamictite (Pu et al., 2016).

Summary. The Trinity diamictite is well-constrained as a regional correlative of the Gaskiers Formation diamictite, deposited at ~579 Ma (Pu et al., 2016). There is good evidence for a glaciogenic origin for the Trinity diamictite, with a thick and intricate diamictite containing glacially worked clasts, as well as evidence for multiple phases of ice expansion and contraction within specific sections (Gómez et al., 2024, 2025a, b; Mills et al., 2024; Pu et al., 2016).

Table S13. Rating of possible glacial influence on the Trinity diamictite (Rocky Harbour Group).

Category	Description	Rating
Outsized clasts	Outsized clasts that disrupt laminae deposited as a massive or stratified diamictite in a flat or distal setting not on or near the base of a slope.	★★★
Clast shape	Clasts are well rounded to angular.	★
Clast surface	Clasts with striated and faceted surfaces (flat-iron and bullet-shaped).	★★★
Clast lithology	Clasts of three lithology classes are reported.	★★
Grain clusters	Uncemented clusters of outsized granules without specific evidence of current flow for their deposition (though surrounding sediment does show signs of current-related deposition).	★★
Summary	Strong: no realistic ice-free depositional environment is likely to produce this evidence.	★★★★

4.3.4 Mercantile diamictite (Rocky Harbour Group)

The Mercantile diamictite is now known to be stratigraphically below the Trinity facies in the lower Rocky Harbour Group and crops out across the northern Bonavista Peninsula, northeast Newfoundland, Canada, where it can be up to 50 m thick (Gómez et al., 2026). Recently published mapping and radiometric dating work allow the Mercantile diamictite to be included in this compilation as a distinct unit.

Sedimentology. The Mercantile diamictite is lithologically similar to the Trinity diamictite and is well documented by Gómez et al. (2026). The stratigraphically adjacent Jones Pond Member and lower Plate Cove East Member are interpreted as glaciofluvial facies associations (Gómez et al., 2026). The Mercantile diamictite comprises clast-rich and clast-poor diamictites as well as minor stratified conglomerates, sandstones, and laminites bearing outsized clasts (Gómez et al., 2026). The basal contact of the Mercantile diamictite is typically sharp and in places scoured up to 1.5 m with ripped up clasts and sand wedges as well as internal faulting of the underlying and overlying deposits (Gómez et al., 2026). The Mercantile diamictite comprises matrix-supported diamictites of varying clast density, with rounded to angular (including elongate) clasts commonly facetted (flat-iron, bullet, rhombic, and triangular shapes) with microstructures including flutes and pits, and rarely striated (Gómez et al., 2026). Outsized clasts have been identified which satisfy criteria for being interpreted as dropstones: clast size independent

of bed thickness, long axes orientated vertically locally, strata below are curved and deformed, strata above draping and bulging over the outsized clasts (Gómez et al., 2026). Clusters of clasts are also reported (Gómez et al., 2026). Diamictite clasts are predominantly red felsic tuffs, with additional rhyolite, basaltic, andesitic, mudstone, sandstone, chert, and quartzite components (Gómez et al., 2026). Glendonites are also present in strata close below and above the main diamictites deposits (Gómez et al., 2026).

The Mercantile diamictite is interpreted as a glaciomarine or glaciolacustrine deposit formed before the nearby Trinity diamictite and the Gaskiers Formation further south (Gómez et al., 2026). Parasequences are developed in strata between the Trinity and Mercantile diamictites, indicating fluctuations in glacial conditions and likely glacial-interglacial cyclicity (Gómez et al., 2026).

Age constraints. The Mercantile diamictite is stratigraphically constrained as being below the well-dated Trinity diamictite (older than 579.63 ± 0.15 Ma) (Pu et al., 2016). The Mercantile diamictite is also constrained to below a tuff in the Monk Bay Member with a zircon U-Pb CA-ID-TIMS date of 584.6 ± 3.6 Ma (Gómez et al., 2025a, b; Mills et al., 2024). Detrital zircons within and stratigraphically adjacent to the Mercantile diamictite indicate a maximum depositional age of ~589 ± 2 Ma (Gómez et al., 2025a). Zircon U-Pb CA-ID-TIMS dates from tuffs in the underlying Plate Cove Formation (which lacks evidence of glacial influence) provide a further maximum depositional age constraint of 591.3 ± 1.3 Ma (Gómez et al., 2025a; Mills et al., 2017, 2024).

Summary. The Mercantile diamictite is well-constrained as a regional correlative of the Gaskiers and Mall Bay glaciogenic deposits, with a likely depositional age between 589 to 584 Ma. There is good evidence for a glaciogenic origin for the Mercantile diamictite, as well as the surrounding Monk Bay Member deposits and overlying Trinity diamictite. Taken together, the lower Rocky Harbour Group deposits record multiple expansions and retreats of ice sheets from ~589 to ~579 Ma.

Table S14. Rating of possible glacial influence on the Mercantile diamictite (Rocky Harbour Group).

Category	Description	Rating
Outsized clasts	Outsized clasts that disrupt laminae deposited as a massive or stratified diamictite in a flat or distal setting not on or near the base of a slope.	★★★
Clast shape	Clasts are well rounded to angular.	★
Clast surface	Clasts with striated and faceted surfaces (flat-iron and bullet-shaped).	★★★
Clast lithology	Clasts of two lithology classes are reported.	★
Grain clusters	Uncemented clusters of outsized granules without specific evidence of current flow for their deposition (though surrounding sediment does show signs of current-related deposition).	★★
Summary	Strong: no realistic ice-free depositional environment is likely to produce this evidence.	★★★★

4.3.5 Gwna Group

Also known as the Llanddwyn Island Conglomerate. Outsized clasts have been reported from the possibly Ediacaran-age mafic mudstones of the Llanddwyn Island Conglomerate, Llanddwyn Island Volcanic Member, Bodorgan Formation, Gwna Group, Ynys Llanddwyn, southwest Anglesey, Wales, United Kingdom (Kawai et al., 2008). The Llanddwyn Island Conglomerate outcrop is fault-bounded and small, perhaps as little as 20 m^2 and 1.5 m thick (Tindal, 2023). Because it is fault-bounded, the precise stratigraphic placement of the Llanddwyn Island Conglomerate within the Llanddwyn Island Volcanic Member is uncertain.

Sedimentology. The Bodorgan Formation consists of crudely bedded conglomerates with a muddy to sandy matrix hosting quartzite, arkose, metamorphosed carbonate, and metamorphosed basic igneous clasts (Dartnall, 2019; Schofield et al., 2021; Tindal, 2023). The Llanddwyn Island Volcanic Member comprises metabasite, after massive brecciated pillow basalts (hyaloclastites), and includes minor components of limestone, mudstone, and sandstone (Dartnall, 2019; Schofield et al., 2021; Tindal, 2023).

The muddy matrix informed Kawai et al.'s (2008) interpretation of a distal marine setting into which sandstone clasts had somehow been introduced, with bent laminae in these mudrocks interpreted as evidence for vertical emplacement of the clasts. Those authors concluded that iceberg dropstones were the most plausible interpretation for the vertically emplaced clasts. Kawai et al. (2008) considered the Llanddwyn Island Conglomerate to be a clast-bearing variant of a ‘mafic mudstone’. Tindal (2023) visited and redescribed two sections where this ‘mafic mudstone’ had been described. The first location is characterized by thinly bedded red and pale green mudstones, whereas the second location is characterized by apparently conglomeratic deposits (Tindal, 2023). At Location 2, Tindal (2023) found the ‘mafic mudstone’ of Kawai et al. (2008) which comprises a matrix of black mudstone with coarse quartz grains and discontinuous lenses of red silicified mudstone, up to 5cm by 10 cm, and white sandstone, up to 15 cm by 50 cm or larger (their fig. 6f). The red silicified mudstone is similar to the mudstone from Location 1, which is a possible source for these clasts. Tindal (2023) inferred a potential tectonic origin for this unit, interpreting the flattened and elongated clasts as possible boudinaged sandstone and mudstone beds of variable original thickness, supported by evidence of tectonically-fused grains and the local fault with which the clasts are aligned.

Also at Location 2 is the Llanddwyn Island Conglomerate which is a matrix-supported (70 % matrix) conglomerate of rounded to well-rounded clasts of red or pale green sandstone and basalt, typically 1 to 5 cm diameter, occasionally up to 15 cm diameter, orientated parallel to cleavage (Tindal, 2023). Note that Kawai et al. (2008) reported large chert pebbles but Tindal (2023) was unable to find any. Wavy, discontinuous, and bifurcating white crystalline veins that pervade the matrix are bent around clasts and concentrated between large clasts, with some veins cutting through clasts (Tindal, 2023). Tindal (2023) inferred that these are the “bent laminae” of Kawai et al. (2008), with the bent veins wrapping equally above and below clasts in a manner that is compatible with tectonic warping but incompatible with the warping and draping of laminae below and above a dropstone.

The Bodorgan Formation is interpreted as submarine volcanic and downslope mass flow deposits of which the conglomerates are one component (Dartnall, 2019; Schofield et al., 2021). The Llanddwyn Island Conglomerate is interpreted as one of several downslope-deposited conglomerates in the Bodorgan Formation, but one which incorporated contemporaneous pillow basalts (Schofield et al., 2021; Tindal, 2023). However, Tindal (2023) makes the cautionary observation that metamorphism and deformation has obliterated most original evidence of the depositional environment of the Llanddwyn Island Conglomerate, so any genetic interpretation can only be tentative.

Age constraints. The Gwna Group is poorly constrained in age. The upper and lower boundaries are faulted contacts and until recently there were no radiometric or other age constraints from the Gwna Group itself, and age interpretations relied on the dates of regional metamorphic events (Kawai et al., 2008). The older age interpretations suggested a possible Gaskiers-correlative depositional age (Kawai et al., 2008), but these are based mostly on older Rb-Sr whole-rock ages. Recent U-Pb detrital zircon dating suggests that the Llanddwyn Island Volcanic Member has a maximum depositional age of 550 ± 24 Ma (Asanuma et al., 2017), and regional litho- and tectonostratigraphy has been used to infer a late Cambrian depositional age (Schofield et al., 2021), though this remains uncertain.

Summary. An Ediacaran age for the Gwna Group Llanddwyn Island Conglomerate is possible, but perhaps not likely (Schofield et al., 2021). Currently, the age of the Llanddwyn Island Conglomerate is best described as "uncertain".

The glaciogenicity of the unit is also uncertain, given the degree of post-depositional alteration. However, there is no good evidence for it being glaciogenic (Dartnall, 2019; Schofield et al., 2021; Tindal, 2023). Rather, a downslope mass flow origin is preferred, with a glaciogenic source for the clasts and matrix unnecessary to explain the deposit. Warped laminae reported beneath dropped stones (Kawai et al., 2008) are in fact deformed diagenetic or metamorphic mineral veins (Tindal, 2023), though post-depositional alteration also makes it impossible to rule out that the clasts did disrupt primary laminae that have since been obliterated (Tindal, 2023). The conglomerate is one of several such deposits in the Bodorgan Formation, and is primarily distinguished from those other coarse siliciclastic units by its association with contemporaneous hyaloclastic basalt (Schofield et al., 2021; Tindal, 2023).

Table S15. Rating of possible glacial influence on the Gwna Group Llanddwyn Island Conglomerate.

Category	Description	Rating
Outsized clasts	Outsized clasts that may disrupt laminae above/below in or associated with reworked deposits and volcanically-emplaced outsized clasts.	★
Clast lithology	Clasts of two lithology classes (siliciclastic, igneous).	★
Summary	Weak: some ice-free depositional environments could produce this evidence.	★★

4.3.6 Squantum Member (Roxbury Conglomerate Formation)

The Squantum Member (Roxbury Conglomerate Formation) crops out in the Boston Basin, northeast USA, and was deposited on the Avalonian portion of Gondwana in the late Neoproterozoic. The Boston Basin represents a back-arc basin setting within the Avalon Terrane, the modern extent of which is strongly demarcated by faults (Carto and Eyles, 2012). The Ediacaran stratigraphy in the Boston Basin is organized into the Boston Bay Group, which comprises two formations: the lower Roxbury Conglomerate, and upper Cambridge Argillite.

Sedimentology. The Roxbury Conglomerate is divided into three members. The lower Brookline Member is predominantly composed of conglomerates, the middle Dorchester Member is primarily fine-grained (argillaceous) turbidites with minor conglomerates, and the upper Squantum Member is mostly diamictite facies interbedded with sandstones and siltstones (Carto and Eyles, 2012). The Cambridge Argillite comprises approximately 5.5 km of tuff-rich finely laminated to thinly bedded fine-grained (argillaceous) turbidites (Carto and Eyles, 2012). Across the Roxbury Conglomerate, three primary and conformably associated facies are recognized: (1) conglomerate and sandstone, (2) diamictite, and (3) mudrock (Carto and Eyles, 2012).

The conglomeratic and sandstone facies (1) are common in the Brookline Member, which can be up to approximately 1.3 km thick (Tierney et al., 1968) and comprise massive clast- and matrix-supported conglomerates with erosive bases that grade up to normally graded sandstones (Carto and Eyles, 2012). The conglomerate clasts are pebble- to boulder-sized, moderately to well sorted, subrounded to rounded, and are predominantly of lithologies found within the Boston Basin, including rhyolites, dacites, basalts, diorites, and granites (Carto and Eyles, 2012). The sandstones which grade out of the conglomerates are mostly massive but some develop low-angle cross-lamination, whilst laminated normally graded sandstones also occur and may have soft sediment deformation structures including convolute laminae and 'dish-and-pillar' structures (Carto and Eyles, 2012). The conglomerate and sandstone facies are often interbedded with diamictites and thick mudrocks (Carto and Eyles, 2012). The conglomerate and sandstone facies is interpreted as the result of rapid deposition from cohesionless gravelly debris flows representing T_a (conglomerate) to T_{b-c} (sandstone) division of the Bouma sequence (Bouma, 1962), with a likely fluvial origin of the clasts (Carto and Eyles, 2012). Rapid deposition is supported by the soft sediment deformation structures observed in the sandstone bodies (Carto and Eyles, 2012).

The diamictite facies (2), typically associated with the upper Squantum Member, comprises massive or chaotic matrix-supported polymict diamictites with pebble- to boulder-sized, moderately to well sorted subrounded to angular clasts of predominantly local lithologies (felsic and mafic volcanics, granodiorite, quartzite, siltstone, and sandstone), similar to the clasts of the conglomerate facies (Carto and Eyles, 2012). The diamictites vary from ~8 m thick in outcrop to 215 m in the subsurface (Carto and Eyles, 2012; Tierney et al., 1968). The diamictite facies is typified by sharp, erosive basal contacts and transitional upper boundaries as the diamictites grade into sandstones or conglomerates (Carto and Eyles, 2012). The chaotic diamictites can show crude stratification with large rafts of conglomerate, sandstone, and mudrock poorly mixed through the diamictite (Carto and Eyles, 2012). Faceted clasts have not been found, and striated clasts identified by earlier workers (Sayles,

1914) were not found by subsequent investigators (Carto and Eyles, 2012). Carto and Eyles (2012) noted that the distinction between the Roxbury Conglomerate diamictite and conglomerate facies is the proportion of matrix (conglomerates: 10 vol.% to 30 vol.%; diamictites: 80 vol.%) with other characteristics, particularly clast composition and form, being remarkably similar – a similarity noted by previous workers who were also sceptical of a glaciogenic origin (Dott, 1961; Socci and Smith, 1990). The diamictite facies is interpreted as the result of early-stage downslope mixing of conglomeratic and muddy material deriving from primary fan or slope-deposited conglomerates, an interpretation that is supported by the conformable, interbedded, relationship between the diamictite facies with coarse- and fine-grained turbidites (Carto and Eyles, 2012).

The argillite facies (3) refers to "rhythmically laminated (0.1 to 1 mm thick) muddy-siltstones that grade subtly into mudstone" (Carto and Eyles, 2012). The argillite facies is typical of the Cambridge Argillite but is interbedded with both the conglomerate and diamictite facies throughout the Boston Bay Group on scales of centimetres to hundreds of metres thickness (Carto and Eyles, 2012). Sedimentary structures include parallel to wavy laminations, cross-lamination, and both large- and small-scale slump folds which occur throughout the unit in argillite, interbedded with conglomerate and diamictite facies as well as with discrete tuff horizons (Carto and Eyles, 2012). The argillite facies has been consistently interpreted as reflecting deep marine (below storm wave base) low-density turbidite deposits (Carto and Eyles, 2012; Dott, 1961; Thompson and Bowring, 2000).

A fourth facies, or perhaps a sub-facies of the argillite facies, is also considered: the pebbly argillite (Carto and Eyles, 2012). Stratigraphically and geographically limited to approximately 0.5 m in total thickness, directly underlying diamictites at Squantum Head, is a laminated argillite with matrix-supported pebbles (approximately 75 vol.% matrix) that is interbedded with non-pebbly laminated and graded argillites (Carto and Eyles, 2012). The clasts are all small, typically gravel-size or smaller, rounded to subrounded, and composed of the same local lithologies as the conglomerate and diamictite facies (Carto and Eyles, 2012). The pebbly layers form couplets with overlying thin laminae of massive pebble-free argillite (Carto and Eyles, 2012). The 'diamictite-argillite couplets' have been interpreted as ice-rafted debris or dropstones – and this remains possible – but an interpretation as debrite-turbidite couplets where finer material is sheared off the top of a dilute debris flow as it transitions to a turbidity current and settles out onto the deposited debrite is more parsimonious with the surrounding facies (Carto and Eyles, 2012). Important to this non-glaciogenic interpretation is the apparent absence of any larger (cobble- or boulder-sized) clasts from the pebbly argillite (Carto and Eyles, 2012). The pebbly argillite is interpreted as a slightly more distal equivalent of the diamictite facies, representing part of a debris flow that ran away from or further than the main flow, resulting in a more dilute flow (Carto and Eyles, 2012).

The weight of evidence reviewed by Carto and Eyles (2012) argues against a primary glaciogenic origin for the 'Squantum Tillite'. However, it does fulfil several criteria for consideration as having some glacial influence. Tindal (2023) considered the Squantum Member a four-star unit with "possible varves, and diamictite and lonestones with angular to subrounded clasts from four lithological groups, some of which are striated". On balance, the most parsimonious interpretation for the deposition of the Squantum Member is as a continuation of downslope remobilization of fan or slope deposits of sandstone, mudstone, and conglomerate. The conglomerates may have an originally glaciogenic origin, but that is not certain and could equally, or perhaps more plausibly given the absence of strongly faceted or striated clasts, derive from a fluvial setting.

Age constraints. Volcanic samples taken for palaeomagnetic study from the Lynn-Mattapan volcanic complex of northern Massachusetts provide maximum age constraints for the Roxbury Group and the Squantum Member (Thompson et al., 2007). Sample MT95-1 (Saugus) rhyolite porphyry from site BOS 18 yielded a weighted mean U-Pb age of 595.8 ± 1.2 Ma (Thompson et al., 2007). Sample MT01-28 (Newton) rhyolite porphyry from site BOS 3B yielded a weighted mean U-Pb age of 597.4 ± 1.5 Ma (Thompson et al., 2007). Sample MT-KK10 (Needham) rhyolitic ash-flow tuff from site BOS 10A yielded a weighted mean U-Pb age of 596.0 ± 1.4 Ma (Thompson et al., 2007). Sample WE7-1A (Hingham) dacitic ash from site BOS 15 yielded a weighted mean U-Pb age of 595.7 ± 1.6 Ma (Thompson et al., 2007). The Squantum Member is therefore younger than 595.8 ± 1.2 Ma. This age agrees with Thompson and Bowring's (2000) earlier study on detrital zircons and tuff clasts within the Squantum Member and Cambridge Argillite. Thompson and Bowring (2000) recovered ages of 593 ± 3 Ma (sample MT99-4; Pb-Pb age of detrital zircons in sandstone), 600 ± 1 Ma (sample AW94-3; Pb-Pb age of crystal-poor tuff clast), 610 ± 2 Ma (sample AW94-4; Pb-Pb age of porphyritic granophyre clast), and 595.5 ± 2.0 Ma (sample MT96-6; Pb-Pb age of welded tuff clast) from the Squantum Member. Thompson and Bowring (2000) recovered ages of 565 ± 5 Ma (sample 198-14; Pb-Pb age of detrital zircons in argillite) and ~568 Ma (sample MT94-2; Pb-Pb age of youngest concordant zircon in ash bed). Older ages of zircons in both the Squantum Member and Cambridge Argillite demonstrate the presence of xenocrysts (in the ash bed) and long-lasting detrital zircons in the Boston Basin. Thompson and Bowring (2000) consider 595.5 ± 2.0 Ma as the maximum age for deposition of the Squantum Member, and that it must have been deposited before approximately 570 Ma, following the Cambridge Argillite ash bed age.

Summary. The Squantum Member was likely deposited between 595 Ma and 570 Ma, potentially correlating with Gaskiers-equivalent glaciogenic deposits regionally and globally, though there remains a substantial uncertainty regarding its depositional age.

Table S16. Rating of possible glacial influence on the Squantum Member (Roxbury Conglomerate). Absence of evidence is noted in this table as the Squantum Member has received a lot of attention and was previously given a higher four-star/strong rating (Tindal, 2023; Wong Hearing et al., 2026).

Category	Description	Rating
Outsized clasts	Outsized clasts that may disrupt laminae above/below in or associated with reworked deposits (pebbly argillite facies).	★
	Outsized clasts deposited as a massive or stratified diamictite in a setting with other reworked deposits.	★
Clast shape	No reported elongate clasts. Clast shape ranges from sub-rounded to sub-angular, occupying only three roundness classes.	–
Clast surface	No faceted clasts. Striated clasts reported by early workers have not been documented since, despite extensive further study of the deposit.	–
Clast lithology	Clasts of local lithologies, similar in composition to the conglomerate facies, from two lithology classes: igneous – felsic and mafic volcanics, and granodiorite – and sedimentary – sandstone, siltstone, and quartzite.	★
Summary	Weak: Some ice-free depositional environments could produce this evidence.	★★

4.4 Baltica

4.4.1 Glussk Formation, Vilchitsy (=Vilchanka) Group (Ukraine, Belarus, Poland)

Sedimentology. Tindal (2023) classed glaciogenic strata in the Blon and Glussk formations (Vilchitsy Group or Vilchitsy Series) as three- and four-star glaciogenic deposits, respectively, and gave these deposits a very broad plausible age range. The Glussk Formation is referred to as the Vlichitsy Formation, overlying the Blon Formation, in Chumakov (1981). The Blon Formation is widely regarded as Cryogenian in age and is not considered here.

The Vilchitsy Group comprises hundreds of metres of siliciclastic stratigraphy including diamictites, sandstones, siltstones, and claystones (Paszkowski et al., 2018). The Ukrainian equivalent of the Vilchitsy Series is the Brody Suite, which is an order of magnitude thinner than the Vilchitsy Group in Poland and Belarus, and comprises claystones and siltstones with irregularly distributed pebbles (Paszkowski et al., 2018).

The Glussk Formation comprises three major diamictite beds separated by sandstones and laminated claystones and siltstones with outsized clasts (Chumakov, 1981, 2004). The laminated claystones and siltstones are interpreted as lacustrine varves with dropstones, and the alternation of diamictites and varved sediments is interpreted as evidence of repeated glacial advance and retreat (Chumakov, 2004). The diamictites are matrix-supported, with a clay-sized matrix with clasts typically 3 % to 8 % of rock volume, though rarely reach up to 15 %, irregularly distributed throughout the diamictite and sometimes occurring in clusters, and ranging from coarse sand to boulder size (<70 cm), typically in the pebble to cobble size range, and ranging from well-rounded to very angular, with most clasts being subangular (Chumakov, 1981). The clasts comprise orange quartzites to sandstones, granites, gneisses, and rarer quartz, quartzite, schist, dolomite, feldspar, diorite, and amphibolite pebble-sized clasts, alongside cobbles to boulders that are dominated by the orange quartzites to sandstones, granites, and gneisses (Chumakov, 1981). Some clasts have flat faceted surfaces with thin to coarse striations, which may occur as single or subparallel striae (Chumakov, 1981). The non-quartzite or sandstone clasts are thought to derive from beyond the depositional basin (Chumakov, 1981).

Age constraints. The Blon Formation, is likely to be Cryogenian in age, but the Glussk Formation, which unconformably overlies the Blon Formation and is unconformably overlain by the Volyn Group, is more challenging to date. Chumakov (2004) ascribes the Blon Formation to a Cryogenian glaciation, with the intervening hiatus equating to either the mid-Cryogenian warmer interval, or the early Ediacaran interval between the Marinoan and Gaskiers glaciations, as well as drawing a clear distinction between the Vilchitsy glacial strata and the late Ediacaran (North African and Baykonur) glaciations. Chumakov (2004) further discusses the similarity of the three major diamictite units separated by varved claystones and siltstones with dropstones to other units that are now recognized as terminal Cryogenian (e.g. the Nantuo, Fiq, and Blaini formations).

Francovschi et al. (2023) ascribe the Blon Suite to the terminal Cryogenian Marinoan glaciation, and correlate the Glussk Suite with the Brody Suite (Ukraine) and the Zukov Suite (Bialystok Group, Poland) together as possible correlatives of the Gaskiers Formation. Shumlyanskyy et al. (2016) provided minimum age constraints on the Brody Suite with radiometric dates of 571

± 13 Ma and 573 ± 14 Ma from igneous zircons in the unconformably overlying Volyn Group. This minimum age constraint is supported by higher precision radiometric dates from the middle Volyn Group of 569.40 ± 0.12 from a sample in Belarus (sample KOB-25, Rataychitsy Formation; Środoń et al., 2023). The Glussk Formation and its local correlatives are therefore reliably older than 570 Ma. However, there is substantial stratigraphic uncertainty around their true depositional age, which could be anything from Cryogenian to >570 Ma.

Summary. The Glussk Formation and correlative strata are reasonably interpreted as glaciogenic on the basis of published descriptions and are plausibly of mid-Ediacaran age (>570 Ma). However, they could be as old as Cryogenian, and Chumakov (2004) discussed the stratigraphic similarity of the Glussk Formation with several deposits now thought to have been deposited during the Marinoan glaciation.

Table S17. Rating of possible glacial influence on the Glussk Formation.

Category	Description	Rating
Outsized clasts	Outsized clasts deposited as massive and stratified diamictites in a setting with other reworked deposits (sandstones interpreted as fluvial).	★
	Outsized clasts that disrupt laminae above/below in a flat or distal setting (varved claystones and siltstones) not on or near the base of a slope.	★★★
Clast shape	Clasts of all grades of roundness are present.	★
Clast surface	Clasts with striated and faceted surfaces (with subparallel aligned striations).	★★★
Clast lithology	Clasts of four lithology classes (siliciclastic, carbonate, igneous, metamorphic).	★★★
Summary	Strong: no realistic ice-free depositional environment is likely to produce this evidence.	★★★★

4.4.2 Tany, Koyva (=Koiva), and Starye Pechi formations (Serebryanka and Sylvitsa groups)

The Serebryanka and Sylvitsa groups in the Central Urals, Russia (Baltica) include three formations which may be glaciogenic (e.g. Chumakov, 2011; Maslov et al., 2013). Stratigraphically, the Tany Formation is the lowest member of the Serebryanka Group and rests unconformably on likely Cryogenian-age (though poorly dated) siliciclastic and volcaniclastic deposits. The Koyva (=Koiva) Formation occurs in the middle of the Serebryanka Group and includes diamictites, volcaniclastics, and possible dropstones. The Starye Pechi Formation is the basal unit of the Sylvitsa Group, variably conformable and unconformable on the upper Serebryanka Group (Chumakov, 2011).

Sedimentology. The Tany Formation is up to 800 m thick and comprises two diamictite members separated by a sandstone and shale member, all of variable internal thickness (Chumakov, 2011). In the Lower Member, diamictites alternate with schists, limestones and dolomites, slump breccias, and mafic volcanic rocks, the lower pillow basalts of which have yielded a radiometric date (Chumakov, 2011; Maslov et al., 2013). The Lower Member diamictite matrix is dark grey and hosts clasts of quartz sandstone, felsic igneous rock (up to 45 %), gneiss, and carbonate, which can be up to 3.5 m diameter and may occur

as clusters of clasts (Chumakov, 2011). Rare shale beds include outsized clasts as well (Chumakov, 2011). In places, there is a dolostone bed at the top of the Lower Member (Chumakov, 2011). The Middle Member comprises quartz-feldspar sandstone beds (Chumakov, 2011). The Upper Member comprises massive and stratified diamictites interbedded with laminated shales hosting outsized clasts, and has a sharp but conformable transition into the overlying Garevka Formation, which consists of interbedded shales and sandstones (Chumakov, 2011).

The Koyva Formation composition is regionally variable (250 m to 600 m thick), and predominantly consists of laminated claystones, siltstones, clay-silt shales, limestones, and dolomites, with either conglomerates (Maslov et al., 2013) and/or diamictites present north of the Sylvitsa River but none to the south (Chumakov, 2011). Where present, the diamictites or conglomerates occur in the upper part of the formation and are interbedded with shales which may, but do not all, have outsized clasts, as well as alkali basalt flows in the northern outcrops (Chumakov, 2011; Maslov et al., 2013). Rhythmically laminated shales are described from throughout the formation which, in the uppermost part of the formation, may have small outsized clasts and dolomite interbeds (Chumakov, 2011; Maslov et al., 2013).

The Starye Pechi Formation is up to 500 m thick and predominantly comprises thinly bedded yellow-green grey siltstones and mudstones, with massive and stratified diamictites interbedded with sandstones and shales with outsized clasts in its lower part (Chumakov, 2011; Maslov et al., 2013). The diamictite matrix is a dark grey sandy siltstone which hosts clasts of unreported roundness but which "vary in size and shape", including some striated and grooved, and predominantly comprise lithologies of the underlying strata alongside some quartz, quartzite, and plagioclase-rich granites (Chumakov, 2011), however Ipat'eva *in* Maslov et al. (2013) pointed out that these clasts are rare. The upper part of the Starye Pechi Formation includes carbonate olistoliths (Chumakov et al., 2013).

Chumakov et al. (2013) interprets some of the dolostones associated with the diamictites, and other lithologies, in the Tany and Koyva formations to be cap carbonates, related to the end of glaciation in the terminal Ediacaran. However, the precise stratigraphic relationships of various lithologies, including the carbonates supposedly overlying the diamictites, within the Koyva Formation are not clear since the original stratigraphy has been disrupted by syn-sedimentary slumping and much later faulting (e.g. Chumakov et al., 2013).

Alongside diamictites, these Middle Urals successions include conglomerates, carbonate breccias, turbidites, flysch, and slumps (Chumakov, 2011; Chumakov et al., 2013; Maslov et al., 2013), all consistent with deposition on the outer shelf and continental slope (Chumakov, 2011). Furthermore, the upper Starye Pechi Formation, as well as the underlying Kernos and Buton formations, include carbonate olistoliths (Chumakov et al., 2013), which are also indicative of gravity-driven deposition on a slope. Such evidence for major downslope deposition calls into question the glaciogenic interpretation of the Tany, Koyva, and Starye Pechi diamictites, which were apparently deposited in a regime of substantial gravitationally-driven mass movement.

Age constraints. Grazhdankin et al. (2011) provided a minimum depositional age of 567.2 ± 3.9 Ma for the Starye Pechi Formation, and therefore also for the underlying Koyva and Tany formations, from tuff bed zircons in the overlying Perevalok

Formation. The Serebryanka and Sylvitsa groups underlie the White Sea assemblage Ediacaran macrofossils of the East European Platform (Grazhdankin et al., 2011), which also indicates deposition before ~557 Ma (Yang et al., 2021).

The minimum depositional age may also tentatively be constrained by carbon isotope stratigraphy, as the uppermost Serebryanka Group (Buton and Kernos formations) and the lowermost Sylvitsa Group (Starye Pechi Formation) have yielded extreme negative (typically –10 ‰ to –15 ‰) carbon isotope values from olistoliths (Chumakov et al., 2013). In particular, very negative carbon isotope values (at least –12 to –14 ‰) have been recovered from the upper Starye Pechi Formation, above the diamictite at the base, and similarly negative values were also recovered from the Kernos and Buton formations, uppermost Serebryanka Group (Chumakov et al., 2013). All of these very negative carbon isotope values are in the range of Shuram excursion values (e.g. Yang et al., 2021). No similarly negative carbon isotope values have been recovered below the Buton Formation, though the upper Koyva Formation carbonates record negative values as low as –9.3 ‰ (mean ± standard deviation: –5.4 ± 1.8 ‰), more typical of the post-Gaskiers excursion.

The maximum depositional age of all three formations is constrained by a zircon date of 598.1 ± 6.0 Ma from pillow basalts at the base of the Tany Formation, underlying all of the potentially glaciogenic strata (Maslov et al., 2013).

Combined, these radiometric constraints indicate that potentially glacial deposition began sometime after 598 Ma and ceased before 567 Ma, before the end of the Shuram isotope excursion. There is tentative evidence for the Shuram isotope excursion above the Koyva Formation, possibly though not certainly spanning the Starye Pechi Formation. Further chemostratigraphic data are needed to properly interpret the depositional age of these rocks, but it is probably that the Tany and Koyva formations were deposited before 575 Ma, and that the lower Starye Pechi Formation was deposited between 575 to 566 Ma.

Summary. The Tany and Koyva formations were most likely deposited between 598 Ma and 575 Ma, making them plausible correlatives of the Gaskiers icehouse. It is possible that the Starye Pechi Formation was also deposited during this interval, but it is also possible that it was deposited after this interval and sometime before 567 Ma (i.e. during the Shuram excursion). Additional radiometric or chemostratigraphic age constraints are required to resolve this question.

The glaciogenicity of all three deposits is questionable. Although all three represent 3-star deposits, there is strong evidence for contemporaneous gravity-driven deposition for the non-diamictite strata in all cases. It is possible that all or some of the diamictites were also the result of gravitational rather than glacial processes, as the features that strongly indicate glaciogenicity are rare at least in the Starye Pechi Formation (Ipat'eva *in* Maslov et al., 2013). The case for glaciogenicity of the Starye Pechi Formation is further questioned because the diamictites are interbedded with massive sandstones and there are substantial olistoliths in both the underlying (Buton and Kernos formations) and overlying (upper Starye Pechi Formation) strata, all indicative of an environment of significant mass transport.

In summary, whilst it is plausible that the Tany, Koyva, and Starye Pechi formations include glaciogenic diamictites deposited between 598 to 567 Ma, the case for glaciogenicity is uncertain and better age constraints are needed to truly determine the minimum depositional age.

Table S18. Rating of possible glacial influence on the Tany Formation.

Category	Description	Rating
Outsized clasts	Outsized clasts deposited as massive and stratified diamictites in a setting with other reworked deposits.	★
	Outsized clasts that disrupt laminae (assumed due to "dropstone" but not explicitly stated or illustrated) in a setting with other reworked deposits.	★
Clast lithology	Clasts of four lithology classes (siliciclastic, carbonate, igneous, metamorphic).	★★★
Summary	Circumstantial: this evidence could be produced by specific, but rare, ice-free depositional environments.	★★★

Table S19. Rating of possible glacial influence on the Koyva Formation.

Category	Description	Rating
Outsized clasts	Outsized clasts deposited as massive and stratified diamictites in a setting with other reworked deposits.	★
	Outsized clasts that disrupt laminae (assumed due to "dropstone" but not explicitly stated or illustrated) in a setting with other reworked deposits.	★
Clast lithology	Clasts of four lithology classes (siliciclastic, carbonate, igneous, metamorphic; assumed, as Chumakov's (2011) description mainly comprises 'similar to Tany Formation').	★★★
Summary	Circumstantial: this evidence could be produced by specific, but rare, ice-free depositional environments.	★★★

Table S20. Rating of possible glacial influence on the Starye Pechi Formation.

Category	Description	Rating
Outsized clasts	Outsized clasts deposited as massive and stratified diamictites in a setting with other reworked deposits.	★
	Outsized clasts that disrupt laminae (assumed due to "dropstone" but not explicitly stated or illustrated) in a setting with other reworked deposits.	★
Clast surface	Rare, striated clasts.	★
Clast lithology	Clasts of three lithology classes (siliciclastic, carbonate, igneous).	★★
Summary	Circumstantial: this evidence could be produced by specific, but rare, ice-free depositional environments.	★★★

4.4.3 Żuków (Zukow) Formation

The Żuków Formation, Białystok Group, is known only from subsurface deposits in the Lublin region of Poland, and particularly in the Kaplonosy IG 1 and Wisznice IG 1 boreholes. It has variably been interpreted as glaciogenic or fluvial and alluvial in origin (Francovschi et al., 2024; Krzemińska et al., 2022; Pacześna, 2014).

Sedimentology. The Żuków Formation comprises polymict conglomerates and coarse sandstones with subordinate thin beds of brown mudstones and fine sandstones (Pacześna, 2014). The "unsorted" polymict conglomerates include quartz and feldspar

clasts up to 10 cm in diameter which have "a good degree of rounding", alongside fragments of crystalline (igneous and metamorphic) basement up to 30 cm, which are "unrounded" (Pacześna, 2014).

At its base, the Żuków Formation makes an angular unconformity with the likely much older Polesie Formation and Mesoproterozoic crystalline basement across various boreholes (Pacześna, 2014). At its top, the Żuków Formation has an unconformable contact with the overlying volcanics of the Sławatycze Formation, Volyn Group (Pacześna, 2014). The combination of low-angle planar crossbedding, repeated fining-upward patterns, and rounding of quartz clasts informed Pacześna (2014) interpretation of the Żuków Formation as a predominantly fluvial (braided river channel) deposit associated with alluvial fans.

Age constraints. The maximum age constraint for the Żuków Formation is provided only by the assumed early Neoproterozoic age of the sedimentary deposits and Mesoproterozoic crystalline basement that they overlies (Pacześna, 2014), though it is lithostratigraphically correlated with the Brody and Glussk formations in Ukraine and Belarus respectively (Francovschi et al., 2024; Pacześna, 2014).

The minimum age of the Żuków Formation is constrained by radiometric dates from the overlying Volyn Group in the Kaplonosy IG 1 borehole. Krzemińska et al. (2022) produced an igneous zircon U-Pb SHRIMP date of at least 567.0 ± 7.8 Ma (MSWD = 0.108) from an andesitic tuff between the basalts of the lower Sławatycze Formation, lower Volyn Group, at -1720 m in the Kaplonosy IG 1 borehole (sample Kap-1720). This date is consistent within uncertainty with the 569.89 ± 0.17 Ma CA-ID-TIMS date obtained by Środoń et al. (2023) from a detrital zircon in a paleosol in the lower Teremiski Formation (upper Volyn Group) at –1449.8 m in the Kaplonosy IG 1 borehole (sample Kaplonosy-3).

Summary. The Żuków Formation is plausibly early or mid-Ediacaran in age and is likely to be older than ~570 Ma. The lack of direct radiometric constraints and angular unconformities above and below the Żuków Formation hamper a more precise age assignment. The sedimentology of the Żuków Formation has been interpreted as glaciogenic in older literature, but it is now regarded as more likely a braided river and alluvial fan deposit (Francovschi et al., 2024; Pacześna, 2014). From the available evidence, a non-glaciogenic interpretation is probable.

Table S21. Rating of possible glacial influence on the Żuków Formation.

Category	Description	Rating
Outsized clasts	Description is of a clast-supported conglomerate, not a diamictite with outsized clasts.	–
Clast shape	Unclear. Clasts in some beds have "a good degree of rounding" whereas in others are described as "unrounded".	★
Clast lithology	Clasts of three lithology classes are reported (igneous, metamorphic, siliciclastic).	★★
Summary	Weak: some ice-free depositional environments could produce this evidence.	★★

4.5 Gondwana: Australia

4.5.1 Bunyeroo Formation (South Australia)

Ediacaran strata in South Australia are organized into the Wilpena Group, which comprises the Nuccaleena, Brachina, ABC Range Quartzite, Bunyeroo, Wonoka, Bonney Sandstone, and Rawnsley Quartzite formations. Ediacaran macrofossils are known from the Rawnsley Quartzite (e.g. Droser and Gehling, 2015; Evans et al., 2020; Gehling and Droser, 2012; Glaessner, 1958, 1959; Sprigg, 1948), and the Wonoka Formation hosts a major negative carbon isotope excursion that has been correlated with the Shuram excursion globally (e.g. Calver, 2000; Husson et al., 2015; Williams and Schmidt, 2018; Yang et al., 2021).

Sedimentology. The Bunyeroo Formation occurs in the Adelaide Geosyncline, South Australia. It is unconformably overlain by the Wonoka Formation (and Wonoka CIE). The lower strata of the Bunyeroo Formation contain the Acraman Impact Ejecta Horizon (AIEH) (Gostin et al., 2010). In the Bunyeroo Formation, lonestones and granule clusters – possible types of IRD – have been recorded from within 10 m above and below the AIEH and are most common in the 1 to 2 m below the AIEH (Gostin et al., 2010; Young, 1995). The Bunyeroo Formation is typically fine-grained, "a monotonous sequence of grayish red and greenish shale", with dolomite concretions in the lower 30 m of the formation (Wallace et al., 1996). Aside from the AIEH, the Bunyeroo Formation lacks sedimentary structures and is thought to have been deposited below storm wave base in a deep shelf setting against the background of rising sea level (Gostin et al., 2010; Haines, 1986; Wallace et al., 1996).
Lonestones and granule clusters are found "sporadically" in units that show "no evidence of grading and slumping" (Gostin et al., 2010). The lonestones and granule clusters "comprise 2 mm, rounded quartz granules and subangular to rounded pebbles 2 to 5 cm in diameter (Young, 1995, *cited in* Gostin et al., 2010). Identified pebble lithologies are siltstone, sandstone and quartzite; no volcanic clasts have been identified, although the AIEH clasts themselves are dacites (Gostin et al., 2010). The pebbles occur in fissile, finely laminated mudstone (shale) that shows no evidence of grading and slumping. Laminae are partly compacted around the pebbles" (Gostin et al., 2010). Only one subrounded lonestone has been figured (Gostin et al., 2010), with a "near-rectangular aggregate of poorly sorted quartzose sand, interpreted as a frozen aggregate" (Gostin et al., 2010).

Age constraints. The Bunyeroo Formation was deposited below the Wonoka excursion and above the Cryogenian Elatina Formation (e.g. Williams and Schmidt, 2018), potentially putting the Bunyeroo Formation and AIEH into the MEIH interval. Such an age assignment is tentatively supported by a (not formally published) Rb-Sr whole rock date of 593 ± 32 Ma (Webb et al., 1983, *cited in* Compston et al., 1987) and with other, similarly uncertain, age constraints (Lloyd et al., 2020). Efforts at better constraining the age of the AEIH by radiometric dating, particularly with zircon U-Pb dates, have not yet been successful (Compston et al., 1987; Gostin et al., 2010; Williams and Schmidt, 2018, 2021).

Summary. The Bunyeroo Formation was deposited in the middle Ediacaran, likely between 595 to 579 Ma. Following the star rating scheme, the Bunyeroo Formation includes sparse rounded to subangular outsized clasts that show some evidence of

disrupting laminae in a low energy setting (Gostin et al., 2010), with no indication of elongated clasts, and clasts from only one of the lithology classes, all of which can be locally sourced.

Table S22. Rating of possible glacial influence on the Bunyeroo Formation.

Category	Description	Rating
Outsized clasts	Outsized clasts that may disrupt laminae in a low energy setting.	★
Clast lithology	Clasts of one lithology class (siliciclastic: siltstone, sandstone, quartzite) which can all be locally sourced.	–
Summary	Equivocal: many ice-free depositional environments could produce this evidence.	★

4.5.2 Dey Dey Mudstone (South Australia and Western Australia)

Sedimentology. The Dey Dey Mudstone includes fresh feldspars and detrital micas, as well as clusters of poorly sorted silt-sized quartz grains in a very fine-grained muddy matrix (Gostin et al., 2010). Laminae in the Dey Dey Mudstone may be graded (Gostin et al., 2010). Scanning electron microscopy (SEM) examination of the Dey Dey Formation quartz granules did not show any indicators of glacial abrasion (Gostin et al., 2010; Young, 1995). Gostin et al. (2010) interpret the clusters of quartz granules as till pellets deposited from melting icebergs. They further suggest that the presence of fresh feldspars supports interpretation of a frigid local/regional climate with limited chemical weathering. Finally, Gostin et al. (2010) explain the absence of dropstones in the Dey Dey Mudstone as being due to sparse sampling of the formation by coring, and the rarity of dropstones in the neighbouring Bunyeroo Formation.

Age constraints. In the Officer Basin, the Dey Dey Mudstone also captures the AIEH horizon and is considered to have been deposited in the middle Ediacaran, between ~595 to 579 Ma (Gostin et al., 2010).

Summary. The Dey Dey Mudstone is likely mid-Ediacaran in age. There is no good evidence for glaciogenicity, though an IRD interpretation of the quartz granules cannot be ruled out.

Table S23. Rating of possible glacial influence on the Dey Dey Mudstone Formation.

Category	Description	Rating
Clast lithology	Clasts of one lithology class (siliciclastic) which can be locally sourced.	–
Grain clusters	Uncemented clusters of outsized clasts without evidence of erosive lower contacts.	★
Summary	Equivocal: many ice-free depositional environments could produce this evidence.	★

Summary of Bunyeroo Formation and Dey Dey Mudstone deposits. If these data are *bona fide* glaciogenic IRD, then the implication is of grounded ice somewhere globally (potentially in the Northern Hemisphere) at the time of deposition. The time of deposition is thought to be approximately 590 Ma to 580 Ma (Compston et al., 1987; Gostin et al., 2010; Williams and

Schmidt, 2021) which is consistent with radiometric age constraints with large uncertainties and chemostratigraphic correlation (i.e. fairly close but unconformably below the Wonoka excursion). The palaeolatitude of these strata as determined from Bunyeroo Formation samples is 15.7° ± 6.5° (Schmidt and Williams, 1996).

If these are Gaskiers-equivalent glaciogenic deposits, then they require either:

a. icebergs calving in the Southern Hemisphere to drift across the palaeo-equator,
b. icebergs calving from a Northern Hemisphere grounded ice sheet, or
c. a reconsideration of the palaeolatitude of South Australia in the mid-Ediacaran.

The first of these options is unlikely, though perhaps possible in an intense icehouse interval. The second of these options requires low altitude grounded ice at low northern latitudes or the presence of a higher latitude continent than is currently known. This also seems unlikely. The final option is always plausible, but there are otherwise robust palaeomagnetic constraints on Wilpena Group strata (Schmidt and Williams, 1996).

Regarding glaciogenicity, none of the pebbles examined show evidence of surface striations (Gostin et al., 2010; Young, 1995), and the illustrated photomicrograph of a "pellet of poorly sorted quartz silt in an ultrafine matrix" from the lower Dey Dey Mudstone (Gostin et al., 2010) includes other silt-sized quartz clasts not in well-defined lenses but occurring in more quartz-rich bands (not quite laminae) alongside the described better-defined quartz-rich lens. A downslope origin for these features is also plausible. Some of the larger clasts in the Bunyeroo Formation are more plausibly dropstones, but they occur sparsely (as described and figured) and do not show signs of surface striation or particular shaping (i.e. faceting) by ice-related processes.

4.5.3 Croles Hill diamictite (northwest Tasmania)

Sedimentology. The Croles Hill Diamictite (Togari Group, Kanunnah Subgroup) crops out in northwest Tasmania, Australia, and is a polymict diamictite up to 250 m thick with basaltic, rhyolitic, and sedimentary (siliciclastic and carbonate) clasts (Calver et al., 2004, 2026; Everard et al., 2007; Mulder et al., 2020). Calver et al. (2004) report intercalations of laminated mudstones with outsized clasts ("dropstones", op. cit. p. 894). The Kanunnah Subgroup is a turbiditic succession of sandstones, shales, diamictite, and basalts (Calver, 2000). The diamictite is only reported from the southern Smithton Synclinorium and its clasts are predominantly basaltic and minor felsic volcanics (Calver, 2000). The tholeiitic basalts (diamictite clasts and *in situ*) have characteristic intraplate rift geochemical signals (Brown, 1986; Calver, 2000; Crawford and Berry, 1992). Rhyolites underlying the Croles Hill Diamictite sometimes form a hyaloclastite (Calver et al., 2004). In section, clasts in the diamictite appear angular and may bend faint laminae in the surrounding sandy-siltstone (Calver et al., 2004). No faceted or striated clasts have been reported but the well-lithified matrix makes it difficult to inspect individual clasts (Calver et al., 2026).

All clasts found in the Croles Hill Diamictite have potential source rocks in the immediately surrounding strata. No striated clasts have been reported. The Kanunnah Subgroup is described as turbiditic and was deposited in a rift-related setting with a large fault (the Roger River Fault) thought to have been active nearby around the time of Croles Hill Diamictite deposition (Mulder et al., 2020).

Age constraints. Calver et al. (2004) dated a rhyolite flow directly underlying the Croles Hill Diamictite at 582.1 ± 4.1 Ma. Recent CA-ID-TIMS U-Pb radiometric dates from rhyodacites immediately below and interbedded with the Croles Hill Diamictite at Robbins Passage provide maximum and syn-depositional age constraints of 579.20 ± 0.65 Ma and 578.86 ± 0.69 Ma, respectively (Calver et al., 2026). The Croles Hill Diamictite is therefore of mid-Ediacaran age, likely deposited at or around 579 Ma.

Summary. Whilst plausibly of Gaskiers glaciation age, evidence of glaciogenicity of the Croles Hill Diamictite is currently rated circumstantial – and the broader tectonic context provides a plausible non-glacial origin for the diamictite as a mass flow deposit.

Table S24. Rating of possible glacial influence on the Croles Hill diamictite.

Category	Description	Rating
Outsized clasts	Outsized clasts deposited as a massive or stratified diamictite in a setting with other reworked deposits.	★
	Outsized clasts which may deflect laminae occurring in a section with known active volcanism (hyaloclastite) and with turbidites in the surrounding strata.	★
Clast lithology	Clasts of three lithology classes (siliciclastic, carbonate, igneous) which can be locally sourced.	★★
Summary	Weak: some ice-free depositional environments could produce this evidence.	★★★

4.6 Gondwana: North Africa

Potentially glaciogenic strata have been identified from several sites in North Africa. Here, we disregard all deposits that are confirmed or highly likely to be Cryogenian in age and focus on three units from Morocco that are thought to be middle to late Ediacaran in age: the Tiddiline Group, the Izdar Member, and the Ouarzazate Group. The Ouarzazate Group is well dated as being younger than 565 Ma and is not further considered here (Vernhet et al., 2012).

4.6.1 Tiddiline Group

The Tiddiline Group, part of the PII Supergroup succession on the West African Craton (Reguibat Shield), comprises 1 to 3 km thick early to mid-Ediacaran siliciclastic deposits and crops out in the Bou Azzer inlier, south of the Anti-Atlas Fault in the Anti-Atlas mountain range (Letsch et al., 2018). Post-depositional deformation and faulting complicates local and regional correlation of the group, and stratigraphic relationships between different sections are difficult if not impossible to reconstruct from sedimentological evidence (Letsch et al., 2018; Vernhet et al., 2012).

Sedimentology. The siliciclastics include matrix-supported diamictites, as well as siltstones, sandstones, and conglomerates (Letsch et al., 2018; Youbi et al., 2020). Matrix-supported diamictites near Ait Ahmane (northeast Bou Azzer inlier) and Cobalt

mine (western Bou Azzer inlier) occur in similar successions and are thought to have been deposited below a >250 m thick coarse-grained micaceous and K-feldspar rich sandstone which shows signs of soft sediment, brittle, and ductile deformation (Letsch et al., 2018). In the Bou Azzer inlier, matrix-supported diamictites can be several tens of metres thick and occur within a succession of siliciclastics (Letsch et al., 2018). At the base of the succession, unconformably overlying sedimentary and crystalline basement, is a clast-supported conglomerate, with predominantly granodiorite clasts and rarer sandstones, which grades into a matrix-supported diamictite with similar clast composition and then to laminated sandy siltstones (Letsch et al., 2018). The main massive diamictite is deposited on these laminated sandy siltstones and comprises a clay- to sandy silt-grade matrix supporting pebble- to boulder-sized clasts randomly distributed throughout the unit (Letsch et al., 2018). The diamictite clasts range from well-rounded to sub-angular, and include quartz sandstones (typically well-rounded, spherical), micritic carbonates, gneisses, granodiorite-diorite intrusive igneous, gabbro, and volcanic rocks, with larger pebble- or cobble-sized clasts sometimes breaking *in situ* (Letsch et al., 2018). Rare striated and faceted pebbles have been reported (Letsch et al., 2018). Bullet-shaped clasts are reported but this may be due to fracturing rather than abrasion (Letsch et al., 2018). Within the matrix-supported diamictite are occasional centimetre-scale sandstone lenses that may show evidence of plastic and brittle deformation, including folding, boudinage, and tearing (Letsch et al., 2018).

Matrix-supported diamictites in the Sirwa inlier, central Anti-Atlas, are interbedded with a variety of siliciclastic sedimentary deposits including shales, greywackes, and breccias, along with igneous units variously interpreted as volcanics or intrusive sills and sometimes called the Imghi Formation assigned to the Saghro Group (Letsch et al., 2018; Thomas et al., 2002). These are reported from near Tizwat and have been assumed to be older than the diamictites of the Bou Azzer inlier (Letsch et al., 2018). The Tizwat matrix-supported diamictites occur within at least three levels in a succession of mudstones, sandstones, conglomerates, and volcanics (Letsch et al., 2018). The matrix-supported diamictites comprise a sandy mudstone matrix, with well-rounded to angular sand grains, hosting well-rounded pebbles to small boulders (1 to 50 cm diameter) randomly scattered throughout, though occasionally clustered (Letsch et al., 2018). Similar to the diamictites of the Bou Azzer inlier, clasts are mainly quartz sandstones with less common rhyolites, cherts, and coarsely crystalline (presumably intrusive) igneous lithologies, as well as one reworked diamictite clast (Letsch et al., 2018). The diamictites are typically massive, but occasionally clasts appear clustered together (Letsch et al., 2018). The diamictites are separated by laminated siltstones and mudstones, which may show evidence of mass movement (slumping), as well as graded sandstone beds with sharp basal contacts, interpreted as turbidites (Letsch et al., 2018). The laminated siltstones and mudstones include outsized clasts which disrupt laminae below and are draped by laminae above (Letsch et al., 2018).

Matrix-supported diamictites have also been reported from the Igherm and Kerdous inliers in the western Anti-Atlas, including near Timzioura (Choubert, 1972; Letsch et al., 2018). The diamictites near Timzioura occur as massive matrix-supported units tens of metres thick, with angular quartz sandstone clasts, similar to the underlying basement, up to 3 m in diameter found near the bottom of the diamictite (Letsch et al., 2018). Clasts range from centimetre-scale to at least 3 m in diameter, are angular to well-rounded, and are predominantly of local basement lithologies, in particular quartz sandstone (Letsch et al., 2018).

In summary, various outcrops show the Tiddiline Group diamictites in the Anti-Atlas Mountains to be massive, matrix-supported units with sub-centimetre- to metre-scale angular to well-rounded clasts of a wide range of lithologies. Some clasts are faceted and some are striated, though bullet-shaped and elongate clasts are not reliably reported. Laminated siltstones and mudstones above and between diamictite beds host outsized clasts showing evidence of vertical emplacement, disrupting laminae below and above. However, these mudstone-siltstone units can be slumped and co-occur with sandstones that show evidence of deposition from a gravity flow.

Age constraints. Inglis et al. (2004) provided maximum age constraints for the end of deposition of the Tiddiline Group diamictites from zircon U-Pb TIMS ages of 579.4 ± 1.2 Ma and 578.5 ± 1.2 Ma from the Bleïda granodiorite, which cuts across the regional fabric of the Tiddiline Group (though the exact contact is not observed). Blein et al. (2014) reported that conglomerates of the basal Ouarzazate Group, which include granodiorite cobbles thought to derive from the Bleïda granodiorite, sit unconformably on stratified Tiddiline Group conglomerates that do not have these granodiorite clasts, suggesting that the Bleïda granodiorite was intruded (or at least exposed at the surface) after deposition of the Tiddiline Group and before deposition of the Ouarzazate Group. The Bleïda granodiorite age constraints are consistent with the depositional age of the Gaskiers and Trinity diamictites in Avalonia (Pu et al., 2016).

Letsch et al. (2018) provide further radiometric (CA-ID-TIMS) constraints from detrital and igneous zircons for both the onset and termination of deposition of the Tiddiline Group diamictites. The majority of detrital zircon ages from within the diamictites, or their interbeds, group around 592 Ma to 593 Ma. In the Ansra section, an ignimbrite from above the main diamictite, but well below the last diamictite and dropstones, yielded a youngest single grain (and interpreted crystallization) age of 593.12 ± 0.14 Ma (sample 14DL21) (Letsch et al., 2018). An igneous zircon from an ignimbrite overlying the glaciogenic strata provides a further U-Pb LA-ICP-MS age constraint of 574.9 ± 3 Ma (sample 14DL15) (Letsch et al., 2018). The maximum depositional age constraints of Inglis et al. (2004) and Letsch et al. (2018) are in close agreement. It is very likely that the termination of Tiddiline Group glaciogenic sediment deposition preceded or was coincident with the termination of Gaskiers and Trinity diamictite deposition at approximately 579 Ma (Pu et al., 2016), and predates the onset of the Shuram carbon isotope excursion, which is likely 574 Ma or younger (Yang et al., 2021).

The maximum age of Tiddiline Group deposition is constrained by detrital zircon dates from diamictite clasts. An ignimbrite clast within the lower diamictites of the Tiddiline Group has yielded a 593.12 ± 0.14 Ma date (sample 14DL21) (Letsch et al., 2018). Several other detrital zircon ages from geographically widespread samples in the lower Tiddiline Group cluster around 592 Ma to 593 Ma (Letsch et al., 2018). Collectively, these dates suggest a maximum depositional age of ~593 Ma for the Tiddiline Group diamictites, which is considerably older than the onset of deposition of the Avalonian Gaskiers and Trinity diamictites (Pu et al., 2016), but is consistent with the discovery of a deeper tail of glaciogenic sediments in the Mall Bay Formation on Avalonia (Fitzgerald et al., 2024).

Summary. The Tiddiline Group deposits are most likely glaciogenic in origin, and include facies interpreted as terrestrial (tillites) and marine (dropstones in laminites, though these may also be interpreted as lacustrine) glaciogenic (Letsch et al.,

2018). Letsch et al. (2018) cite as further evidence supporting a glaciogenic interpretation the presence of both brittle and ductile deformation, including planar microfabrics with high birefringence clay seams, which are commonly found in Quaternary tills that have been subglacially deformed (van der Meer, 1994; van der Meer et al., 2003; Menzies, 2000). The generally massive and chaotic diamictites are similar to Quaternary till deposits, and the Tizwat diamictite pebble clusters have been interpreted as iceberg dumps (Letsch et al., 2018) which are also found in Quaternary glaciolacustrine and glaciomarine deposits. These perhaps provide additional circumstantial evidence for a glaciogenic interpretation for the Tiddiline Group diamictites, though other mass flow deposition mechanisms remain possible.

It is likely impossible to unpick the number and nature of glacial advances and retreats, except to say that at least one of them occurred over "considerable pre-glacial topography" (Letsch et al., 2018), suggesting that this may have been the first glaciation in the region for a substantial interval of time, possibly since the Cryogenian. Letsch et al. (2018) conclude that the most parsimonious explanation for the number, variety, and extent of glaciogenic rocks in the Tiddiline Group, along with the consistency of radiometric dates recovered from these strata, is that they were deposited during a single icehouse interval. It is likely that there were at least local, more probably global, advances and retreats of an icesheet proximal to the Anti-Atlas region during deposition of the Tiddiline Group from the three diamictite beds, interpreted as terrestrial tillites, found in the Sirwa inlier which are separated by alternating sandy siltstone and claystone laminae and which sometimes host outsized clasts with evidence of vertical emplacement, interpreted as ice-rafted dropstones (Letsch et al., 2018). Letsch et al. (2018) further interpret the depositional setting of the laminites as lacustrine (based on the absence of evidence for coastal deposits) which perhaps makes local rather than global icesheet fluctuations a more plausible explanation for changing depositional conditions.

Table S25. Evidence of glacial influence in the Tiddiline Group diamictites.

Category	Description	Rating
Outsized clasts	Outsized clasts deposited as massive diamictites in a setting with evidence for gravity-flow deposition of stratigraphically adjacent units.	★
	Outsized clasts that disrupt laminae above/below in a setting with evidence of downslope deposition.	★
Clast shape	Clasts are well-rounded to angular.	★
Clast surface	Clasts striated (alignment not reported) and faceted.	★★★
Clast lithology	Clasts of four lithology classes (siliciclastic, carbonate, metamorphic, igneous).	★★★
Summary	Strong: no realistic ice-free depositional environment is likely to produce this evidence.	★★★★

4.6.2 Izdar Member

Rocks assigned to the Izdar Member crop out in the Zenaga inlier, eastern Anti-Atlas Mountains, between the Bou Azzer (east) and Timjich (wester) inliers, near the reservoir and dam of Taghdout (Letsch et al., 2018). The Izdar Member includes diamictites and has been identified as lying on top of a polished surface (Letsch et al., 2018). Letsch et al. (2018) identify the

Zenaga inlier Izdar Member as distinct from the rest of the Ouarzazate Group polished surfaces and diamictites discussed in Vernhet et al. (2012).

Sedimentology. The contact between the Izdar Member and underlying PII Group shallow marine sediments is a polished and striated angular unconformity with irregular but smooth micro-scale topography of divots, fractures, and steps, as well as metre-scale undulations of dips and bumps or swells, similar to roches moutonnées (Letsch et al., 2018). Fault-related slickensides are well-developed elsewhere in both the PII sandstones and the Izdar Member diamictites, but are not observed on the plane of the angular unconformity between the two units (Letsch et al., 2018). The lower part of the Izdar Member comprises typically chaotic matrix- and clast-supported diamictites with intermittent sandstone lenses (Letsch et al., 2018). The diamictite clasts are predominantly quartz sandstones, and more rarely basement lithologies, ranging from coarse sand to boulder grade, well-rounded to very angular, occasionally bullet- or triangle-shaped (possibly due to fracturing) (Letsch et al., 2018). The upper Izdar Member is well-bedded, with siltstones, sandstones, and conglomerates interbedded with the diamictites.

The Izdar Member diamictites thin laterally toward the west and are gradually replaced by shales, sandstones, and less common stratified diamictites which have typically been associated with the Saghro Group (Letsch et al., 2018). The silty shales contain boudinaged sandstones and outsized clasts of quartz sandstones and carbonates ranging from pebble-grade to very angular megaclasts of 40 m long, with the smaller clasts being typically subrounded to well-rounded, though these also have angular fractured or faceted surfaces (Letsch et al., 2018). The outsized clasts may be draped by surrounding laminae (Letsch et al., 2018), though this is hard to see.

Age constraints. The Izdar Member has been assigned to the basal Ouarzazate Group (or PIII). In the Zenaga inlier, the Izdar Member typically rests on a polished and striated unconformity over shallow marine sandstones of the PII Group, which is thought to be of earlier Neoproterozoic (Tonian to Cryogenian) age (Letsch et al., 2018). In places, a thin unit of thinly bedded intercalated green-grey shale to fine sandstone units over a basal boulder bed is sandwiched between the PII and Izdar Member deposits (Letsch et al., 2018). Detrital zircon dates from the Izdar Member show a similar age spectrum to that of the Tiddiline Group, with significant populations at ~2090 Ma and ~590 Ma, including a youngest single grain age of 592.31 ± 0.18 Ma (Letsch et al., 2018).

The upper contact of the Izdar Member is poorly constrained due to tectonic activity on the major Anti-Atlas fault, which has complicated field relationships (Letsch et al., 2018). The Oufalla granite, which abuts the Izdar Member with an uncertain contact relationship, and the Izdar Member are unconformably overlain by siliciclastics and volcaniclastics of the Ouarzazate Group (Letsch et al., 2018). An ignimbrite at the base of the Ouarzazate Group near Tamazarra was dated at 574.9 ± 3.0 Ma (sample 14DL15) (Letsch et al., 2018).

The shale-with-outsized-clasts facies to the west of the main Izdar Member may be its lateral equivalent, which would give the same radiometric constraints for each, but this relationship has not been fully resolved in the field (Letsch et al., 2018).

The shale facies rests on an ignimbrite dated at 593.12 ± 0.14 Ma (youngest single grain in sample 14DL21) (Letsch et al., 2018). Detrital zircons from a sandstone bed in the Izdar Member gave a typical bimodal age distribution, with the younger mode at approximately 593 Ma (sample 14DL22) (Letsch et al., 2018). The upper contact constraint for this shale facies is the same basal Ouarzazate Group ignimbrite as for the diamictite facies of the Izdar Member: 574.9 ± 3.0 Ma (Letsch et al., 2018).

Summary. The Izdar Member is likely of the same depositional age as the Tiddiline Group diamictites (approximately 593 Ma to 579 Ma), though strictly it has a younger minimum age constraint (574 Ma). It was deposited before the Ouarzazate Group. The Izdar Member diamictites display glaciogenic characteristics, but are not as clear as other Ediacaran examples. In particular, the large 40 m long block may be more plausibly explained by downslope mass flow rather than glacial deposition. The polished eroded surface is more convincingly glaciogenic, however, and contributes to an overall four-star rating.

Table S26. Evidence of glacial influence in the Izdar Member.

Category	Description	Rating
Outsized clasts	Outsized clasts deposited as massive diamictites in a setting with evidence for gravity-flow deposition of stratigraphically adjacent units.	★
	Outsized clasts that disrupt laminae above/below in a setting with evidence of downslope deposition.	★
Clast shape	Clasts are well-rounded to very angular.	★
Clast surface	Some faceted (bullet-shaped) clasts present.	★
Clast lithology	Clasts of (at least) three lithology classes (siliciclastic, carbonate, basement – unspecified but described as being metamorphic intruded by igneous rocks).	★★
Geomorphology	Extensive surfaces with striae and/or small surfaces with crescentic gouges, chatter marks, and s-forms.	★★★
Summary	Strong: no realistic ice-free depositional environment is likely to produce this evidence.	★★★★

4.7 Laurentia

4.7.1 Fauquier Formation (upper Lynchburg Group, northern Virginia)

Deposited on the margin of Laurentia (Virginia, USA) during the Ediacaran (Hebert et al., 2010), the Fauquier Formation is part of the upper Lynchburg Group and overlies the lower Lynchburg Group Mechum River Formation, which has also been interpreted as glaciogenic but is generally considered to be Cryogenian in age (Bailey and Peters, 1998; Tollo and Hutson, 1996), being correlated with Sturtian deposits (Hebert et al., 2010). Here, we follow the Cryogenian age interpretation for the Mechum River Formation and discuss the plausibly Ediacaran age for the Fauquier Formation.

Sedimentology. The Fauquier Formation comprises a basal diamictite, followed by a thick sandstone-dominated unit, and finally a thin carbonate with low $\delta^{13}C$ values, and is overlain by the Catoctin Volcanic Formation (Evans and Raub, 2011; Hebert et al., 2010). The basal diamictite comprises rounded to angular cobble- and boulder-grade clasts in a matrix of cross-

bedded coarse sandstone (Hebert et al., 2010). The diamictite clasts primarily comprise basement granite and gneiss, and the boulder-grade clasts reduce in frequency up-section (Hebert et al., 2010). The basal diamictite has been interpreted as a pro-glacial outwash deposit (Hebert et al., 2010).

Overlying the diamictite unit throughout the basin are thick deposits of immature siliciclastic rocks including greywackes, argillites, arkoses, and pebbly sandstones (Hebert et al., 2010). The greywackes and argillites are interpreted as gravity-driven deposits including turbidites, and the arkoses and pebbly sandstones are interpreted as proximal marine or even fluvial deposits (Hebert et al., 2010). Further up section, these units pass into calcareous siltstones and shallow marine limestones which include an intra-formational breccia, laminated rhythmite, and microbial limestones (Hebert et al., 2010). Pillow basalts of the Catoctin volcanics overlying the shallow marine limestones and appear to have been deposited before the carbonate was fully lithified (Hebert et al., 2010).

Age constraints. Hebert et al. (2010) consider the volcanic Catoctin Formation to conformably overly the Fauquier Formation, with the implication of very little temporal hiatus between the two units. They argue that radiometric dates from the lower Catoctin Formation can therefore provide a minimum depositional age for the Fauquier Formation. Zircons from Catoctin Formation volcanics have yielded radiometric dates of 570 ± 12 Ma (Bluemont Quadrangle, northern Virginia) and 564 ± 9 Ma (South Mountain, Pennsylvania), as well as a 572 ± 5 Ma date from a Catoctin-related dyke (Aleinikoff et al., 1995). Further zircon U-Pb dates from the lower 50 m of the Catoctin Formation basalts have been dated at 571 ± 1 Ma (Southworth et al., 2009), which further supports a minimum depositional age of about 570 Ma for the Fauquier Formation.

Hebert et al. (2010) infer that the Catoctin Formation is conformable with the carbonates of the upper Fauquier Formation due to observations of soft sediment deformation in those carbonates. They further argue that the upper Lynchburg Group (Fauquier Formation) is closer in age to the overlying Catoctin Formation volcanics than it is to the underlying lower Lynchburg Group (Mechum River and Bunker Hill formations), which are putatively glaciogenic deposits dated at around 700 Ma (Bailey and Peters, 1998; Tollo and Hutson, 1996).

Summary. The Fauquier Formation diamictite is likely mid-Ediacaran in age, deposited before 571 Ma. The glaciogenicity of the Fauquier Formation is uncertain.

Table S27. Rating of possible glacial influence on the Fauquier Formation diamictite.

Category	Description	Rating
Outsized clasts	Outsized clasts deposited as a massive or stratified diamictite in a setting with other reworked deposits.	★
Clast shape	Clasts are rounded to angular.	★
Clast lithology	Clasts of two lithology classes (metamorphic, igneous) which can be locally sourced.	★
Summary	Equivocal: many ice-free depositional environments could produce this evidence.	★★

4.7.2 Inishowen (=Inishowan) beds

Condon and Prave (2000) described candidate Ediacaran glaciogenic deposits from the Southern Highland Group on the Inishowen (also spelled 'Inishowan') Peninsula, County Donegal, Republic of Ireland. These deposits are generally correlated with the Dalradian Supergroup in Scotland, bounded in the southwest by the Highland Boundary Fault (Scotland) and equivalent Clew Bay – Fair Head faults in Ireland.

Sedimentology. The Inishowen beds comprise five candidate dropstone diamictites, each between a few centimetres to a few decimetres thick, occurring sporadically, separated by tens of metres, in a ~500 m thick succession of arkosic sandstones and mudstones (Condon et al., 2002; Condon and Prave, 2000). Three of the five candidate dropstone-bearing beds consist of granule to pebble grade (up to 25 mm) angular to well-rounded quartzite, gneiss, schist, and igneous clasts, at least some of which are exotic to the local stratigraphy, which can pierce laminae and have laminae draped over them, separated by decimetre to metre thick mudstone deposits lacking outsized clasts (Condon et al., 2002; Condon and Prave, 2000; Prave and Fallick, 2011). Where the outsized clasts are present they are not graded (Condon and Prave, 2000).

In the two stratigraphically higher horizons, the outsized clasts occur predominantly in pelagic mudstones between relatively clast-poor mudstone turbidites, and this is interpreted as a relatively continuous rainout of iceberg dropstones with background sedimentation punctuated by turbidity currents (Condon and Prave, 2000). One of the outsized clasts in the second lowest diamictite, up to ~10 cm diameter, is made up of a cluster of rounded to angular small pebbles (~4 to 8 mm) of quartz and feldspar in a sand-mud matrix (Condon and Prave, 2000). This was interpreted as a frozen aggregate dropped from the base of an iceberg (Condon and Prave, 2000).

In the lowest outsized clast-bearing interval is a convex-up dome-shaped structure with a planar non-erosive base and irregular edge that is up to 20 cm thick and 1 to 2 m in diameter and comprises poorly sorted coarse-grained material described as a diamictite (Condon et al., 2002; Prave and Fallick, 2011). This was interpreted as an iceberg dump structure (Condon et al., 2002).

The strata between the five identified horizons with outsized clasts consist of a heterolithic suite of thin bedded normally graded and cross bedded sandstones, (up to 2 m) thick bedded graded to massive arkoses with sharp erosive bases, pebbly sandstones, and finely laminated or ripple-topped mudstones, all indicating unidirectional flow in a deep marine slope setting (Condon et al., 2002; Condon and Prave, 2000).

The deposits stratigraphically adjacent to the ~500 m thick arkosic succession are quartzitic, with the abundant feldspar in the arkosic units being interpreted as the result of cold climate weathering with limited chemical breakdown (Condon et al., 2002; Condon and Prave, 2000).

Age constraints. There are no direct age constraints on the Inishowen beds. An Ediacaran age interpretation is dependent on correlation with the poorly constrained Dalradian Supergroup in Scotland. Regarding the Inishowen beds, this correlative

framework hinges on a lithostratigraphic correlation between the Culdaff Limestone (Ireland, below Inishowen beds) and the Tayvallich Limestone (Scotland, below the Tayvallich keratophyre) and between the upper Inishowen beds and the Loch na Cille Boulder Bed (Condon and Prave, 2000; Harris et al., 1994). The Tayvallich keratophyre was dated at 595 ± 4 Ma (Halliday et al., 1989) and this was considered a likely age for both the Inishowen beds and Loch na Cille Boulder Bed (Condon et al., 2002; Condon and Prave, 2000). However, (Dempster et al., 2002) highlighted the uncertain stratigraphic relationship between the dated keratophyre and the Dalradian deposits, notably that it might intrude and crosscut adjacent deposits, and that there is likely an inherited component to the 595 Ma age determined by Halliday et al. (1989) who used a standard multigrain analysis. More recently, the 601 ± 4 Ma tuff bed zircon U-Pb date from the Tayvallich Volcanics (Dempster et al., 2002) has been used as the maximum age constraint for the Inishowen beds (Prave and Fallick, 2011).

Summary. The age of the Inishowen beds is likely Ediacaran, and possibly mid- to late Ediacaran, but the dating evidence is weak and its age assignment is here considered uncertain. The evidence for glaciogenicity is not conclusive, but is stronger than that for the supposedly correlative Loch na Cille Boulder Bed (see below). Notably, well rounded to angular granule to pebble grade outsized clasts of three lithological categories occur across multiple horizons (Condon and Prave, 2000; Prave and Fallick, 2011); some of the clasts apparently disrupt laminae both below (warping and penetrating) and above (draping) (Condon et al., 2002; Condon and Prave, 2000); clasts occur in both event (turbidite) and background (pelagic mudstone) beds (Condon and Prave, 2000); some clasts comprise aggregates of granules, interpreted as frozen aggregates (Condon and Prave, 2000); one large patch of diamictite in mudstone is up to 2 m in diameter and has been interpreted as an iceberg dump structure (Condon et al., 2002).

The pebble-bearing horizons are separated by tens of metres in a ~500 m thick heterolithic arkosic succession (Condon et al., 2002; Condon and Prave, 2000). The arkosic succession is situated with hundreds of metres of quartzitic arenites, with the compositional change to arkose inferred to represent a cooler weathering regime, spanning the interval of the pebble beds (Condon et al., 2002; Condon and Prave, 2000). This could also reflect a change to a more proximal source region.

Table S28. Rating of possible glacial influence on the Inishowen beds.

Category	Description	Rating
Outsized clasts	Outsized clasts that may disrupt laminae above/below in or associated with reworked deposits.	★
Clast shape	Clasts are well rounded to angular.	★
Clast lithology	Clasts of three lithology classes (siliciclastic, igneous, metamorphic), at least some of which are considered exotic.	★★
Grain clusters	Uncemented clusters of outsized granules without specific evidence of current flow for their deposition (though surrounding sediment does show signs of current-related deposition).	★★
Summary	Circumstantial: this evidence could be produced by specific, but rare, ice-free depositional environments.	★★★

4.7.3 Loch na Cille Boulder bed (Tayvallich Formation, southwest Scotland)

Sedimentology. The Loch na Cille Boulder Bed is part of the Tayvallich Subgroup, Argyll Group, Dalradian Supergroup, and crops out on the Tayvallich Peninsula, western Scotland, United Kingdom. The Tayvallich Subgroup comprises fine-grained turbidites, limestones, and intrusive and extrusive basaltic rocks and rarer felspar-porphyritic rocks, as well as the Loch na Cille polymict conglomerate, deposited on a submarine slope (Tindal, 2023). Tayvallich Subgroup lithologies on the eponymous Peninsula include (pillowed) basalts, tuffs, feldspar porphyry, keratophyre, pale grey to brown limestone, conglomerate, and mudstone (Tindal, 2023).

There are four distinct conglomerate groups in the Tayvallich Subgroup (Tindal, 2023): basalt + limestone clasts in a basalt + limestone matrix; finely crystalline keratophyre + minor basalt in an epidotized fine-grained matrix; clast-supported basalt + feldspar porphyry conglomerate; polymict conglomerate comprising feldspar-porphyry, keratophyre, basalt, quartzite, and limestone clasts in a dark green mudstone matrix with rare quartz sand. The last of these has generally been considered as the key representative of the Loch na Cille Boulder Bed (Tindal, 2023) and has been interpreted as a candidate Ediacaran glaciogenic deposit on the basis of supposedly exotic clasts (Condon and Prave, 2000; Elles, 1935; McCay et al., 2006; Prave, 1999; Prave and Fallick, 2011). Tindal (2023) comprehensively demonstrated that the lithologies of all the clasts known from the Loch na Cille Boulder Bed can be found "in outcrop within one kilometre" of the boulder bed outcrops. The clasts of the Loch na Cille Boulder Bed show no specific signs of being glacially reworked (e.g. striations, faceted surfaces, warped laminae), nor are any of the clasts truly exotic in origin; rather it can be parsimoniously interpreted as one end member of the gravity-driven conglomerate deposits on a volcanic-carbonate slope (Tindal, 2023).

Age constraints. The Loch na Cille Boulder Bed has a maximum depositional age constraint of 601 ± 4 Ma from a tuff bed zircon U-Pb date several hundred metres stratigraphically below it (Dempster et al., 2002). Cambrian rocks overlie the Dalradian Supergroup and provide the minimum depositional age constraint.

Summary. The Loch na Cille Boulder Bed is likely mid- to late Ediacaran in age, following loose radiometric and lithostratigraphic constraints (Dempster et al., 2002; Prave and Fallick, 2011). However, it is unlikely to be of glaciogenic origin. There are no diagnostic glaciogenic features, and the broad range of clast lithologies can be found both geographically and stratigraphically in close proximity to the boulder bed (Tindal, 2023).

Table S29. Rating of possible glacial influence on the Loch na Cille Boulder Bed.

Category	Description	Rating
Outsized clasts	Outsized clasts deposited as massive diamictites in a setting with other reworked deposits.	★
Clast lithology	Clasts of three lithology classes (siliciclastic, carbonate, igneous).	★★
Summary	Weak: Some ice-free depositional environments could produce this evidence.	★★

4.8 North China Craton

4.8.1 Fengtai Formation

The Fengtai Formation crops out on the southeast margin of the North China Craton where its sedimentology has recently been described from the Huainan and Huoqiu sections (Yue et al., 2025). The Fengtai Formation unconformably overlies the Tonian Sidingshan Formation and is unconformably overlain by the Cambrian Houjiashan Formation (Yue et al., 2025).

Sedimentology. The Fengtai Formation crops out across the Huainan and Huoqiu regions on the North China Craton where it can reach up to 100 m thick, typically thinning south and east (Yue et al., 2025). The source of most clasts in the diamictites can be found within the basin, notably various carbonate lithologies in the Sidingshan Formation, which unconformably underlies the Fengtai Formation with a scratched and scoured erosional contact surface (Yue et al., 2025).

In the Huainan area (Bagongshan section and surrounding area), there are four facies associations. The massive matrix-supported diamictites are several to tens of metres thick, massive in structure, with the exclusively carbonate (locally-derived) angular to subrounded clasts comprising up to 50 % of the rock and typically 1 to 50 cm in diameter, exceptionally >1 m diameter, in a carbonate matrix (Yue et al., 2025). Some clasts are striated, with striations having a consistent orientation, variable length, and widths and depths of 1 to 3 mm (Yue et al., 2025). However, Yue et al. (2025) observe these striations continuing into the diamictite matrix, i.e. they are not confined to clast surfaces, and therefore interpret the striations as evidence of post-depositional processes including fault plane movement and much later erosion. Approximately 0.5 to 2 m thick dolostones, with or without 'dropstones' overlie the massive diamictites and are up to 10 m thick (Yue et al., 2025). These units are typically massive dolostones with bedding rarely visible and rare, poorly sorted, outsized clasts of 5 to 15 cm (rarely 30 cm) diameter throughout (Yue et al., 2025). The overlying units are generally flat-based with an erosive contact (Yue et al., 2025). Thin-bedded matrix-supported stratified diamictites and thin to medium-bedded clast-bearing sandstones overlie the dolostones (Yue et al., 2025). The sandstones host subangular carbonate clasts up to 3 cm diameter that are randomly distributed throughout the beds (Yue et al., 2025). Yue et al. (2025) interpret these clasts as disrupting (breaking underlying and being draped by overlying) laminae in the sandstones, but the figured outcrop photograph (their fig. 5c) appears to show a series of chemical alteration fronts rather than sedimentary laminae. A fourth facies association – laminated sandstones, shales, and limestones – occurs in the upper Fengtai Formation and lacks outsized clasts, though some of the alternations are considered by Yue et al. (2025) to be rhythmites. This facies association is conformable above the diamictites below, and unconformable below the (Cambrian) Houjiasjan Formation above with an erosional contact with evidence for subaerial exposure and intense, lateritic, weathering (Yue et al., 2025). Tan et al. (2025) describe the Fengtai Formation at the Bagongshan section as comprising cyclic units of dolomitic breccia that broadly fines upwards to become breccia-bearing muddy dolostone, with the lower breccia being massive and hosting angular to subangular gravel clasts and the upper breccia-bearing muddy dolostone being laminated and hosting gravel-sized clasts with their long-axis typically aligned with bedding.

Tan et al. (2025) also note that outsized clasts can reach up to 1.3 m (typically 0.5 to 25 cm) and are predominantly dolostone, with minor chert, sandstone, and hematite grains.

In the Huoqiu area (Xiaomeiyoa section and surrounding area) there are also four facies associations. The massive grey diamictites association is up to 20 m thick, with pebble to boulder grade (up to 50 cm diameter) subrounded to angular carbonate clasts, and occasionally displays weak stratification with discontinuous wavy and parallel laminae (Yue et al., 2025). There are truly stratified diamictites as well, comprising thick-bedded matrix-supported diamictites and clast-supported (conglomeratic?) units with subrounded to angular clasts up to 10 cm diameter, sometimes displaying normal grading and parallel lamination (Yue et al., 2025). Clasts are typically aligned with laminations (Yue et al., 2025). One figured thin section from this facies (Yue et al., 2025, fig. 8a) does show an angular (quartz?) gravel clast disrupting underlying micritic carbonate laminae and draped by overlying laminae, suggesting a plausible interpretation of this clast as a dropstone. Where calcareous shales and limestones alternate, they are separated by an erosional surface at the top of the limestones (Yue et al., 2025). A dark shale plus limestone association comprises (rhythmic?) alternation of organic-rich shales and parallel laminated limestones lacking any outsized clasts (Yue et al., 2025). A third diamictite facies association is also identified with normally graded sandstones and shales, directly overlying the dark shales and limestones association (Yue et al., 2025). These diamictites are massive, clast-rich (up to 50 %), with subrounded to angular carbonate clasts up to 10 cm diameter, and are overlain by graded, and parallel and cross-laminated sandstones which themselves grade into calcareous shales with abundant phosphate nodules (Yue et al., 2025).

The depositional interpretation of the Fengtai Formation has been of gravity flow deposits close to the coarse material (due to the poor sorting, high angularity of clasts, and the predominance of local lithologies) (Li et al., 2018), but Yue et al. (2025) and others challenge this interpretation because of the rapid stratigraphic transitions from massive diamictite to dolostones and sandstones with outsized clasts interpreted as dropstones, all of which they infer to be glaciogenic in origin. The dropstone interpretation is questionable based on the field photographic evidence (Yue et al., 2025, fig. 5c) but there is some supportive thin-section evidence (Yue et al., 2025, fig. 8a).

Age constraints. The depositional age of the Fengtai Formation is poorly constrained. It rests unconformably on the Sidingshan Formation which is considered to be Tonian in age, and is unconformably overlain by the Cambrian Series 2 Houjiashan Formation (Tan et al., 2025; Yue et al., 2025). Detrital zircon LA-ICP-MS U-Pb dates from Fengtai Formation shales yield an ~640 ± 18 Ma maximum depositional age (Niu, 2016, unpublished MSc thesis cited in Yue et al., 2025). More detailed detrital zircon study has not led to tighter radiometric age constraints (Tan et al., 2025). The Fengtai Formation is lithostratigraphically correlated with the Luoquan and Zhengmuguan formations of the North China Craton (Yue et al., 2025), but the detrital zircon U-Pb age spectra of these units are quite different to that of the Fengtai Formation, except for parts of the Zhengmuguan Formation in the Helanshan area (Tan et al., 2025)

Summary. The Fengtai Formation is plausibly though not demonstrably Ediacaran in age, and it could reasonably be interpreted as late Cryogenian based on (unpublished) low resolution zircon U-Pb dates. There is little evidence for glaciogenicity. Whilst plausibly deposited in or close to a glaciated area there is only one figure of a clast reasonably interpreted as a dropstone (Yue et al., 2025, p.8a). Other supposed dropstone evidence (Yue et al., 2025, p.5c) is more likely to be misinterpreted chemical alteration haloes, which undermines the validity of the general statements of dropstones being present. The pre-existing interpretation for the depositional conditions of this unit are of downslope debris flow deposits, and that interpretation remains plausible.

Table S30. Rating of possible glacial influence on the Fengtai Formation diamictite.

Category	Description	Rating
Outsized clasts	Outsized clasts deposited as a massive and stratified diamictite in a setting with other reworked deposits.	★
	Outsized clasts that may disrupt laminae above/below in or associated with reworked deposits.	★
Clast lithology	Clasts of one lithology classes (siliciclastic, igneous) which can be locally sourced.	–
Clast roundness	Clasts with three grades of roundness (subrounded, subangular, angular).	–
Summary	Equivocal: many ice-free depositional environments could produce this evidence.	★★

4.9 Río de la Plata Craton

The Maldonado Group includes the Playa Hermosa and Las Ventanas formations, and the San Carlos Formation is considered to be a lateral equivalent of the Las Ventanas Formation (Pecoits et al., 2011). The Maldonado Group was deposited over an angular unconformity with Paleoproterozoic to Neoproterozoic basement rocks of the Lavalleja Group in southeast Uruguay on the Río de Plata craton (Pecoits et al., 2011). Upper Ediacaran to lower Cambrian rocks unconformably overlie the Maldonado Group (Pecoits et al., 2011).

4.9.1 Las Ventanas Formation (Maldonado Group)

Sedimentology. The Las Ventanas Formation comprises siliciclastic sediments including a basal conglomerate, diamictites, sandstones, and siltstones, with fine-grained rhythmites towards the top of the up to 1250 m thick formation (Pecoits et al., 2011). The approximately 250 m thick San Carlos Formation comprises conglomerates, sandstones, and siltstones, which fine upwards to mudstones, and does not have any evidence of glaciogenic sediments (Pecoits et al., 2011).

During deposition of the Maldonado Group, this part of the Río de Plata craton experienced active strike-slip and normal faulting, and active volcanism with the intrusion and extrusion of calc-alkaline and alkaline granites and shoshonitic basalts during the transition from a back-arc basin (pre-Maldonado Group) to a strike-slip basin (syn-Maldonado Group) and finally a foreland basin (post-Maldonado Group) (Pecoits et al., 2011). This geotectonic setting provides several non-glaciogenic emplacement mechanisms for often putatively glaciogenic features.

Putative evidence for glacial influence in deposition of the Las Ventanas Formation comes from outsized clasts with faceted surfaces in fine-grained rhythmites (Gaucher et al., 2008; Pecoits, 2003; Pecoits et al., 2008, 2011). Diamictites and dropstones have been reported from the middle of the Las Ventanas Formation near Minas (Gaucher et al., 2008). The diamictite comprises angular to subrounded carbonate, sandstone, quartzite, metasiltstone, granitoid, and rhyolite clasts up to 25 cm in diameter embedded in a ferruginous clay-silt mudstone matrix, with the matrix typically comprising 35 to 40 % but up to 100 % by volume (Gaucher et al., 2008). The diamictites range from massive to slightly normally graded (Gaucher et al., 2008). Carbonate and metasiltstone clasts occur as lonestones, which may be elongate or 'bullet-shaped' (Gaucher et al., 2008).

The Las Ventanas Formation diamictites range from massive to weakly graded, occasionally reverse graded, with granule to boulder sized clasts of carbonate, siliciclastic, igneous, and metamorphic rocks, some of which are allochthonous to the basin, ranging from angular to rounded and occasionally bullet-shaped (Gaucher et al., 2008; Pecoits, 2003; Pecoits et al., 2008, 2011). Pecoits et al. (2011) identify two different diamictite types: pebble- to cobble-grade clasts in a massive muddy matrix, and cobble- to boulder-grade clasts in a massive to laminated mudstone matrix that form thick (2 to 10 m) beds with clasts sometimes faceted and striated. Rhythmites throughout but particularly in the upper part of the formation, have millimetre- to centimetre-scale alternations of silt and sand sized sediments with clays, and are punctuated with outsized clasts that deform the laminae (Pecoits et al., 2011).

Age constraints. Radiometric dates constrain Maldonado Group deposition to a middle Ediacaran age (Pecoits et al., 2011). Igneous intrusions provide minimum age constraints for the deposition of the Las Ventanas Formation. Syenites intruding the Las Ventanas Formation have yielded a Rb-Sr date of 520 ± 5 Ma (Bossi et al., 1993). The Pan de Azucar pluton intrudes the Las Ventanas Formation and has yielded a Rb-Sr date of 559 ± 28 Ma (Gaucher et al., 2008; Preciozzi et al., 1993) and an Ar-Ar date of 579 ± 1.5 Ma from hornblende in the syenite (Oyhantçabal et al., 2007). Maximum age constraints for deposition of the Las Ventanas Formation come from (meta)basalts at the base of the formation, which have yielded a K-Ar date of 615 ± 30 Ma (Sánchez Bettucci and Linares, 1996), or from the uppermost Lavalleja Group which has yielded a U-Pb zircon date of 590 ± 2 Ma (Mallmann et al., 2007). Acritarchs from the Las Ventanas Formation are characterized by low diversity assemblages of large sphaeromorphs, dominated by *Leiosphaeridia* alongside *Soldadophycus*, with the assemblage being considered typical of lower to middle Ediacaran strata (Gaucher et al., 2008). There are no chemostratigraphic constraints on the Maldonado Group.

Summary. There is strong evidence for glacial influence on the deposition of the Las Ventanas Formation. There is reasonable evidence that the Las Ventanas Formation was likely deposited after 600 Ma, probably after 590 Ma, and before 579 Ma, which is supported by biostratigraphic evidence for deposition before approximately 580 Ma.

Table S31. Evidence of glacial influence in the Las Ventanas Formation.

Category	Description	Rating
Outsized clasts	Outsized clasts deposited as massive and stratified diamictites in proximal settings with evidence for current deposition of other stratigraphically adjacent units.	★
	Outsized clasts that disrupt laminae above/below in a flat setting (rhythmites).	★★★
Clast shape	Clasts are rounded to angular.	★
Clast surface	Clasts striated (alignment not reported) and faceted.	★★★
Clast lithology	Clasts of four lithology classes (siliciclastic, carbonate, metamorphic, igneous).	★★★
Summary	Strong: no realistic ice-free depositional environment is likely to produce this evidence.	★★★★

4.9.2 Playa Hermosa Formation (Maldonado Group)

The Playa Hermosa Formation is considered to be a lateral equivalent of the Las Ventanas Formation (e.g. Pazos et al., 2011; Pecoits et al., 2011), which is consistent with radiometric dates for both units (Mallmann et al., 2007; Oyhantçabal et al., 2007; Rapalini et al., 2015).

Sedimentology. The Playa Hermosa Formation comprises a lower member of conglomerates, diamictites, fine sandstones, pelites, and laminated fine-grained sediments, and an upper member of conglomerates, sandstones, diamictites, and volcanic (hyaloclastic) rocks (Pazos et al., 2003, 2011). The lower member is interpreted to have a glaciogenic influence. The lower member conglomerates include predominantly subrounded though up to angular pebble-grade clasts of felsic igneous rocks, mylonitic rocks, and deformed rhythmites, and have been interpreted as sediment gravity flow deposits (Pazos et al., 2003, 2011). The diamictites include abundant rhythmite clasts and angular feldspathic clasts, are massive, with pebble-sized angular clasts and substantial lateral variability in clast density (Pazos et al., 2003). Syn-sedimentary soft sediment deformation occurs throughout the lower member but is concentrated towards the top (Pazos et al., 2011). The conglomerates have irregular bases, sometimes with evidence of loading, are discontinuous at outcrop scale, and are clast-supported (Pazos et al., 2011). Gravel and sand layers alternate with mud to form coarse rhythmites which contain outsized bullet-shaped quartzite clasts of boulder-grade (Pazos et al., 2011). There are also fine-grained rhythmites of silt and clay layers, some of which alternate with normally graded and rippled sandstones (Pazos et al., 2011). The diamictites typically have sharp basal contacts and may interbed with normally graded sandstones and claystones (Pazos et al., 2011).

Age constraints. The Playa Hermosa Formation rests unconformably on a tonalite gneiss dated at ~1.7 Ga (Pazos et al., 2011; Sánchez-Bettucci et al., 2009). The depositional age of the Playa Hermosa Formation is constrained by radiometric dates above and below. A sample from the basal Playa Hermosa Formation has yielded a detrital zircon U-Pb SHRIMP date of 594 ± 16 Ma (based on an Isoplot youngest detrital zircon analysis) (Rapalini et al., 2015). The minimum depositional age of the Playa Hermosa Formation is constrained by three zircon U-Pb SHRIMP-dated samples from a microsyenite dyke intruding the Playa

Hermosa Formation (sample SA-20 / SdAn-1), a syenite (sample SA-8 / SdAn3), and a flow-banded rhyolite from the El Tambo Formation (sample SA-12 / SdAn-2), all belonging to the Sierra de las Animas igneous complex (Rapalini et al., 2015). These samples were dated at 574.5 ± 8.1 Ma, 587.4 ± 7.3 Ma, and 581.8 ± 3.4 Ma respectively, with a grand mean weighted U-Pb age of 578.0 ± 4.3 Ma (Rapalini et al., 2015).

Summary. The Playa Hermosa Formation was likely deposited after 594 Ma, though there is a large uncertainty associated with this date, and before 578 Ma (Rapalini et al., 2015).

Table S32. Evidence of glacial influence in the Playa Hermosa Formation.

Category	Description	Rating
Outsized clasts	Outsized clasts deposited as massive diamictites in a setting with evidence for reworking of these and stratigraphically adjacent deposits.	★
	Outsized clasts that may disrupt laminae above/below in or associated with reworked deposits.	★
Clast surface	Faceted (bullet-shaped) clasts are reported.	★
Clast lithology	Clasts of three lithology classes (siliciclastic, metamorphic, igneous).	★★
Summary	Circumstantial: this evidence could be produced by specific, but rare, ice-free depositional environments.	★★★

4.10 Sao Francisco Craton

4.10.1 Iporanga Formation

The Iporanga Formation is part of the Neoproterozoic to early Paleozoic succession formed on the Riberira Belt during the Brasiliano Orogeny (Campanha et al., 2008). The Ribeira Belt formed during the collision of the São Francisco, Congo, and Paraná cratons (Campanha et al., 2008).

Sedimentology. The Iporanga Formation comprises polymict breccias and conglomerates interbedded with sandstones and rhythmic pelites, and has been variably interpreted as glaciogenic (tillite), turbidites and other mass flow deposits, and reworked tillites (Campanha et al., 2008). The Iporanga Formation conglomerates comprise millimetre- to decimetre-scale clasts of claystone, rhythmite, quartz, sandstone, conglomerate, amphibolite, gneiss, granitoid, and volcanic lithologies in a fine-grained (pelitic) matrix (Campanha et al., 2008). In the lower units, the conglomerates are clast-rich and massive, with slaty and crenulation cleavage developed through matrix and clasts (Campanha et al., 2008). The conglomerates transition into fine-grained turbidites with interbedded sandstones and conglomerates with a coarser, sandy, matrix (Campanha et al., 2008). There is no evidence of striated clasts or surfaces, and the initial interpretation of a glaciogenic origin for the unit hung on the polymict nature of the conglomerates and breccias, which certainly include some clasts not currently known from the region, whilst subsequent workers have favoured a downslope mass flow deposition model (Campanha et al., 2008).

Age constraints. Campanha et al. (2008) produced radiometric age constraints for the Iporanga Formation from an underlying volcanic unit (sample IP808) and granite clasts in the basal breccia of the formation (sample F203) using zircon U-Pb SHRIMP dating. Sample IP808 yielded a SHRIMP age of 579 ± 34 Ma from the youngest population of zircons, and sample F203 yielded a SHRIMP age of 593 ± 15 Ma from two granite clasts with similar zircon populations (Campanha et al., 2008).

Summary. The Iporanga Formation was likely deposited in the mid-Ediacaran (Campanha et al., 2008) and is plausibly of MEIH interval age, though precise age constraints are lacking. The glaciogenicity of the Iporanga Formation is also questionable, with most recent work supporting a gravity-driven mass flow depositional interpretation in keeping with the tectonic setting proximal to a collisional orogen (Campanha et al., 2008). Although a glaciogenic, or reworked glaciogenic, origin cannot be ruled out, this interpretation is not strongly supported by the evidence.

Table S33. Evidence of glacial influence in the Iporanga Formation.

Category	Description	Rating
Outsized clasts	Outsized clasts deposited as massive conglomerates and breccias (sometimes described as diamictites) in proximal settings with evidence for current deposition of stratigraphically adjacent units.	★
Clast lithology	Clasts of three lithology classes (siliciclastic, metamorphic, igneous).	★★
Summary	Weak: Some ice-free depositional environments could produce this evidence.	★★

4.11 South China

4.11.1 Doushantuo Formation: karst surfaces and glendonites

There is no reliable evidence of glaciogenic sediments or glacial erosion surfaces in the Doushantuo Formation of South China, though Retallack (2022) mentions that karst surfaces within the formation may be due to glacioeustasy without expansion on this point. However, abundant glendonites have been well-documented from several (but not all) sections in the lower to middle Doushantuo Formation, between the EN1 and EN2 negative $\delta^{13}C$ excursions (Wang et al., 2017, 2020). The Doushantuo Formation is an organic-rich and phosphate-rich deep-water deposit – all of which are factors strongly associated with enhanced ikaite precipitation and stabilization (Bischoff et al., 1993; Zhou et al., 2015). The Doushantuo Formation glendonites indicate cool (<10 °C, likely < 4°C) bottom water temperatures during deposition.

Glendonite occurrences in the Doushantuo Formation have all been reported between the negative $\delta^{13}C$ excursions EN1 and EN2 (Wang et al., 2017, 2020). The EN1 excursion is associated with the basal Ediacaran Nantuo cap carbonate, whereas the EN2 excursion is commonly considered a (terminal-) Gaskiers-related (~580 Ma) excursion, and the EN3 excursion at the top of the Doushantuo Formation is thought to correlate with the Shuram $\delta^{13}C$ excursion (Yang et al., 2021).

In the Zhangcunping section, Hubei Province, glendonites are reported from Unit 6 above an unnamed minor negative $\delta^{13}C$ excursion and below the larger EN2 excursion (Wang et al., 2017). The unnamed minor excursion is dated at 609 ± 5 Ma (SIMS zircon U-Pb) (Zhou et al., 2017) and ≤612.5 ± 0.9 Ma (sample 18SC25; CA-ID-TIMS youngest detrital zircon U-Pb date) (Yang et al., 2021). The minor unnamed excursion is correlated into the Jiulongwan section, Yangtze Gorges area, western Hubei Province, to a horizon dated at 587.2 ± 3.6 Ma (sample F1404; Re-Os whole-rock isochron) (Yang et al., 2021). No glendonites are reported above the EN2 excursion. The nearest overlying radiometric age constraint is from the top of the Miaohe Member, Doushantuo Formation, Jiajawan section, western Hubei Province, which is above EN3 and is dated at 550.1 ± 0.6 Ma (sample 16JJW-3; CA-ID-TIMS zircon U-Pb date) (Yang et al., 2021). The onset of the Shuram excursion is considered to be approximately 574 Ma, and not earlier than 578.7 Ma (Rooney et al., 2020; Yang et al., 2021).

The Doushantuo Formation glendonites are considered here to indicate cool (<10 °C) or cold (<4 °C) bottom waters at least around parts of the South China craton between 610 Ma (or perhaps 587 Ma) and 575 Ma.

4.12 Tarim

4.12.1 Xichangjing Formation

The Xichangjing Formation was deposited in the Altaids orogenic belt on the northern margin of the Tarim and North China cratons (Niu et al., 2024). The Xichangjing Formation is particularly well studied in the Beishan region, on the Hanshan and Shuangyingshan blocks (Niu et al., 2024).

Sedimentology. In the Xichangjing Formation, 18 facies have been identified, comprising four clast-rich diamictite facies, four matrix-rich diamictite facies, and 10 apparently non-glacial facies, arranged into eight facies associations (Niu et al., 2024). The proglacial marine facies association includes cherts, limestones, shales, and mudstones, which may be slumped, interbedded with matrix-rich stratified and massive diamictites with a very fine-grained (siliceous flour) matrix hosting unsorted outsized clasts (0.5 mm to 2 m) of marble, biogenic limestones, crystalline limestones, quartzites, and volcanic lithologies, that sometimes deform laminae and may be abraded (flat-iron or bullet shaped) and striated (Niu et al., 2024). Some diamictites show evidence of syn-sedimentary shearing, with bounding shear planes and aligned elongate clasts (Niu et al., 2024). Some of the diamictites have planar, non-erosive, bases and have heterogeneously distributed clusters of clasts, interpreted as iceberg overturning deposits (Niu et al., 2024).

Matrix-supported massive diamictites also occur in the submarine retreat and marginal marine facies associations, the latter of which also includes stratified diamictites, and with diamictites interbedded with laminated limestones and calcareous shales laterally traceable over wide areas (Niu et al., 2024). Both diamictite types include faceted (flat-iron) and striated clasts which range from 1 mm to 0.5 m in diameter and are interpreted as the result of proximal glacial outwash flows (Niu et al., 2024).

The fan-delta and submarine fan facies associations predominantly comprise conglomerates and massive sandstones that are typically lenticular at outcrop scale and not traceable beyond ~50 m (Niu et al., 2024). The conglomerate clasts are well-sorted,

rounded pebbles of quartzite, carbonate, and volcanic lithologies, and the sandstones represent the coarser Bouma sequence turbidite divisions (T_{a-c}), and both show no evidence of direct glacial influence (Niu et al., 2024). The inner and outer shelf facies associations also show no evidence of direct glacial influence and include laterally continuous limestones interbedded with chert, tuffaceous mudstone, and manganiferous deposits (Niu et al., 2024). Finally, a cap carbonate facies association has been described comprising dolomite and limestone beds (Niu et al., 2024).

In the glacially-influenced facies associations, alternations between the different diamictite facies and between diamictites and other lithologies have been interpreted as cyclical signals of glacial advance and retreat (Niu et al., 2024).

Age constraints. The Xichangjing Formation rests unconformably on Mesoproterozoic basement rocks and is unconformably overlain by trilobite-bearing Cambrian rocks of the Pochengshan and Shuangyingshan formations (Niu et al., 2024). Detrital zircon analyses from the Xichangjing, Pochengshan, and Shuangyingshan formations provide a radiometric age control for the deposition of the Xichangjing Formation (Niu et al., 2024). In particular, maximum depositional ages from three samples in the Xichangjing Formation are 601.3 ± 6.4 Ma (sample A2), 594.5 ± 6.5 Ma (sample A1), and 591.1 ± 5.6 Ma (sample E1), suggesting a maximum depositional age for the formation of ~591 Ma (Niu et al., 2024). Detrital zircons from the overlying Cambrian formations include an age peak at 561 Ma that is absent from the Xichangjing Formation, perhaps indicating that it was deposited before this time and providing a minimum depositional age constraint of 561.9 ± 4.8 Ma (Niu et al., 2024).

Summary. The Xichangjing Formation was most likely deposited between ~591 to 561 Ma (Niu et al., 2024). The Xichangjing Formation includes abundant sedimentological evidence of glacial influence in its deposition; most of this evidence indicates proximal subaqueous (likely submarine) deposition and reworking of glacially-derived material from a glacier or icesheet that waxed and waned repeatedly (Niu et al., 2024). A glaciogenic interpretation for this unit is highly parsimonious.

Table S34. Evidence of glacial influence in the Xichangjing Formation.

Category	Description	Rating
Outsized clasts	Outsized clasts deposited as massive and stratified diamictites in proximal settings with evidence for current deposition of other stratigraphically adjacent units.	★
	Outsized clasts deposited as a massive or stratified diamictite in a setting with other reworked deposits.	★
Clast surface	Clasts striated (alignment not reported) and faceted (flat-iron and/or bullet-shaped).	★★★
Clast lithology	Clasts of four lithology classes (siliciclastic, carbonate, metamorphic, igneous).	★★★
Summary	Strong: no realistic ice-free depositional environment is likely to produce this evidence.	★★★★

5 SUPPLEMENTARY FIGURES

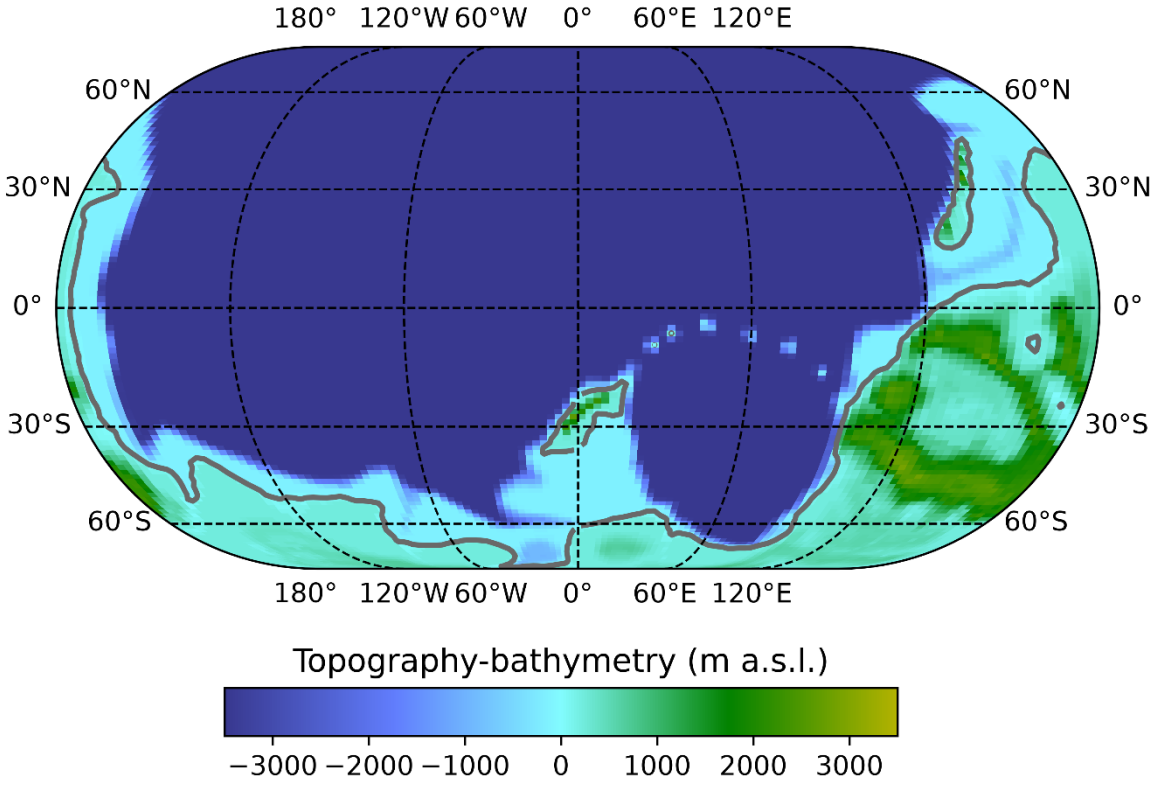

Fig. S1. Mid-Ediacaran (600 Ma) PALEOMAP palaeogeographic reconstruction (Scotese, 2016; Scotese and Wright, 2018) which provided the topographic-bathymetric boundary conditions for our climate and ice sheet model simulations, in an Eckert IV projection. Colours indicate altitude in metres above sea level (m a.s.l.). Thick grey lines indicate the 0 m a.s.l. contour.

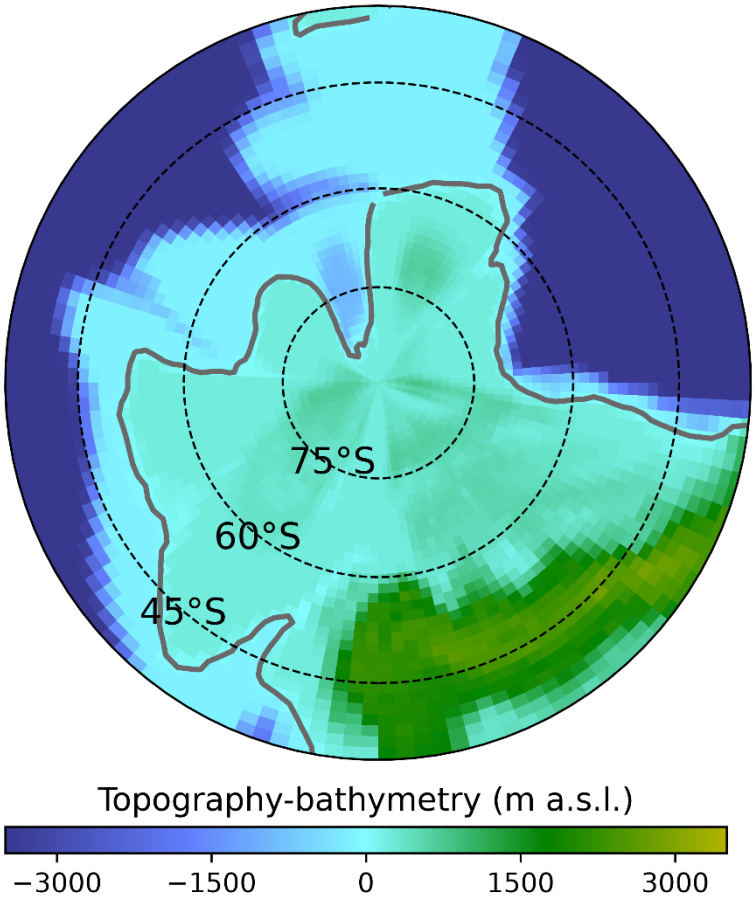

Fig. S2. Mid-Ediacaran (600 Ma) PALEOMAP palaeogeographic reconstruction (Scotese, 2016; Scotese and Wright, 2018) which provided the topographic-bathymetric boundary conditions for our climate and ice sheet model simulations, in a south polar stereographic projection to emphasize the South Pole region used for ice sheet simulations. Colours indicate altitude in metres above sea level (m a.s.l.). Thick grey lines indicate the 0 m a.s.l. contour.

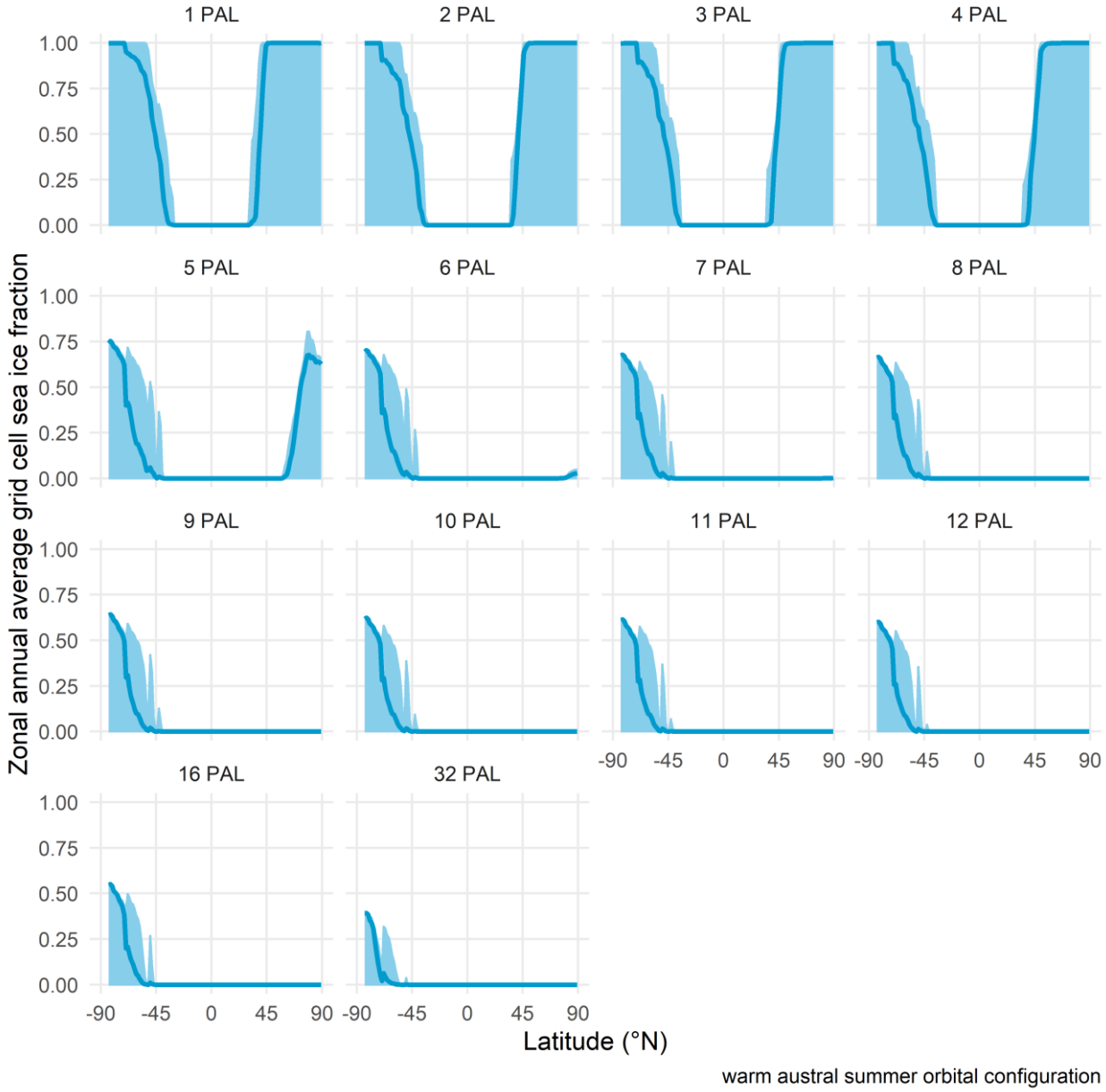

1615

Fig. S3. Zonally-averaged sea-ice cover fraction simulated by FOAM at different pCO_2 levels (warm austral summer orbital configuration). Dark blue line: mean annual zonally-averaged sea-ice cover fraction; light blue envelope: shaded zero to maximum annual zonally-averaged sea ice cover fraction.

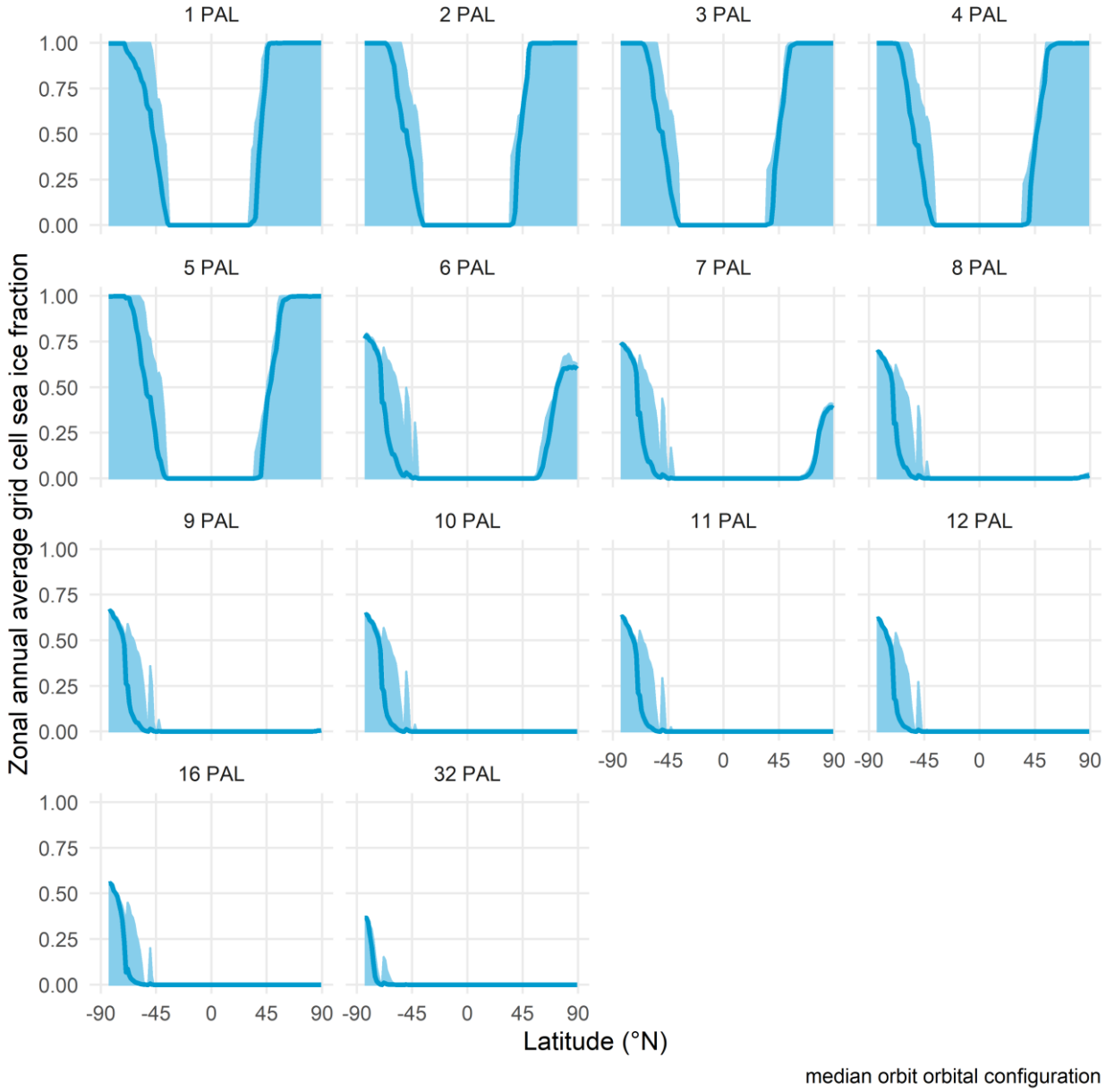

Fig. S4. Zonally-averaged sea-ice cover fraction simulated by FOAM at different pCO_2 levels (median orbital configuration). Dark blue line: mean annual zonally-averaged sea ice cover fraction; light blue envelope: shaded zero to maximum annual zonally-averaged sea ice cover fraction.

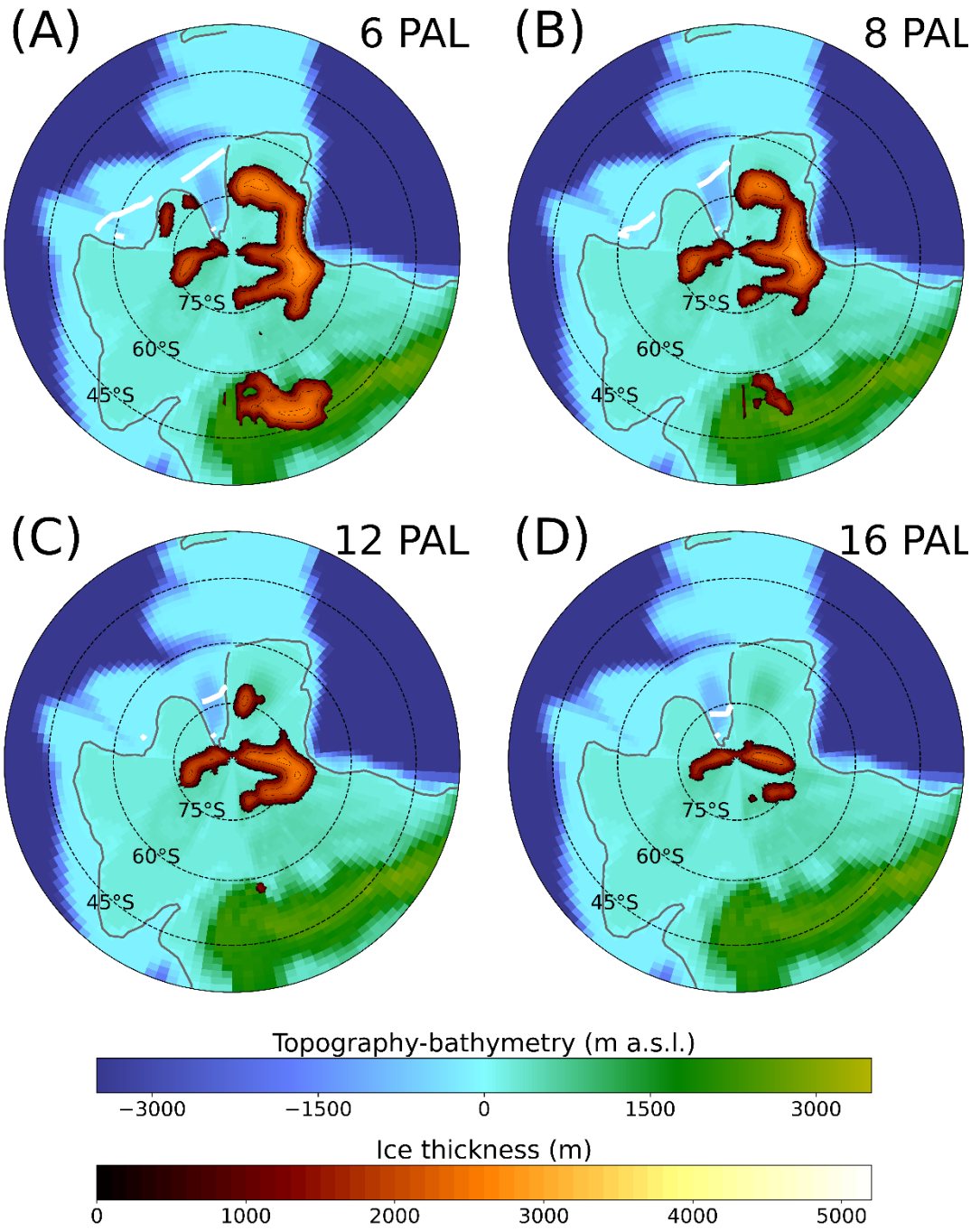

Fig. S5. Ice sheets simulated using the GRISLI ice sheet model after 10 kyr of model integration for (A) 6, (B) 8, (C) 12, and (D) 16 times pre-industrial atmospheric level (PAL) pCO_2 (1 PAL = 280 ppmv). Each panel shows the GRISLI-simulated ice sheet thickness (heatmap colours) and the extent of the FOAM-simulated mean annual 50 % sea ice fraction (thick white lines). Contrast with Fig. 4, which shows ice sheet thickness simulated at equilibrium after 300 kyr of ice sheet model integration. The map is a south polar projection with latitudes shown every 15° between 90 to 45 °S and map margin at 35 °S.

6 References

Aleinikoff, J. N., Zartman, R. E., Walter, M., Rankin, D. W., Lyttle, P. T., and Burton, W. C.: U-Pb Ages of Metarhyolites of the Catoctin and Mount Rogers Formations, Central and Southern Appalachians; Evidence for Two Pulses of Iapetan Rifting, American Journal of Science, 295, 428–454, https://doi.org/10.2475/ajs.295.4.428, 1995.

Al-Husseini, M. I.: Proposed correlation of Oman's Abu Mahara Supergroup and Saudi Arabia's Jibalah Group, GeoArabia, 19, 17–48, https://doi.org/10.2113/geoarabia190217, 2014.

Allen, P. A. and Etienne, J. L.: Sedimentary challenge to Snowball Earth, Nature Geosci, 1, 817–825, https://doi.org/10.1038/ngeo355, 2008.

Alvarenga, C. J. S., Figueiredo, M. F., Babinski, M., and Pinho, F. E. C.: Glacial diamictites of Serra Azul Formation (Ediacaran, Paraguay belt): Evidence of the Gaskiers glacial event in Brazil, Journal of South American Earth Sciences, 23, 236–241, https://doi.org/10.1016/j.jsames.2006.09.015, 2007.

Alvarenga, C. J. S., Boggiani, P. C., Babinski, M., Dardenne, M. A., Figueiredo, M. F., Dantas, E. L., Uhlein, A., Santos, R. V., Sial, A. N., and Trompette, R.: Chapter 45 Glacially influenced sedimentation of the Puga Formation, Cuiabá Group and Jacadigo Group, and associated carbonates of the Araras and Corumbá groups, Paraguay Belt, Brazil, Geological Society, London, Memoirs, 36, 487–497, https://doi.org/10.1144/M36.45, 2011.

Asanuma, H., Fujisaki, W., Sato, T., Sakata, S., Sawaki, Y., Aoki, K., Okada, Y., Maruyama, S., Hirata, T., Itaya, T., and Windley, B. F.: New isotopic age data constrain the depositional age and accretionary history of the Neoproterozoic-Ordovician Mona Complex (Anglesey-Lleyn, Wales), Tectonophysics, 706–707, 164–195, https://doi.org/10.1016/j.tecto.2017.03.017, 2017.

Babinski, M., Trindade, R., Alvarenga, C., Boggiani, Liu, D., Santos, R., and Neves, B. B.: Chronology of Neoproterozoic ice ages in central Brazil, in: Short Papers, South American Symposium on Isotope Geology, 2006.

Bailey, C. M. and Peters, S. E.: Glacially influenced sedimentation in the late Neoproterozoic Mechum River Formation, Blue Ridge province, Virginia, Geology, 26, 623–626, https://doi.org/10.1130/0091-7613(1998)026%3C0623:GISITL%3E2.3.CO;2, 1998.

Bennett, M. R., Doyle, P., and Mather, A. E.: Dropstones: their origin and significance, Palaeogeography, Palaeoclimatology, Palaeoecology, 121, 331–339, https://doi.org/10.1016/0031-0182(95)00071-2, 1996.

Bischoff, J. L., Fitzpatrick, J. A., and Rosenbauer, R. J.: The Solubility and Stabilization of Ikaite ($CaCO3 \cdot 6H2O$) from 0° to 25°C: Environmental and Paleoclimatic Implications for Thinolite Tufa, The Journal of Geology, 101, 21–33, https://doi.org/10.1086/648194, 1993.

Blein, O., Baudin, T., Chèvremont, P., Soulaimani, A., Admou, H., Gasquet, P., Cocherie, A., Egal, E., Youbi, N., Razin, P., Bouabdelli, M., and Gombert, P.: Geochronological constraints on the polycyclic magmatism in the Bou Azzer-El Graara inlier (Central Anti-Atlas Morocco), Journal of African Earth Sciences, 99, 287–306, https://doi.org/10.1016/j.jafrearsci.2014.04.021, 2014.

Bossi, J., Cingolani, C. A., Llambías, E. J., Varela, R., and Campal, N.: Características del magmatismo post-orogénico finibrasiliano en el Uruguay: formaciones Sierra de Ríos y Sierra de Ánimas, The magmatic characteristics of the post-orogenic late Brazilian magmatism from Uruguay: Sierra de Ríos and Sierra de Ánimas formations, 23, no. 3, https://doi.org/10.5327/rbg.v23i3.469, 1993.

Bouma, A. H.: Sedimentology of some flysch deposits: A graphic approach to facies interpretation, Elsevier, Amsterdam, 168 pp., 1962.

Brown, A. V.: Geology of the Dundas–Mount Lindsay–Mount Youngbuck Region, Geological Survey of Tasmania, 1986.

Brückner, D. and Anderson, M. M.: Late Precambrian glacial deposits in southeastern Newfoundland—a preliminary note, Geological Association of Canada Proceedings, 24, 95–102, 1971.

Buchardt, B., Seaman, P., Stockmann, G., Vous, M., Wilken, U., Düwel, L., Kristiansen, A., Jenner, C., Whiticar, M. J., Kristensen, R. M., Petersen, G. H., and Thorbjørn, L.: Submarine columns of ikaite tufa, Nature, 390, 129–130, https://doi.org/10.1038/36474, 1997.

Calver, C. R.: Isotope stratigraphy of the Ediacarian (Neoproterozoic III) of the Adelaide Rift Complex, Australia, and the overprint of water column stratification, Precambrian Research, 100, 121–150, https://doi.org/10.1016/S0301-9268(99)00072-8, 2000.

Calver, C. R., Black, L. P., Everard, J. L., and Seymour, D. B.: U-Pb zircon age constraints on late Neoproterozoic glaciation in Tasmania, Geology, 32, 893–896, https://doi.org/10.1130/G20713.1, 2004.

Calver, C. R., Cumming, G. V., Halverson, G. P., Crowley, J. L., Roberts, N. J., and Schmitz, M.: High-resolution U-Pb dating of the Croles Hill Diamictite, Tasmania: Near-synchroneity of widely separated mid-Ediacaran glacial deposits, Precambrian Research, 432, 107958, https://doi.org/10.1016/j.precamres.2025.107958, 2026.

Campanha, G. A. C., Basei, M. S., Tassinari, C. C. G., Nutman, A. P., and Faleiros, F. M.: Constraining the age of the Iporanga Formation with SHRIMP U-Pb zircon: Implications for possible Ediacaran glaciation in the Ribeira Belt, SE Brazil, Gondwana Research, 13, 117–125, https://doi.org/10.1016/j.gr.2007.05.010, 2008.

Carto, S. L. and Eyles, N.: Chapter 42 The deep-marine glaciogenic Gaskiers Formation, Newfoundland, Canada, Geological Society, London, Memoirs, 36, 467–473, https://doi.org/10.1144/M36.42, 2011.

Carto, S. L. and Eyles, N.: Sedimentology of the Neoproterozoic (c. 580 Ma) Squantum 'Tillite', Boston Basin, USA: Mass flow deposition in a deep-water arc basin lacking direct glacial influence, Sedimentary Geology, 269–270, 1–14, https://doi.org/10.1016/j.sedgeo.2012.03.011, 2012.

Choubert, G.: Complément à la séance de discussion d'Ouarzazate. Problème de certains quartzites; problème des tillites., Notes et Mémoires du Service Géologique du Maroc, 236, 363–365, 1972.

Chumakov, N. M.: E25. Late Precambrian glacial deposits of the Vilchitsy Formation of western regions of the U.S.S.R., in: Earth's pre-pleistocene glacial record, edited by: Hambrey, M. J. and Harland, W. B., Cambridge University Press, Cambridge, UK, 655–659, 1981.

Chumakov, N. M.: Trends in global climatic changes inferred from geological date, Stratigraphy and Geological Correlation, 12, 117–138, 2004.

Chumakov, N. M.: Chapter 24 The Neoproterozoic glacial formations of the North and Middle Urals, in: The Geological Record of Neoproterozoic Glaciations, edited by: Arnaud, E., Halverson, G. P., and Shields-Zhou, G., Geological Society of London, 289–296, https://doi.org/10.1144/M36.23, 2011.

Chumakov, N. M., Pokrovskii, B. G., and Maslov, A. V.: Stratigraphic position and significance of carbonate rocks related to neoproterozoic glacial horizons of the Urals, Stratigr. Geol. Correl., 21, 573–591, https://doi.org/10.1134/S0869593813060038, 2013.

Clark, P. U., Dyke, A. S., Shakun, J. D., Carlson, A. E., Clark, J., Wohlfarth, B., Mitrovica, J. X., Hostetler, S. W., and McCabe, A. M.: The Last Glacial Maximum, Science, 325, 710–714, https://doi.org/10.1126/science.1172873, 2009.

Compston, W., Williams, I. S., Jenkins, R. J. F., Gostin, V. A., and Haines, P. W.: Zircon age evidence for the Late Precambrian Acraman ejecta blanket, Australian Journal of Earth Sciences, 34, 435–445, https://doi.org/10.1080/08120098708729424, 1987.

Condon, D. J. and Prave, A. R.: Two from Donegal: Neoproterozoic glacial episodes on the northeast margin of Laurentia, Geology, 28, 951–954, https://doi.org/10.1130/0091-7613(2000)28%3C951:TFDNGE%3E2.0.CO;2, 2000.

Condon, D. J., Prave, A. R., and Benn, D. I.: Neoproterozoic glacial-rainout intervals: Observations and implications, Geology, 30, 35–38, https://doi.org/10.1130/0091-7613(2002)030%3C0035:NGRIOA%3E2.0.CO;2, 2002.

Council, T. C. and Bennett, P. C.: Geochemistry of ikaite formation at Mono Lake, California: Implications for the origin of tufa mounds, Geology, 21, 971–974, https://doi.org/10.1130/0091-7613(1993)021%3C0971:GOIFAM%3E2.3.CO;2, 1993.

Crawford, A. J. and Berry, R. F.: Tectonic implications of Late Proterozoic-Early Palaeozoic igneous rock associations in western Tasmania, Tectonophysics, 214, 37–56, https://doi.org/10.1016/0040-1951(92)90189-D, 1992.

Dartnall, R.: Depositional framework of the Gwna Group mélanges of Anglesey and North-West Wales, UK, d_ph, University of Birmingham, 288 pp., https://doi.org/10/13/Dartnall2019PhD.pdf, 2019.

Davies, T. A. and Laughton, A. S.: Sedimentary processes in the North Atlantic, Initial Report of the Deep Sea Drilling Project, 12, 905–934, 1972.

Dempster, T. J., Rogers, G., Tanner, P. W. G., Bluck, B. J., Muir, R. J., Redwood, S. D., Ireland, T. R., and Paterson, B. A.: Timing of deposition, orogenesis and glaciation within the Dalradian rocks of Scotland: constraints from U–Pb zircon ages, Journal of the Geological Society, 159, 83–94, https://doi.org/10.1144/0016-764901061, 2002.

Dieckmann, G. S., Nehrke, G., Papadimitriou, S., Göttlicher, J., Steininger, R., Kennedy, H., Wolf-Gladrow, D., and Thomas, D. N.: Calcium carbonate as ikaite crystals in Antarctic sea ice, Geophysical Research Letters, 35, https://doi.org/10.1029/2008GL033540, 2008.

Dietrich, P., Griffis, N. P., Le Heron, D. P., Montañez, I. P., Kettler, C., Robin, C., and Guillocheau, F.: Fjord network in Namibia: A snapshot into the dynamics of the late Paleozoic glaciation, Geology, 49, 1521–1526, https://doi.org/10.1130/G49067.1, 2021.

Dott, R. H., Jr.: Squantum "Tillite", Massachusetts—Evidence of Glaciation or Subaqueous Mass Movements?, GSA Bulletin, 72, 1289–1305, https://doi.org/10.1130/0016-7606(1961)72%5B1289:STMOGO%5D2.0.CO;2, 1961.

Droser, M. L. and Gehling, J. G.: The advent of animals: The view from the Ediacaran, Proceedings of the National Academy of Sciences, 112, 4865–4870, https://doi.org/10.1073/pnas.1403669112, 2015.

Elles, G. L.: The Loch na Cille Boulder Bed and its place in the Highland Succession, Quarterly Journal of the Geological Society of London, 91, 111–149, https://doi.org/10.1144/GSL.JGS.1935.091.01-04.05, 1935.

Etienne, J. L., Allen, P. A., Rieu, R., and Le Guerroué, E.: Neoproterozoic Glaciated Basins: A Critical Review of the Snowball Earth Hypothesis by Comparison with Phanerozoic Glaciations, in: Glacial Sedimentary Processes and Products, John Wiley & Sons, Ltd, 343–399, https://doi.org/10.1002/9781444304435.ch19, 2007.

Evans, D. J. A. and Benn, D. I. (Eds.): A Practical Guide to the Study of Glacial Sediments, 1st ed., Taylor & Francis Group, London, UK, 297 pp., 2004.

Evans, David. A. D.: A fundamental Precambrian–Phanerozoic shift in earth's glacial style?, Tectonophysics, 375, 353–385, https://doi.org/10.1016/S0040-1951(03)00345-7, 2003.

Evans, David. A. D. and Raub, T. D.: Chapter 7. Neoproterozoic glacial palaeolatitudes: a global update, in: The Geological Record of Neoproterozoic Glaciations, edited by: Arnaud, E., Halverson, G. P., and Shields-Zhou, G. A., Geological Society of London, London, UK, 93–112, 2011.

Evans, S. D., Hughes, I. V., Gehling, J. G., and Droser, M. L.: Discovery of the oldest bilaterian from the Ediacaran of South Australia, PNAS, 117, 7845–7850, https://doi.org/10.1073/pnas.2001045117, 2020.

Everard, J. L., Seymour, D. B., Reed, A. R., McClenaghan, M. P., Green, D. C., Calver, C. R., and Brown, A. V.: Regional Geology of the Southern Smithton Synclinorium: Explanatory Report for the Roger, Sumac and Dempster 1:25,000 Map Sheets, Far Northwestern Tasmania, Mineral Resources Tasmania, Hobart, Tasmania, 2007.

Eyles, N. and Boyce, J. I.: Kinematic indicators in fault gouge: tectonic analog for soft-bedded ice sheets, Sedimentary Geology, 116, 1–12, https://doi.org/10.1016/S0037-0738(97)00122-X, 1998.

Eyles, N. and Eyles, C. H.: Glacially-influenced deep-marine sedimentation of the Late Precambrian Gaskiers Formation, Newfoundland, Canada, Sedimentology, 36, 601–620, https://doi.org/10.1111/j.1365-3091.1989.tb02088.x, 1989.

Eyles, N., Eyles, C. H., and Miall, A. D.: Lithofacies types and vertical profile models; an alternative approach to the description and environmental interpretation of glacial diamict and diamictite sequences, Sedimentology, 30, 393–410, https://doi.org/10.1111/j.1365-3091.1983.tb00679.x, 1983.

Fenton, I. S., Aze, T., Farnsworth, A., Valdes, P., and Saupe, E. E.: Origination of the modern-style diversity gradient 15 million years ago, Nature, 614, 708–712, https://doi.org/10.1038/s41586-023-05712-6, 2023.

Field, L. P., Milodowski, A. E., Shaw, R. P., Stevens, L. A., Hall, M. R., Kilpatrick, A., Gunn, J., Kemp, S. J., and Ellis, M. A.: Unusual morphologies and the occurrence of pseudomorphs after ikaite ($CaCO_3 \cdot 6H_2O$) in fast growing, hyperalkaline speleothems, Mineralogical Magazine, 81, 565–589, https://doi.org/10.1180/minmag.2016.080.111, 2017.

Figueiredo, M. F., Babinski, M., and Alvarenga, C. J. S.: Chapter 46 The Serra Azul Formation, Paraguay Belt, Brazil, Geological Society, London, Memoirs, 36, 499–502, https://doi.org/10.1144/M36.46, 2011.

Fitzgerald, D. M., Narbonne, G. M., Pufahl, P. K., and Dalrymple, R. W.: The Mall Bay Formation (Ediacaran) and the protracted onset of the Gaskiers glaciation in Newfoundland, Canada, Precambrian Research, 405, 107369, https://doi.org/10.1016/j.precamres.2024.107369, 2024.

Flint, R. F., Sanders, J. E., and Rodgers, J.: Diamictite, a substitute term for symmictite, GSA Bulletin, 71, 1809–1810, https://doi.org/10.1130/0016-7606(1960)71%5B1809:DASTFS%5D2.0.CO;2, 1960a.

Flint, R. F., Sanders, J. E., and Rodgers, J.: Symmictite: a name for nonsorted terrigenous sedimentary rocks that contain a wide range of particle sizes, GSA Bulletin, 71, 507–510, https://doi.org/10.1130/0016-7606(1960)71%5B507:SANFNT%5D2.0.CO;2, 1960b.

Francovschi, I., Shumlyanskyy, L., Soesoo, A., Tarasko, I., Melnychuk, V., Hoffmann, A., Kovalick, A., Love, G., and Bekker, A.: U–Pb geochronology of detrital zircon from the Ediacaran and Cambrian sedimentary successions of NE Estonia and Volyn region of Ukraine: Implications for the provenance and comparison with other areas within Baltica, Precambrian Research, 392, 107087, https://doi.org/10.1016/j.precamres.2023.107087, 2023.

Francovschi, I., Shumlyanskyy, L., Grytsenko, V., Hoffmann, A., Wilde, S. A., and Bekker, A.: U–Pb geochronology and Hf isotope systematics of detrital zircon from the basal part of the late Ediacaran sedimentary succession of the Moldova-Podillya basin (SW Baltica): Implications for glacial vs. alluvial origin, Precambrian Research, 413, 107572, https://doi.org/10.1016/j.precamres.2024.107572, 2024.

Gaucher, C., Blanco, G., Chiglino, L., Poiré, D., and Germs, G. J. B.: Acritarchs of Las Ventanas Formation (Ediacaran, Uruguay): Implications for the timing of coeval rifting and glacial events in western Gondwana, Gondwana Research, 13, 488–501, https://doi.org/10.1016/j.gr.2007.05.008, 2008.

Gee, M. J. R., Gawthorpe, R. L., and Friedmann, J. S.: Giant striations at the base of a submarine landslide, Marine Geology, 214, 287–294, https://doi.org/10.1016/j.margeo.2004.09.003, 2005.

Gehling, J. G. and Droser, M. L.: Ediacaran stratigraphy and the biota of the Adelaide Geosyncline, South Australia, Episodes, 35, 236–246, https://doi.org/10.18814/epiiugs/2012/v35i1/023, 2012.

Ghienne, J.-F., Desrochers, A., Vandenbroucke, T. R. A., Achab, A., Asselin, E., Dabard, M.-P., Farley, C., Loi, A., Paris, F., Wickson, S., and Veizer, J.: A Cenozoic-style scenario for the end-Ordovician glaciation, Nat Commun, 5, 4485, https://doi.org/10.1038/ncomms5485, 2014.

Gilbert, R.: Rafting in glacimarine environments, Geological Society, London, Special Publications, 53, 105–120, https://doi.org/10.1144/GSL.SP.1990.053.01.06, 1990.

Glaessner, M. F.: New fossils from the base of the Cambrian in South Australia (Preliminary Account), Transactions of the Royal Society of South Australia, Incorporated, 81, 185–188, 1958.

Glaessner, M. F.: The oldest fossil faunas of South Australia, Geologische Rundschau, 47, 522–531, https://doi.org/10.1007/BF01800671, 1959.

Goldschmidt, P. M., Pfirman, S. L., Wollenburg, I., and Henrich, R.: Origin of sediment pellets from the Arctic seafloor: sea ice or icebergs?, Deep Sea Research Part A. Oceanographic Research Papers, 39, S539–S565, https://doi.org/10.1016/S0198-0149(06)80020-8, 1992.

Gómez, N., Lowe, D., Mills, A., Slaney, N., and Arnott, B.: Ediacaran proximal glaciomarine sedimentation in the Bonavista Peninsula, Avalon Zone (Newfoundland) , Copernicus Meetings, https://doi.org/10.5194/egusphere-egu24-6919, 2024.

Gómez, N., Lowe, D., Mills, A., Kommescher, S., and Lam, R.: Interplay of Ediacaran glaciation and sediment provenance revealed by detrital zircon U-Pb geochronology and Hf isotope geochemistry in the Bonavista Peninsula (Newfoundland), GSA Bulletin, https://doi.org/10.1130/B38347.1, 2025a.

Gómez, N., Lowe, D., Kommescher, S., and Mills, A.: Unraveling recycling and climate influence on detrital U-Pb geochronology of titanite and apatite: An example from the Gaskiers Glaciation in Newfoundland, Precambrian Research, 427, 107871, https://doi.org/10.1016/j.precamres.2025.107871, 2025b.

Gómez, N., Lowe, D., Mills, A., Slaney, N., and Arnott, R. W. C.: Ediacaran proximal glaciomarine sedimentation in the Bonavista Peninsula, Avalon Zone, Newfoundland, Canada, Journal of Sedimentary Research, 96, 130–157, https://doi.org/10.2110/jsr.2025.022, 2026.

Gostin, V. A., McKirdy, D. M., Webster, L. J., and Williams, G. E.: Ediacaran ice-rafting and coeval asteroid impact, South Australia: insights into the terminal Proterozoic environment, Australian Journal of Earth Sciences, 57, 859–869, https://doi.org/10.1080/08120099.2010.509408, 2010.

Grace, K. and Lowe, D. G.: The record of Ediacaran basin transformation from the deepwater Mistaken Point Formation, Avalon Terrane, Newfoundland, Journal of Sedimentary Research, https://doi.org/10.2110/jsr.2024.170, 2025.

Gravenor, C. P.: Heavy minerals and sedimentological studies on the glaciogenic Late Precambrian Gaskiers Formation of Newfoundland, Can. J. Earth Sci., 17, 1331–1341, https://doi.org/10.1139/e80-140, 1980.

Grazhdankin, D. V., Marusin, V. V., Meert, J., Krupenin, M. T., and Maslov, A. V.: Kotlin regional stage in the South Urals, Dokl. Earth Sc., 440, 1222–1226, https://doi.org/10.1134/S1028334X11090170, 2011.

Haines, P.: The upper Wilpena Group at Bunyeroo Gorge - a one day excursion, in: Proterozoic Clastic Sedmentation in relation to Glaciations and Tectonism, Flinders Ranges, South Australia, edited by: Gostin, V. A., A8–A11, 1986.

Halliday, A. N., Graham, C. M., Aftalion, M., and Dymoke, P.: Short Paper: The depositional age of the Dalradian Supergroup: U-Pb and Sm-Nd isotopic studies of the Tayvallich Volcanics, Scotland, Journal of the Geological Society, 146, 3–6, https://doi.org/10.1144/gsjgs.146.1.0003, 1989.

Hambrey, M. J. and Harland, W. B.: Criteria for the identification of glacigenic deposits, in: Earth's pre-pleistocene glacial record, edited by: Hambrey, M. J. and Harland, W. B., Cambridge University Press, Cambridge, UK, 14–21, 1981.

Harris, A. L., Haselock, P. J., Kennedy, M. J., Mendum, J. R., Long, C. B., Winchester, J. A., and Tanner, P. W. G.: The Dalradian Supergroup in Scotland, Shetland and Ireland, in: A revised correlation of Pre-Cambrian rocks in the British Isles, vol. 22, edited by: Gibbons, W. and Harris, A. L., Geological Society of London, 0, https://doi.org/10.1144/SR22.4, 1994.

Headland, R. K., Hughes, N. E., and Wilkinson, J. P.: Historical occurrence of Antarctic icebergs within mercantile shipping routes and the exceptional events of the 1890s, Journal of Glaciology, 69, 2046–2058, https://doi.org/10.1017/jog.2023.80, 2023.

Hebert, C. L., Kaufman, A. J., Penniston-Dorland, S. C., and Martin, A. J.: Radiometric and stratigraphic constraints on terminal Ediacaran (post-Gaskiers) glaciation and metazoan evolution, Precambrian Research, 182, 402–412, https://doi.org/10.1016/j.precamres.2010.07.008, 2010.

Hill, J. C. and Condron, A.: Subtropical iceberg scours and meltwater routing in the deglacial western North Atlantic, Nature Geosci, 7, 806–810, https://doi.org/10.1038/ngeo2267, 2014.

Hoffman, P. F., Kaufman, A. J., Halverson, G. P., and Schrag, D. P.: A Neoproterozoic Snowball Earth, Science, 281, 1342–1346, https://doi.org/10.1126/science.281.5381.1342, 1998.

Hoffman, P. F., Abbot, D. S., Ashkenazy, Y., Benn, D. I., Brocks, J. J., Cohen, P. A., Cox, G. M., Creveling, J. R., Donnadieu, Y., Erwin, D. H., Fairchild, I. J., Ferreira, D., Goodman, J. C., Halverson, G. P., Jansen, M. F., Le Hir, G., Love, G. D., Macdonald, F. A., Maloof, A. C., Partin, C. A., Ramstein, G., Rose, B. E. J., Rose, C. V., Sadler, P. M., Tziperman, E., Voigt, A., and Warren, S. G.: Snowball Earth climate dynamics and Cryogenian geology-geobiology, Science Advances, 3, e1600983, https://doi.org/10.1126/sciadv.1600983, 2017.

Huggett, Q. J. and Kidd, R. B.: Identification of ice-rafted and other exotic material in deep-sea dredge hauls, Geo-Marine Letters, 3, 23–29, https://doi.org/10.1007/BF02463438, 1983.

Husson, J. M., Higgins, J. A., Maloof, A. C., and Schoene, B.: Ca and Mg isotope constraints on the origin of Earth's deepest δ13C excursion, Geochimica et Cosmochimica Acta, 160, 243–266, https://doi.org/10.1016/j.gca.2015.03.012, 2015.

Inglis, J. D., MacLean, J. S., Samson, S. D., D'Lemos, R. S., Admou, H., and Hefferan, K.: A precise U–Pb zircon age for the Bleïda granodiorite, Anti-Atlas, Morocco: implications for the timing of deformation and terrane assembly in the eastern Anti-Atlas, Journal of African Earth Sciences, 39, 277–283, https://doi.org/10.1016/j.jafrearsci.2004.07.041, 2004.

Judd, E. J., Tierney, J. E., Lunt, D. J., Montañez, I. P., Huber, B. T., Wing, S. L., and Valdes, P. J.: A 485-million-year history of Earth's surface temperature, Science, 385, eadk3705, https://doi.org/10.1126/science.adk3705, 2024.

Kawai, T., Windley, B., Terabayashi, M., Yamamoto, H., Isozaki, Y., and Maruyama, S.: Neoproterozoic glaciation in the mid-oceanic realm: An example from hemi-pelagic mudstones on Llanddwyn Island, Anglesey, UK, Gondwana Research, 14, 105–114, https://doi.org/10.1016/j.gr.2007.12.008, 2008.

Kennedy, M. J. and Christie-Blick, N.: Condensation origin for Neoproterozoic cap carbonates during deglaciation, Geology, 39, 319–322, https://doi.org/10.1130/G31348.1, 2011.

Kidd, R. B. and Huggett, Q. J.: Rock debris on abyssal plains in the Northeast Atlantic: a comparison of epibenthic sledge hauls and photographic surveys, Oceanologica Acta, 4, 99–104, 1981.

Kirschvink, J. L.: Late Proterozoic Low-Latitude Global Glaciation: the Snowball Earth, in: The Proterozoic Biosphere: a Multidisciplinary Study, vol. 52, edited by: Schopf, J. W. and Klein, C., Cambridge University Press, New York, USA, 51–52, 1992.

Knight, J.: The environmental significance of ventifacts: A critical review, Earth-Science Reviews, 86, 89–105, https://doi.org/10.1016/j.earscirev.2007.08.003, 2008.

Krogh, T. E., Strong, D. F., O'Brien, S. J., and Papezik, V. S.: Precise U–Pb zircon dates from the Avalon Terrane in Newfoundland, Can. J. Earth Sci., 25, 442–453, https://doi.org/10.1139/e88-045, 1988.

Krzemińska, E., Poprawa, P., Pacześna, J., and Krzemiński, L.: From initiation to termination: The evolution of the Ediacaran Volyn large igneous province (SW East European Craton) constrained by comparative geochemistry of proximal tuffs versus lavas and zircon geochronology, Precambrian Research, 370, 106560, https://doi.org/10.1016/j.precamres.2022.106560, 2022.

Kusky, T. M. and Matsah, M. I.: Neoproterozoic dextral faulting on the Najd Fault System, Saudi Arabia, preceded sinistral faulting and escape tectonics related to closure of the Mozambique Ocean, in: Proterozoic East Gondwana: Supercontinent Assembly and Breakup, vol. 206, edited by: Yoshida, M., Windley, B. F., and Dasgupta, S., Geological Society of London, 327–361, https://doi.org/10.1144/GSL.SP.2003.206.01.16, 2003.

Lamoso, I. S. M., Babinski, M., Caetano-Filho, S., Paula-Santos, G. M., and Hollanda, M. H. B. M.: A Record of the Snowball Earth Events? The Parecis Basin May Encompass Three Major Neoproterozoic Glaciations on the Amazonian Craton, Journal of South American Earth Sciences, 127, 104411, https://doi.org/10.1016/j.jsames.2023.104411, 2023.

Le Heron, D. P.: An exhumed Paleozoic glacial landscape in Chad, Geology, 46, 91–94, https://doi.org/10.1130/G39510.1, 2017.

Leather, J., Allen, P. A., Brasier, M. D., and Cozzi, A.: Neoproterozoic snowball Earth under scrutiny: Evidence from the Fiq glaciation of Oman, Geology, 30, 891–894, https://doi.org/10.1130/0091-7613(2002)030%3C0891:NSEUSE%3E2.0.CO;2, 2002.

Letsch, D., Large, S. J. E., Buechi, M. W., Winkler, W., and von Quadt, A.: Ediacaran glaciations of the west African Craton – Evidence from Morocco, Precambrian Research, 310, 17–38, https://doi.org/10.1016/j.precamres.2018.02.015, 2018.

Li, Z., Zhao, Z., Li, J., Li, Q., and Niu, H.: Provenance Analysis of the Black Clastic Rock Series at the Cambrian Base in the Southeastern Margin of North China Craton and Its Constraints on the Late Precambrian Geologic Evolution, Acta Geologica Sinica, 92, 1803–1828, 2018.

Lloyd, J. C., Blades, M. L., Counts, J. W., Collins, A. S., Amos, K. J., Wade, B. P., Hall, J. W., Hore, S., Ball, A. L., Shahin, S., and Drabsch, M.: Neoproterozoic geochronology and provenance of the Adelaide Superbasin, Precambrian Research, 350, 105849, https://doi.org/10.1016/j.precamres.2020.105849, 2020.

Macdonald, F. A., Swanson-Hysell, N. L., Park, Y., Lisiecki, L., and Jagoutz, O.: Arc-continent collisions in the tropics set Earth's climate state, Science, 364, 181–184, https://doi.org/10.1126/science.aav5300, 2019.

Mallmann, G., Chemale, F., Ávila, J. N., Kawashita, K., and Armstrong, R. A.: Isotope geochemistry and geochronology of the Nico Pérez Terrane, Rio de la Plata Craton, Uruguay, Gondwana Research, 12, 489–508, https://doi.org/10.1016/j.gr.2007.01.002, 2007.

Maslov, A., Meert, J., Levashova, N., Yu, R., Grazhdankin, D., Kuznetsov, N., Krupenin, M., Fedorova, N. M., and Ipat`eva, I. S.: New Constraints for the Age of Vendian Glacial Deposits (Central Urals), Doklady Earth Sciences, 449, 303–308, https://doi.org/10.1134/S1028334X13030203, 2013.

Matthews, J. J., Liu, A. G., Yang, C., McIlroy, D., Levell, B., and Condon, D. J.: A Chronostratigraphic Framework for the Rise of the Ediacaran Macrobiota: New Constraints from Mistaken Point Ecological Reserve, Newfoundland, GSA Bulletin, 133, 612–624, https://doi.org/10.1130/B35646.1, 2021.

McCay, G. A., Prave, A. R., Alsop, G. I., and Fallick, A. E.: Glacial trinity: Neoproterozoic Earth history within the British-Irish Caledonides, Geology, 34, 909–912, https://doi.org/10.1130/G22694A.1, 2006.

McGee, B., Collins, A. S., and Trindade, R. I. F.: A Glacially Incised Canyon in Brazil: Further Evidence for Mid-Ediacaran Glaciation?, The Journal of Geology, 121, 275–287, https://doi.org/10.1086/669979, 2013.

McGee, B., Collins, A. S., Trindade, R. I. F., and Payne, J.: Age and provenance of the Cryogenian to Cambrian passive margin to foreland basin sequence of the northern Paraguay Belt, Brazil, GSA Bulletin, 127, 76–86, https://doi.org/10.1130/B30842.1, 2015a.

McGee, B., Collins, A. S., Trindade, R. I. F., and Jourdan, F.: Investigating mid-Ediacaran glaciation and final Gondwana amalgamation using coupled sedimentology and 40Ar/ 39Ar detrital muscovite provenance from the Paraguay Belt, Brazil, Sedimentology, 62, 130–154, https://doi.org/10.1111/sed.12143, 2015b.

Means, W. D.: A newly recognized type of slickenside striation, Journal of Structural Geology, 9, 585–590, https://doi.org/10.1016/0191-8141(87)90143-X, 1987.

van der Meer, D. G., Scotese, C. R., Mills, B. J. W., Sluijs, A., van den Berg van Saparoea, A.-P., and van de Weg, R. M. B.: Long-term Phanerozoic global mean sea level: Insights from strontium isotope variations and estimates of continental glaciation, Gondwana Research, 111, 103–121, https://doi.org/10.1016/j.gr.2022.07.014, 2022.

van der Meer, J. J. M.: Microscopic evidence of subglacial deformation, Quaternary Science Reviews, 12, 553–587, 1994.

van der Meer, J. J. M., Menzies, J., and Rose, J.: Subglacial till: the deforming glacier bed, Quaternary Science Reviews, 22, 1659–1685, 2003.

Menzies, J.: Micromorphological analyses of microfabrics and microstructures indicative of deformation processes in glacial sediments, Geological Society, London, Special Publications, 176, 245–257, 2000.

Merdith, A. S., Gernon, T. M., Maffre, P., Donnadieu, Y., Goddéris, Y., Longman, J., Müller, R. D., and Mills, B. J. W.: Phanerozoic icehouse climates as the result of multiple solid-Earth cooling mechanisms, Science Advances, 11, eadm9798, https://doi.org/10.1126/sciadv.adm9798, 2025.

Micheels, A. and Montenari, M.: A snowball Earth versus a slushball Earth: Results from Neoproterozoic climate modeling sensitivity experiments, Geosphere, 4, 401–410, https://doi.org/10.1130/GES00098.1, 2008.

Mills, A. J., Dunning, G. R., Murphy, M., and Langille, A.: New geochronological constraints on the timing of magmatism for the Bull Arm Formation, Musgravetown Group, Avalon Terrane, northeastern Newfoundland, St. John's, Newfoundland, 2017.

Mills, A. J., Normore, L., Gomez, N., Dunning, G. R., and Lowe, D. G.: A tale of two basins: juxtaposition of the Ediacaran fossil-bearing St. John's Basin against the Ediacaran glaciovolcanic Bonavista Basin on the Bonavista Peninsula, Avalon Zone, Newfoundland, Atlantic Geoscience, 60, 131–150, https://doi.org/10.4138/atlgeo.2024.007, 2024.

Moeller, P. and Ingolefsson, O.: Gravel and sand flotation; a sediment dispersal process important in certain nearshore marine environments, Journal of Sedimentary Research, 64, 894–898, https://doi.org/10.1306/D4267EFB-2B26-11D7-8648000102C1865D, 1994.

Montañez, I. P. and Poulsen, C. J.: The Late Paleozoic Ice Age: An Evolving Paradigm, Annual Review of Earth and Planetary Sciences, 41, 629–656, https://doi.org/10.1146/annurev.earth.031208.100118, 2013.

Mulder, J. A., Everard, J. L., Cumming, G., Meffre, S., Bottrill, R. S., Merdith, A. S., Halpin, J. A., McNeill, A. W., and Cawood, P. A.: Neoproterozoic opening of the Pacific Ocean recorded by multi-stage rifting in Tasmania, Australia, Earth-Science Reviews, 201, 103041, https://doi.org/10.1016/j.earscirev.2019.103041, 2020.

Munn, C. A.: Huge icebergs in the Southern Ocean, Scientific American, 105, 544–545, 1911.

Myrow, P. M. and Kaufman, A. J.: A newly discovered cap carbonate above Varanger-age glacial deposits in Newfoundland, Canada, Journal of Sedimentary Research, 69, 784–793, https://doi.org/10.2110/jsr.69.784, 1999.

Nettle, D., Halverson, G. P., Cox, G. M., Collins, A. S., Schmitz, M., Gehling, J., Johnson, P. R., and Kadi, K.: A middle–late Ediacaran volcano-sedimentary record from the eastern Arabian-Nubian shield, Terra Nova, 26, 120–129, https://doi.org/10.1111/ter.12077, 2014.

Nielsen, T. and Kuijpers, A.: Geohazard studies offshore the Faroe Islands: slope instability, bottom currents and sub-seabed sediment mobilisation, GEUS Bulletin, 4, 57–60, https://doi.org/10.34194/geusb.v4.4785, 2004.

Niu, Y., Shi, G. R., Zhang, Q., Jones, B. G., Wang, X., and Zhao, G.: Ediacaran Cordilleran-type mountain ice sheets and their erosion effects, Earth-Science Reviews, 249, 104671, https://doi.org/10.1016/j.earscirev.2023.104671, 2024.

Normore, L. S.: Preliminary findings on the geology of the Trinity map area (NTS 2C/06), Newfoundland, St. John's, Newfoundland, 2011.

Ovenshine, A. T.: Observations of iceberg rafting in Glacier Bay, Alaska, and the identification of ancient ice-rafted deposits, GSA Bulletin, 81, 891–894, https://doi.org/10.1130/0016-7606(1970)81%5B891:OOIRIG%5D2.0.CO;2, 1970.

Oyhantçabal, P., Siegesmund, S., Wemmer, K., Frei, R., and Layer, P.: Post-collisional transition from calc-alkaline to alkaline magmatism during transcurrent deformation in the southernmost Dom Feliciano Belt (Braziliano–Pan-African, Uruguay), Lithos, 98, 141–159, https://doi.org/10.1016/j.lithos.2007.03.001, 2007.

Pacześna, J.: Litostratygrafia utworów ediakaru w lubelsko-podlaskim basenie sedymentacyjnym (wschodnia i południowo-wschodnia Polska), Biuletyn Państwowego Instytutu Geologicznego, 460, 1–23, 2014.

Paszkowski, M., Kędzior, A., and Shumlyanskyy, L.: Well-preserved Proterozoic pre- and post Vilchitsy peryglacial phenomena on Western Baltica Paleocontinent, in: Book of Abstracts, Geology and Mineral Resources of Ukraine: 100-years Anniversary Conference of the Institute of Geology, Mineralogy, and Mineral Resources of National Academy of Sciences, 190–191, 2018.

Pauly, H.: "Ikaite", a New Mineral from Greenland, ARCTIC, 16, 263–264, https://doi.org/10.14430/arctic3545, 1963.

Pazos, P. J., Sánchez-Bettucci, L., and Tofalo, O. R.: The Record of the Varanger Glaciation at the Río De La Plata Craton, Vendian-Cambrian of Uruguay, Gondwana Research, 6, 65–77, https://doi.org/10.1016/S1342-937X(05)70644-4, 2003.

Pazos, P. J., Rapalini, A. E., Bettucci, L. S., and Tófalo, O. R.: Chapter 52 The Playa Hermosa Formation, Playa Verde Basin, Uruguay, Geological Society, London, Memoirs, 36, 547–553, https://doi.org/10.1144/M36.52, 2011.

Pecoits, E.: Sedimentología y consideraciones estratigráficas de la Formación Las Ventanas en su área tipo, Departamento de Maldonado, Uruguay, Revista de la Sociedad Uruguaya de Geologia Publicacion Especial, 1, 124–140, 2003.

Pecoits, E., Gingras, M., Aubet, N., and Konhauser, K.: Ediacaran in Uruguay: palaeoclimatic and palaeobiological implications, Sedimentology, 55, 689–719, https://doi.org/10.1111/j.1365-3091.2007.00918.x, 2008.

Pecoits, E., Gingras, M. K., and Konhauser, K. O.: Chapter 53 Las Ventanas and San Carlos formations, Maldonado Group, Uruguay, Geological Society, London, Memoirs, 36, 555–564, https://doi.org/10.1144/M36.53, 2011.

Powers, M. C.: A new roundness scale for sedimentary particles, Journal of Sedimentary Research, 23, 117–119, https://doi.org/10.1306/D4269567-2B26-11D7-8648000102C1865D, 1953.

Prave, A. R.: The Neoproterozoic Dalradian Supergroup of Scotland: an alternative hypothesis, Geological Magazine, 136, 609–617, https://doi.org/10.1017/S0016756899003155, 1999.

Prave, A. R. and Fallick, A. E.: The Neoproterozoic glaciogenic deposits of Scotland and Ireland, in: The Geological Record of Neoproterozoic Glaciations, vol. 36, edited by: Arnaud, E., Halverson, G. P., and Shields-Zhou, G., Geological Society of London, 0, https://doi.org/10.1144/M36.63, 2011.

Prave, A. R., Condon, D. J., Hoffmann, K. H., Tapster, S., and Fallick, A. E.: Duration and nature of the end-Cryogenian (Marinoan) glaciation, Geology, 44, 631–634, https://doi.org/10.1130/G38089.1, 2016.

Preciozzi, F., Masquelin, H., and Sanchez Bettucci, L.: Geología de la Porción Sur del Cinturón Cuchilla de Dionisio, La Paloma, Uruguay, Primer Simposio Internacional Del Neoproterozoico- Cambriano de la Cuenca Del Plata, Guía de Excursiones, 1–38, 1993.

Pu, J. P., Bowring, S. A., Ramezani, J., Myrow, P., Raub, T. D., Landing, E., Mills, A., Hodgin, E., and Macdonald, F. A.: Dodging snowballs: Geochronology of the Gaskiers glaciation and the first appearance of the Ediacaran biota, Geology, 44, 955–958, https://doi.org/10.1130/G38284.1, 2016.

Qu, Y., Teichert, B. M. A., Birgel, D., Goedert, J. L., and Peckmann, J.: The prominent role of bacterial sulfate reduction in the formation of glendonite: a case study from Paleogene marine strata of western Washington State, Facies, 63, 10, https://doi.org/10.1007/s10347-017-0492-1, 2017.

Rapalini, A. E., Tohver, E., Bettucci, L. S., Lossada, A. C., Barcelona, H., and Pérez, C.: The late Neoproterozoic Sierra de las Ánimas Magmatic Complex and Playa Hermosa Formation, southern Uruguay, revisited: Paleogeographic implications of new paleomagnetic and precise geochronologic data, Precambrian Research, 259, 143–155, https://doi.org/10.1016/j.precamres.2014.11.021, 2015.

Raymond, A. and Metz, C.: Ice and Its Consequences: Glaciation in the Late Ordovician, Late Devonian, Pennsylvanian-Permian, and Cenozoic Compared, The Journal of Geology, 112, 655–670, https://doi.org/10.1086/424580, 2004.

Retallack, G. J.: Towards a glacial subdivision of the Ediacaran Period, with an example of the Boston Bay Group, Massachusetts, Australian Journal of Earth Sciences, 69, 223–250, https://doi.org/10.1080/08120099.2021.1954088, 2022.

Rooney, A. D., Strauss, J. V., Brandon, A. D., and Macdonald, F. A.: A Cryogenian chronology: Two long-lasting synchronous Neoproterozoic glaciations, Geology, 43, 459–462, https://doi.org/10.1130/G36511.1, 2015.

Rooney, A. D., Cantine, M. D., Bergmann, K. D., Gómez-Pérez, I., Al Baloushi, B., Boag, T. H., Busch, J. F., Sperling, E. A., and Strauss, J. V.: Calibrating the coevolution of Ediacaran life and environment, Proceedings of the National Academy of Sciences, 117, 16824–16830, https://doi.org/10.1073/pnas.2002918117, 2020.

Sánchez Bettucci, L. and Linares, E.: Primeras edades en Basaltos del Complejo Sierra de las Animas, XIII Congreso Geológico Argentino y III Congreso de Exploración de Hidrocarburos, Actas, 1, 399–404, 1996.

Sánchez-Bettucci, L., Koukharsky, M., Pazos, P. J., and Stareczek, S.: Neoproterozoic subaqueous extrusive–intrusive rocks in the Playa Hermosa Formation in Uruguay: Regional and stratigraphic significance, Gondwana Research, 16, 134–144, https://doi.org/10.1016/j.gr.2009.01.002, 2009.

Sayles, S. D.: The Squantum Tillite, Museum of Comparative Zoology Bulletin, 66, 141–175, 1914.

Schmidt, P. W. and Williams, G. E.: Palaeomagnetism of the ejecta-bearing Bunyeroo Formation, late Neoproterozoic, Adelaide fold belt, and the age of the Acraman impact, Earth and Planetary Science Letters, 144, 347–357, https://doi.org/10.1016/S0012-821X(96)00169-0, 1996.

Schofield, D. I., Leslie, A. G., Wilby, P. R., Dartnall, R., Waldron, J. W. F., and Kendall, R. S.: Tectonic evolution of Anglesey and adjacent mainland North Wales, Geological Society, London, Special Publications, 503, 371–390, https://doi.org/10.1144/SP503-2020-9, 2021.

Scotese, C. R.: PALEOMAP PaleoAtlas for GPlates and the PaleoData Plotter Program, PALEOMAP Project, 2016.

Scotese, C. R. and Wright, N.: PALEOMAP paleodigital elevation models (PaleoDEMS) for the Phanerozoic, PALEOMAP Proj, 2018.

Scotese, C. R., Song, H., Mills, B. J. W., and van der Meer, D. G.: Phanerozoic paleotemperatures: The earth's changing climate during the last 540 million years, Earth-Science Reviews, 215, 103503, https://doi.org/10.1016/j.earscirev.2021.103503, 2021.

Shaw, J., Gilbert, R. G., Sharpe, D. R., Lesemann, J.-E., and Young, R. R.: The origins of s-forms: Form similarity, process analogy, and links to high-energy, subglacial meltwater flows, Earth-Science Reviews, 200, 102994, https://doi.org/10.1016/j.earscirev.2019.102994, 2020.

Shumlyanskyy, L., Nosova, A., Billström, K., Söderlund, U., Andréasson, P.-G., and Kuzmenkova, O.: The U–Pb zircon and baddeleyite ages of the Neoproterozoic Volyn Large Igneous Province: implication for the age of the magmatism and the nature of a crustal contaminant, GFF, 138, 17–30, https://doi.org/10.1080/11035897.2015.1123289, 2016.

Socci, A. D. and Smith, G. W.: Stratigraphic implications of facies within the Boston Basin, in: Geology of the Composite Avalon Terrane of Southern New England, vol. 245, edited by: Socci, A. D., Skehan, J. W., and Smith, G. W., Geological Society of America, 0, https://doi.org/10.1130/SPE245-p55, 1990.

Southworth, S., Tollo, R. P., Aleinikoff, J. N., Bailey, C., Burton, W. C., Crider, E., Hackley, P. C., Kunk, M. J., Mundil, R., Naeser, C. N., and others: New geologic map and geochronology of the Shenandoah National Park region, Virginia, in: Geological Society of America Abstracts with Programs, 365, 2009.

Spencer, A. M.: Mechanisms and environments of deposition of late precambrian geosynclinal tillites: Scotland and East Greenland, Palaeogeography, Palaeoclimatology, Palaeoecology, 51, 143–157, https://doi.org/10.1016/0031-0182(85)90083-5, 1985.

Sprigg, R. C.: Jellyfish from the Basal Cambrian in South Australia, Nature, 161, 568–569, https://doi.org/10.1038/161568a0, 1948.

Środoń, J., Condon, D. J., Golubkova, E., Millar, I. L., Kuzmenkova, O., Paszkowski, M., Mazur, S., Kędzior, A., Drygant, D., Ciobotaru, V., and Liivamägi, S.: Ages of the Ediacaran Volyn-Brest trap volcanism, glaciations, paleosols, Podillya Ediacaran soft-bodied organisms, and the Redkino-Kotlin boundary (East European Craton) constrained by zircon single grain U-Pb dating, Precambrian Research, 386, 106962, https://doi.org/10.1016/j.precamres.2023.106962, 2023.

Stein, C. L. and Smith, A. J.: Authigenic Carbonate Nodules in the Nankai Trough, Site 583, Initial Reports of the Deep Sea Drilling Project, https://doi.org/10.2973/dsdp.proc.87.115.1986, 1986.

Suess, E., Balzer, W., Hesse, K.-F., Müller, P. J., Ungerer, C. A., and Wefer, G.: Calcium Carbonate Hexahydrate from Organic-Rich Sediments of the Antarctic Shelf: Precursors of Glendonites, Science, 216, 1128–1131, https://doi.org/10.1126/science.216.4550.1128, 1982.

Tan, M., Li, Z., Lan, Z., An, W., and Wang, D.: Rodinia supercontinent assembly in the southeastern North China Craton: Detrital zircon evidence from the late Ediacaran Fengtai Formation, Precambrian Research, 422, 107775, https://doi.org/10.1016/j.precamres.2025.107775, 2025.

Tasistro-Hart, A. R., Macdonald, F. A., Crowley, J. L., and Schmitz, M. D.: Four-million-year Marinoan snowball shows multiple routes to deglaciation, Proceedings of the National Academy of Sciences, 122, e2418281122, https://doi.org/10.1073/pnas.2418281122, 2025.

Tedesco, J., Cagliari, J., Coitinho, J. dos R., da Cunha Lopes, R., and Lavina, E. L. C.: Late Paleozoic paleofjord in the southernmost Parana Basin (Brazil): Geomorphology and sedimentary fill, Geomorphology, 269, 203–214, https://doi.org/10.1016/j.geomorph.2016.06.035, 2016.

Thomas, R. J., Chevallier, L. P., Gresse, P. G., Harmer, R. E., Eglington, B. M., Armstrong, R. A., de Beer, C. H., Martini, J. E. J., de Kock, G. S., Macey, P. H., and Ingram, B. A.: Precambrian evolution of the Sirwa Window, Anti-Atlas Orogen, Morocco, Precambrian Research, 118, 1–57, https://doi.org/10.1016/S0301-9268(02)00075-X, 2002.

Thompson, M. D. and Bowring, S. A.: Age of the Squantum "tillite," Boston Basin, Massachusetts; U-Pb zircon constraints on terminal Neoproterozoic glaciation, American Journal of Science, 300, 630–655, https://doi.org/10.2475/ajs.300.8.630, 2000.

Thompson, M. D., Grunow, A. M., and Ramezani, J.: Late Neoproterozoic paleogeography of the Southeastern New England Avalon Zone: Insights from U-Pb geochronology and paleomagnetism, GSA Bulletin, 119, 681–696, https://doi.org/10.1130/B26014.1, 2007.

Tierney, F. L., Billings, M. P., and Cassidy, M. M.: Geology of the city tunnel, Greater Boston, Massachusetts, Boston Society of Civil Engineers, 55, 60–96, 1968.

Tindal, B.: Geological constraints on Neoproterozoic glacial episodes, PhD, University of Cambridge, Cambridge, UK, 275 pp., https://doi.org/10.17863/CAM.93553, 2023.

Tollefsen, E., Balic-Zunic, T., Mörth, C.-M., Brüchert, V., Lee, C. C., and Skelton, A.: Ikaite nucleation at 35 °C challenges the use of glendonite as a paleotemperature indicator, Sci Rep, 10, 8141, https://doi.org/10.1038/s41598-020-64751-5, 2020.

Tollo, R. P. and Hutson, F. E.: 700 Ma rift event in the Blue Ridge province of Virginia: A unique time constraint on pre-Iapetan rifting of Laurentia, Geology, 24, 59–62, https://doi.org/10.1130/0091-7613(1996)024%3C0059:MREITB%3E2.3.CO;2, 1996.

Van Hoesen, J. G. and Orndorff, R. L.: Using GIS to Evaluate an Enigmatic Diamicton in the Spring Mountains, Southern Nevada, The Professional Geographer, 55, 206–215, https://doi.org/10.1111/0033-0124.5502008, 2003.

Van Hoesen, J. G. and Orndorff, R. L.: A comparative SEM study on the micromorphology of glacial and nonglacial clasts with varying age and lithology, Can. J. Earth Sci., 41, 1123–1139, https://doi.org/10.1139/e04-056, 2004.

Vandyk, T. M., Kettler, C., Davies, B. J., Shields, G. A., Candy, I., and Le Heron, D. P.: Reassessing classic evidence for warm-based Cryogenian ice on the western Laurentian margin: The "striated pavement" of the Mineral Fork Formation, USA, Precambrian Research, 363, 106345, https://doi.org/10.1016/j.precamres.2021.106345, 2021.

Várkonyi, P. L. and Laity, J. E.: Formation of surface features on ventifacts: Modeling the role of sand grains rebounding within cavities, Geomorphology, 139–140, 220–229, https://doi.org/10.1016/j.geomorph.2011.10.021, 2012.

Vernhet, E., Youbi, N., Chellai, E. H., Villeneuve, M., and El Archi, A.: The Bou-Azzer glaciation: Evidence for an Ediacaran glaciation on the West African Craton (Anti-Atlas, Morocco), Precambrian Research, 196–197, 106–112, https://doi.org/10.1016/j.precamres.2011.11.009, 2012.

Vickers-Rich, P., Ivantsov, A., Kattan, F., Johnson, P., Al Qubsani, A., Kashghari, W., Leonov, M., Rich, T., Linnemann, U., Hofmann, M., Trusler, P., Smith, J., Yazedi, A., Rich, B., Al Garni, S. M., Shamari, A., Al Barakati, A., and Al Kaff, M. H.: Reconnaissance for an Ediacaran fauna, Kingdom of Saudi Arabia, Saudi Geological Survey, Jeddah, Saudi Arabia, 2012.

Wallace, M., Gostin, V., and Keays, R.: Sedimentology of the Neoproterozoic Acraman impact-ejecta horizon, South Australia, AGSO Journal of Australian Geology and Geophysics, 16, 443–451, 1996.

Wang, Z., Wang, J., Suess, E., Wang, G., Chen, C., and Xiao, S.: Silicified glendonites in the Ediacaran Doushantuo Formation (South China) and their potential paleoclimatic implications, Geology, 45, 115–118, https://doi.org/10.1130/G38613.1, 2017.

Wang, Z., Chen, C., Wang, J., Suess, E., Chen, X., Ma, X., Wang, G., and Xiao, S.: Wide but not ubiquitous distribution of glendonite in the Doushantuo Formation, South China: Implications for Ediacaran climate, Precambrian Research, 338, 105586, https://doi.org/10.1016/j.precamres.2019.105586, 2020.

Wicander, R., Clayton, G., Marshall, J. E. A., Troth, I., and Racey, A.: Was the latest Devonian glaciation a multiple event? New palynological evidence from Bolivia, Palaeogeography, Palaeoclimatology, Palaeoecology, 305, 75–83, https://doi.org/10.1016/j.palaeo.2011.02.016, 2011.

Williams, G. E. and Schmidt, P. W.: Shuram–Wonoka carbon isotope excursion: Ediacaran revolution in the world ocean's meridional overturning circulation, Geoscience Frontiers, 9, 391–402, https://doi.org/10.1016/j.gsf.2017.11.006, 2018.

Williams, G. E. and Schmidt, P. W.: Dating the Acraman asteroid impact, South Australia: the case for deep drilling the 'hot shock' zone of the central uplift, Australian Journal of Earth Sciences, 68, 355–367, https://doi.org/10.1080/08120099.2020.1808066, 2021.

Williams, G. E., Schmidt, P. W., and Young, G. M.: Strongly seasonal Proterozoic glacial climate in low palaeolatitudes: Radically different climate system on the pre-Ediacaran Earth, Geoscience Frontiers, 7, 555–571, https://doi.org/10.1016/j.gsf.2016.01.005, 2016.

Williams, H. and King, A. F.: Trepassey map area, Newfoundland / by H. Williams and A.F. King.: M46-389E-PDF - Government of Canada Publications - Canada.ca, Geological Survey of Canada, 1979.

Wong Hearing, T. W., Tindal, B. H., Vandyk, T. M., Na, L., Pohl, A., Liu, A. G., Harvey, T. H. P., and Williams, M.: Ediacaran coupling of climate and biosphere dynamics, GSA Bulletin, accepted, 2026.

Woodhouse, A., Swain, A., Fagan, W. F., Fraass, A. J., and Lowery, C. M.: Late Cenozoic cooling restructured global marine plankton communities, Nature, 614, 713–718, https://doi.org/10.1038/s41586-023-05694-5, 2023.

Yang, C., Rooney, A. D., Condon, D. J., Li, X.-H., Grazhdankin, D. V., Bowyer, F. T., Hu, C., Macdonald, F. A., and Zhu, M.: The tempo of Ediacaran evolution, Science Advances, 7, eabi9643, https://doi.org/10.1126/sciadv.abi9643, 2021.

Ye, Y., Wang, X., Wang, H., Wu, C., and Zhang, S.: Exploring climate variability during the Marinoan glaciation: A study of black shale geochemistry, Gondwana Research, 128, 315–324, https://doi.org/10.1016/j.gr.2023.10.022, 2024.

Youbi, N., Ernst, R. E., Söderlund, U., Boumehdi, M. A., Lahna, A. A., Tassinari, C. C. G., Moume, W. E., and Bensalah, M. K.: The Central Iapetus magmatic province: An updated review and link with the ca. 580 Ma Gaskiers glaciation, in: Mass Extinctions, Volcanism, and Impacts: New Developments, edited by: Adatte, T., Bond, D. P. G., and Keller, G., Geological Society of America, 0, https://doi.org/10.1130/2020.2544(02), 2020.

Young, T.: The Bunyeroo Formation and its possible cold-water marine setting, BSc (Honours) thesis, University of Adelaide, Adelaide, Australia, 1995.

Yue, L., Ji, Y., Chu, Z., Zhang, C., Cui, Y., Vandeginste, V., Zong, Y., and Yan, G.: Ediacaran glaciogenic deposits within a carbonate platform background: insights from the Fengtai formation in the southeastern margin of the North China Craton, Geosci J, 29, 342–361, https://doi.org/10.1007/s12303-025-00034-3, 2025.

Zhou, C., Li, X.-H., Xiao, S., Lan, Z., Ouyang, Q., Guan, C., and Chen, Z.: A new SIMS zircon U–Pb date from the Ediacaran Doushantuo Formation: age constraint on the Weng'an biota, Geological Magazine, 154, 1193–1201, https://doi.org/10.1017/S0016756816001175, 2017.

Zhou, X., Lu, Z., Rickaby, R. E. M., Domack, E. W., Wellner, J. S., and Kennedy, H. A.: Ikaite Abundance Controlled by Porewater Phosphorus Level: Potential Links to Dust and Productivity, The Journal of Geology, 123, 269–281, https://doi.org/10.1086/681918, 2015.